

REPUBLIC OF TURKEY
AYDIN ADNAN MENDERES UNIVERSITY
GRADUATE SCHOOL OF NATURAL AND APPLIED SCIENCES
MASTER'S PROGRAMME IN MECHANICAL ENGINEERING

**PERFORMANCE ANALYSIS OF PARABOLIC TROUGH
SOLAR COLLECTORS**

MEHMET AKTAŞ

MASTER'S THESIS

SUPERVISOR

Prof. Dr. Yunus ÇERÇİ

AYDIN-2021

ACCEPTANCE AND APPROVAL

The thesis titled “PERFORMANCE ANALYSIS OF PARABOLIC TROUGH SOLAR COLLECTORS”, prepared by Mehmet AKTAŞ, a student of Department of Mechanical Engineering Program at Republic of Turkey, Aydın Adnan Menderes University, Graduate School Of Natural And Applied Science, was accepted as a Master’s Thesis by the jury below.

Date of Thesis Defence: 26/07/2021

Member : Prof. Dr. Yunus Çerçi ADU Engineering Faculty
(Thesis adv.)

Member : Assoc. Prof. Dr. Ali Yurddaş CBU Engineering Faculty

Member : Asst. Prof. Dr. Mustafa Timur ADU Engineering Faculty

APPROVAL:

This thesis was approved by the jury above in accordance with the relevant articles of the Aydın Adnan Menderes University Graduate Education and Examination Regulations and was approved on the by from the Board of Directions of the Graduate School of Science in thenumbered decision.

Prof. Dr. Gönül AYDIN
Institute Director

ACKNOWLEDGEMENTS

I would like to thank very much my precious thesis advisor Prof. Dr. Yunus ERI whose courses I chose with great excitement, and listened since I have started master program, and tried not to miss his any of courses, and who adds new one to my knowledges in every course, motivated and encouraged me, and is always with me during my thesis study, guided me with his precious knowledge.

I also would like to thank very much my dear family who has always with me and supports me financially /spiritually during my life, and feels same emotion with me during my thesis study, and encourages me in every step of my academic dreams, and believes in me.

I sincerely thank my brother Ahmet GÜLDEMİR who has always with me and helped me to complete my thesis, always listened to me, motivated and encouraged me to realize my academic dreams.

I sincerely thank my brother Yusuf Enes AKDOĞAR who has always motivated me to realize my dreams, listened me on the phone in every thesis speech, calmed me down and believed in me.

Finally, I would like to thank dear jury members Assoc. Prof. Dr. Ali YURDDAŞ and Asst. Prof. Dr. Mustafa TİMUR for joined my thesis defense and their valuable comments.

Mehmet AKTAŞ
Mechanical Engineer

TABLE OF CONTENTS

ACCEPTANCE AND APPROVAL	i
ACKNOWLEDGEMENTS	ii
TABLE OF CONTENTS	iii
LIST OF SYMBOLS AND ABBREVIATIONS.....	v
LIST OF FIGURES	vii
LIST OF TABLES	xii
ÖZET	xiii
ABSTRACT	xv
1 . INTRODUCTION	1
1.1 Solar Concentrators.....	6
1.2 PTSC.....	6
1.3 Industrial Usage Area of PTSC	9
1.4 PTSC Applications in Turkey	15
2 . LITERATURE REVIEW	16
2.1 Objective of Thesis and Outlines.....	24
3 . MATERIAL AND METHOD.....	25
3.1 Material.....	25
3.1.1 Components of PTSC.....	25
3.1.1.1 Mirror Reflectors	25
3.1.1.2 Receiver Tube or HCE	28
3.1.1.3 HTF.....	29
3.1.1.4 Supporting Structure.....	30

3.1.1.5 Control and Tracking System.....	31
3.1.2 Optical Modelling and Geometry of PTSC.....	33
3.2 Method.....	37
3.2.1 Optical Efficiency of the Collector.....	38
3.2.2 Thermal Modelling of the PTSC.....	41
3.2.3 Description of ADU Solar Field.....	44
3.2.4 Heat Transfers Occurred in PTSC.....	51
3.2.4.1 Heat Transfer Between the HTF and the Absorber Pipe.....	51
3.2.4.2 Heat Transfer Through the Absorber Wall.....	53
3.2.4.3 Heat Transfers from the Absorber Pipe to the Glass Envelope.....	54
3.2.4.4 Heat Transfer Through the Glass Envelope.....	58
3.2.4.5 Heat Transfers from Glass Envelope to the Atmosphere.....	59
3.2.4.6 Heat Transfer Through the HCE Support Bracket.....	62
3.2.4.7 Heat Transfers Occurred due to Other Pipes in ADU Solar Field.....	63
3.2.5 Performance Analysis of ADU Solar Field with EES.....	71
4 . RESULTS.....	77
5 . DISCUSSIONS.....	84
6 . CONCLUSION AND RECOMMENDATIONS.....	88
REFERENCES.....	90
APPENDICES.....	99
SCIENTIFIC ETHICAL STATEMENT.....	143

LIST OF SYMBOLS AND ABBREVIATIONS

ADU	: Aydın Adnan Menderes University
AISI	: American Iron and Steel Institute
ANI	: Aperture Normal Insolation
ANN	: Artificial Neural Network
CFD	: Computational Fluid Dynamics
CSP	: Concentrated Solar Power
CPV	: Concentrated Photo Voltaic
DI	: Deionized Water
DN	: Diameter Nominal
DNI	: Direct Normal Irradiance
EES	: Engineering Equation Solver
EU	: European Union
E-W	: East - West
FO	: Forward Osmosis
HCE	: Heat Collecting Element
HTF	: Heat Transfer Fluids
LPM	: Litters Per Minute
MED	: Multi Effect Distillation
NaCl	: Sodium Chloride
NPV	: Net Present Value
N-S	: North - South
ORC	: Organic Rankine Cycle
PTSC	: Parabolic Trough Solar Collectors

PVs	: Photovoltaics
RO	: Reverse Osmosis
SAM	: System Advisor Model
SCs	: Selective Coatings
SG	: Steam Generation
SODIS	: Solar Water Disinfection
UV	: Ultraviolet
α	: Solar Altitude Angle
A_{co}	: Glass Envelope Outer Area
$D_{pipe,outer}$: Outer Diameter of DN50 / DN80 Pipe
ϵ_{glass}	: Emissivity of Glass Envelope
$\dot{q}'_{other\ pipes}$: Amount of Heat Transfer Occurred in Other Pipes
h_{out}	: Convective Heat Transfer Coefficient from Glass Envelope Outer Surface to Ambient
$h_{rad,ge-atm}$: Radiative Heat Transfer Coefficient from Glass Envelope to Atmosphere
$\eta_{opt,env}$: Optical Efficiency of Glass Envelope
Pr	: Prandtl Number
Re	: Reynolds Number
U_L	: Overall Heat Loss Coefficient
v_6	: Wind Speed
\dot{Q}_s	: Solar Radiation Coming to Collector
$\dot{Q}_{u,exp}$: Experimental Useful Heat
θ_z	: Zenith Angle
δ	: Declination Angle

LIST OF FIGURES

Figure 1.1. The structure of the sun	3
Figure 1.2. The observed maximum ozone hole in Sep 2019.....	4
Figure 1.3. Solar energy distribution of Turkey	5
Figure 1.4. Solar energy potential atlas of Turkey.....	5
Figure 1.5. Solar collectors	6
Figure 1.5a. Solar tower	6
Figure 1.5b. Parabolic dish and linear fresnel collectors.....	6
Figure 1.5c. Linear fresnel collectors	6
Figure 1.6. PTSC	7
Figure 1.7. Schematic illustration of PTSC when oil is used as HTF	8
Figure 1.8. Schematic illustration of PTSC water oil is used as HTF	8
Figure 1.9. Industrial implementation classification	9
Figure 1.10. CSP diagrams	11
Figure 1.10a. Direct SG	11
Figure 1.10b. Indirect SG united with a combined cycle	11
Figure 1.11. Solar absorption.....	12
Figure 1.11a. Single effect.....	12
Figure 1.11b. Double effect.....	12
Figure 1.12. Solar adsorption diagram.....	12
Figure 1.13. Classification of seawater desalination	13
Figure 1.14. Diagram of desalination	14
Figure 1.14a. Phase changing	14

Figure 1.14b. Single phase	14
Figure 1.15. Solar assisted wastewater disinfection diagram	14
Figure 3.1. Geometrical errors in mirrors	27
Figure 3.2. Silvered mirror reflectors of PTSC at ADU Solar Field	28
Figure 3.3. Evacuated tube parabolic trough applications	29
Figure 3.4. Structural sections of PTSC at ADU Solar Field	30
Figure 3.4a. Brackets and main supports.....	30
Figure 3.4b. Frames	30
Figure 3.5. Flexible connectors of PTSC at ADU Solar Field	31
Figure 3.5a. Flexible hose.....	31
Figure 3.5b. Ball joints	31
Figure 3.6. Working of active trackers	32
Figure 3.6a. Closed loop.....	32
Figure 3.6b. Open loop	32
Figure 3.7. Monitoring methods	33
Figure 3.7a. North-South	33
Figure 3.7b. East-West	33
Figure 3.8. Beam transfer illustration of PTSC	34
Figure 3.9. 2D cross section view of PTSC with circular absorber.....	35
Figure 3.10. End effect and blocking of PTSC.....	39
Figure 3.11. Thermal modeling of HCE	42
Figure 3.12. Thermal network diagram of HCE.....	42
Figure 3.13. Collector placement in ADU Solar Field	44
Figure 3.14. ADU Solar Field.....	45

Figure 3.15. Panoramic view of ADU Solar Field	45
Figure 3.16. Inner and outer diameters of glass cover and absorber pipe	47
Figure 3.17. PTSC true energy input	49
Figure 3.18. Solar angles	50
Figure 3.19. The cross section of HCE	56
Figure 3.20. Support bracket of HCE at ADU Solar Field	62
Figure 3.21. The cross section of pipes	64
Figure 3.21a. DN50	64
Figure 3.21b. DN80	64
Figure 3.22. The oil inlet and outlet vertical pipes in 1 loop	65
Figure 3.23. First pipe	65
Figure 3.23a. Horizontal pipes in 1 loop	65
Figure 3.23b. Closed-up image.....	65
Figure 3.24. Other pipe next to the horizontal pipe	66
Figure 3.25. Bare-short elbow pipe	66
Figure 3.25a. 304L material	66
Figure 3.25b. Remote view.....	66
Figure 3.26. Flex pipe	67
Figure 3.26a. Rockwool.....	67
Figure 3.26b. Remote view.....	67
Figure 3.27. Short cylindrical pipes	68
Figure 3.28. Bare-long elbow pipe	68
Figure 3.29. The annular brackets	69
Figure 3.30. Long-cylindrical pipe	69

Figure 3.30a. Remote view	69
Figure 3.30b. Close-up image.....	69
Figure 3.31. Isolated-long elbow pipe	70
Figure 3.32. The T-shaped pipe	70
Figure 3.32a. Remote view	70
Figure 3.32b. Closed-up image.....	70
Figure 3.33. Pipe between two parallel rows	71
Figure 3.33a. J-shaped pipe	71
Figure 3.33b. Pipe at the end of it.....	71
Figure 3.34. Pipes above.....	71
Figure 3.34a. Between two rows	71
Figure 3.34b. Side pipes coming to building.....	71
Figure 3.34c. Other side pipes coming from other rows.....	71
Figure 3.35. Creating lookup table	73
Figure 3.36. Properties defined to lookup table	74
Figure 3.37. Defining of constant parameters.....	74
Figure 3.38. An example image of variable data input.....	75
Figure 3.39. Defining variable parameters	75
Figure 3.40. EES windows	76
Figure 3.40a. Creating new parametric table.....	76
Figure 3.40b. Solving table.....	76
Figure 3.41. Displaying results	76
Figure 4.1. Variation of average outlet temperatures with respect to date	77
Figure 4.2. Variation of modeled and experimental average outlet temperatures (ΔT).....	78

Figure 4.3. Variation of average collected energy with respect to date.....	78
Figure 4.4. Variation of average heat loss with respect to date	79
Figure 4.5. Variation of average thermal efficiency with respect to date.....	79
Figure 4.6. Variation of experimental inlet and outlet temperatures	80
Figure 4.7. Variation of optical efficiency with respect to date.....	80
Figure 4.8. Variation of inlet and outlet annual average temperatures	81
Figure 4.9. Variation of average annual heat gain	81
Figure 4.10. Variation of average annual thermal efficiency	82
Figure 4.11. Variation of average annual optical efficiency.....	82
Figure 4.12. Variation of average annual heat loss.....	83

LIST OF TABLES

Table 1.1. Industrial processes and their temperature range.....	9
Table 1.2. Pros and cons of PTSC for disinfection processes	14
Table 3.1. Selected parameters for optical efficiency.....	38
Table 3.2. Typical features of Therminol 54	46
Table 3.3. Specifications of PTSC located in ADU Solar Field.....	46
Table 3.4. Day number for each month	50
Table 3.5. C and m coefficients corresponding Re numbers range	60

ÖZET

PARABOLİK OLUKLU GÜNEŞ KOLLEKTÖRLERİNİN PERFORMANS ANALİZİ

Aktaş M. Aydın Adnan Menderes Üniversitesi, Fen Bilimleri Enstitüsü, Makine Mühendisliği Programı, Yüksek Lisans Tezi, Aydın, 2021.

Amaç: Bu tez çalışması ADÜ Merkez Kampüste bulunan parabolik oluk güneş sahasının verileri ile Mühendislik Denklem Çözücüsü (EES) programından elde edilen teorik verileri karşılaştırmak, ve sahanın çalıştığı Mayıs, Haziran, Ağustos ayları ve 2020 yılı için güneş sahasının ortalama ısı kazançlarını, kayıplarını, optik ve ısı verimlerini belirlemek amacıyla yapılmıştır.

Materyal ve Yöntem: ADÜ Parabolik Oluk Güneş Sahası analitik olarak modellenmiş, tüm hesaplamalar ve analizler sahanın tam gün çalıştığı günlere ait veriler kullanılarak gerçekleştirilmiştir. Teorik hesaplamalar ve sahanın genel performansını belirlemek için EES programı kullanılmıştır. Giriş değerleri olarak direk güneş ışınımı, rüzgar hızı, hava sıcaklığı ve ısı transfer sıvısı giriş sıcaklıkları, güneşin geliş açısı verileri EES'e tanımlanmış ve Mayıs, Haziran, Temmuz ayları için sistemin model doğrulaması yapılmış ve elde edilen grafik sonuçları incelenmiştir. Yıllık ortalama analizde ise 2020 yılına ait belirli aylar için ayda ortalama 1 gün göz önüne alınmış, ve bu günlere ait veriler EES'e tanımlanmış ve gerekli hesaplamalar gerçekleştirilmiştir.

Bulgular: EES'den elde edilen ortalama teorik değerlerin ortalama faydalı ısı için %4,54, ısı transfer sıvısı sıcaklık çıkış değerleri için %11,62, ısı kayıpları için %8,51, ısı verim için %4,38 lik farklarla gerçek değerlere yaklaştığı tespit edilmiştir.

Sonuç: Model doğrulama sonucu olarak Mayıs, Haziran, ve Ağustos ayları için ortalama hatanın %11,62 yi geçmediği, ve güneş sahasının ortalama 470,89 kW yararlı ısı ürettiği, ortalama %41,96 ısı verim ve %80,16 optik verimle çalıştığı saptanmıştır. Ayrıca, güneş

sahası yıllık ortalama %69,85 optik verim, %35,1 ortalama ısıl verim, 209,3 kW ortalama ısı kaybı, 323,93 kW ortalama ısı kazancı olarak performans göstermiştir.

Anahtar kelimeler: EES, Güneş Enerjisi, Parabolik Oluklu Güneş Kollektörleri

ABSTRACT

PERFORMANCE ANALYSIS OF PARABOLIC TROUGH SOLAR COLLECTORS

Aktaş M. Aydın Adnan Menderes University, Graduate School of Natural and Applied Sciences, Mechanical Engineering Program, Master Thesis, Aydın, 2021.

Objective: This thesis study was conducted to compare the data of parabolic trough solar field located in ADU Central Campus with the theoretical data obtained from the Engineering Equation Solver (EES) program, and to determine the average heat gains, losses, optical and thermal efficiencies of the solar field for the months of May, June, August and for the year 2020 in which the field operated full time.

Material and Methods: ADU Parabolic Trough Solar Field was analytically modeled, all calculations and analyses were carried out using data belong to the days in which the field operated full time. EES program was used to determine theoretical calculations and general performance of the field. Data of Direct Normal Insolation (DNI), wind speed, ambient temperature and inlet temperatures of heat transfer fluid (HTF), angle of incidence were introduced to EES program, and model validation of the system was performed and graphic results obtained were examined. Average 1 day in month was considered for the specific days belong to year 2020 in annual analysis, and data belong to these days were introduced to EES and needed calculations were performed.

Results: It was determined that the average theoretical values obtained from EES converged to actual values with the differences of 4,54% for the average useful heat; 11,62% for outlet temperatures; 8,51 % for heat losses; 4,38% for thermal efficiency.

Conclusion: As a result of model validation, it was determined that the average error did not exceed 11,62% for the months of May, June and August, and the solar field operated with an average useful heat of 470,89 kW, an average thermal efficiency of 41,96% and optical

efficiency of 80,16%. Moreover, the solar field was exhibited the performance as annual average optical efficiency of 69,85%, average thermal efficiency of 35,1%, average heat loss of 209,3 kW, average heat gain of 323,93 kW.

Keywords: EES, Solar Energy, Parabolic Trough Solar Collectors

1. INTRODUCTION

In today's world which develops day by day, energy consumption is increasing due to reasons such as rapid population growth, technological developments, industrialization and rising living standards. Therefore, this leads to an increase in the difference between energy production and consumption from day to day. Developed and developing countries are in an effort to increase energy production according to the amount of energy they consume in order to reduce this difference (Bakır, 2014).

On the one hand, energy resources are the most important problem of all countries in the world, on the other hand, efforts of countries to have energy deposits, to meet their energy needs and to control energy trade cause war in the world. The problems caused by the oil crisis that occurred in the 1970s, the fact that countries do not want to lose their power, the constant increase in trade volumes causes them to consume natural energy sources and therefore need new energy sources. For this reason, all countries have started to follow renewable energy sources closely by turning to inexhaustible, environmentally friendly and cheap energy sources using developing technology (Soylu, 2019).

There are eight renewable or alternative energy resources as tidal energy, geothermal energy, wave energy, solar energy, hydropower, biomass, wind energy, hydrogen energy.

Compared to other renewable resources, solar energy has the most usage area and is easily accesible (Cicibiyık, 2012). Heating, drying, obtaining hot water and cooking are the first applications of solar energy. Steam and electricity generation are also included in these application areas thanks to the developing technology. In particular, the work of obtaining electricity using solar energy was focused on, and electricity began to be produced thanks to steam obtained at high temperatures. Of course, it is possible to obtain electricity from steam and steam turbines at high temperatures. For this purpose, solar concentrating systems have been developed (Bakır, 2014). The reasons why these systems are used and preferred can be listed as follows (Atlıoğlu, 1991):

- Creating a more ergonomic and inexpensive collector.
- Achieving better collector efficiency by reducing the surface where heat losses occur.
- Obtaining higher temperatures with energy converted from solar energy.

Solar concentrating systems is divided into two as point concentrator and linear concentrator. Parabolic trough and fresnel mirrors are linear concentrators, dish collectors and solar towers are point concentrators.

Compared to other solar concentrating systems, PTSC has the most usage area (Demirci, 2015). PTSC consists of receiver or absorber tube, mirror material, bearing structure, HTF. First, rays coming from the sun hit the system's parabola shaped mirror. Then, this mirror concentrates the rays on the absorber or receiver tube located at the focal point of the parabola. At the end of this process, heat transfer occurs by transferring energy from absorber pipe, whose temperature rises, to the HTF passing through the pipe. The purpose of the system is to transmit the energy obtained from the sun to the heat transfer fluid with minimum loss.

The Sun is a star that is the source of life. This star consists of 73,46% hydrogen and 24,85% helium, 0,77% oxygen, 0,29% carbon, 0,16% iron, 0,12% neon, 0,12% nitrogen, 0,07% silicon, 0,05% magnesium, 0,04% sulfur. Although the size of the Sun star is very large compared to the earth, it is a medium-sized star compared to other stars in the universe. If there was no Sun, there would be no life on earth. The weight of the Sun, which is 330 thousand times heavier than the earth, is $1,9891 \times 10^{30}$ kilograms. With a diameter of 1.4 million kilometers, the sun is about 109 times the size of the earth and its density is $\frac{1}{4}$ of the World. It completes its rotation around its axis in about 90 days. The temperature of the sun increases towards its center, and this increase reaches up to 20 million degrees. The sun's radiation occurs at about 6000 K, and electrons that can not withstand this temperature leave the atomic nucleus. Therefore, in the sun, there are free electrons and atomic nuclei called plasma, while there are no atoms and molecules. The combination of 4 hydrogen nuclei to form 1 helium nucleus at a very high temperature is called fusion (thermonuclear reaction). The amount of hydrogen spent in the sun is more than the amount of helium formed. The difference between these two expresses the energy that occurs in the sun according to the theory of relativity put forward by Einstein. This energy is calculated utilizing $E = mc^2$, where m is mass (kg) and c is the speed of light (3×10^8 m/s). The amount of energy produced by the sun in 1 second is more than the total amount of energy people have used from the past to the present (Yiğit & Atmaca, 2018). The structure of the sun is shown in Fig. 1.1.

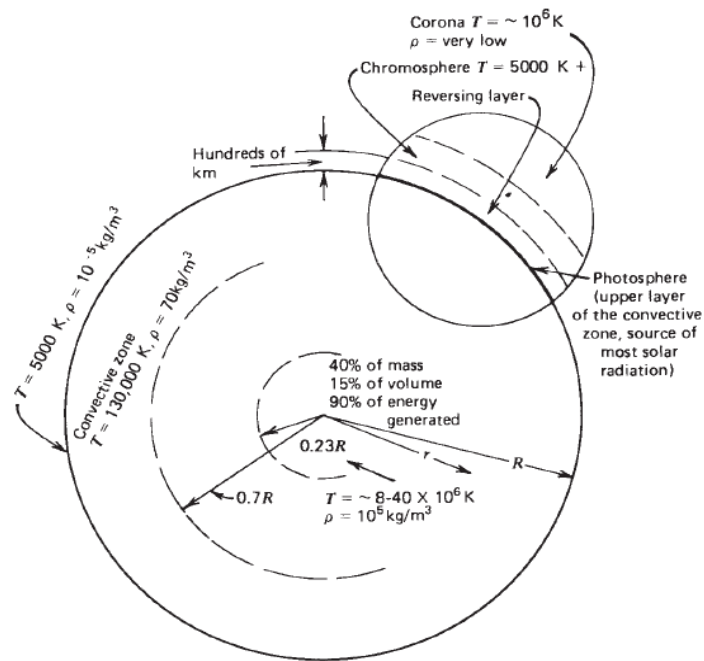


Figure 1.1. The structure of the Sun (Duffie & Beckman, 2013)

Not all rays from the sun reach the earth, more than half of them are reflected back from the atmosphere. 564 million tons of H is transformed into 560 million tons of He in 1 second in the sun, and a difference of 4 million tons is formed between them. This H difference first converts into energy and then reflects into space from the sun as a source of heat and light. The sun sends about 170 billion megawatts of radiant energy to the world. This energy corresponds to a very small fraction compared to the total energy produced in the sun. In addition, the total energy that people have used from the past to the present is 15-16 per thousand of this 170 billion megawatts of energy. Finally, to talk about ozone layer, ozone layer acts as a filter by keeping the burning and harmful rays coming from the sun about 22 kilometers above the earth and protecting living things from harmful UV rays. In recent years, the damage to the ozone layer has led people to panic, and the use of harmful substances that cause this damage has been restricted (Yiğit & Atmaca, 2018). The maximum ozone layer depletion recorded on 8 September 2019 is shown in Fig. 1.2.

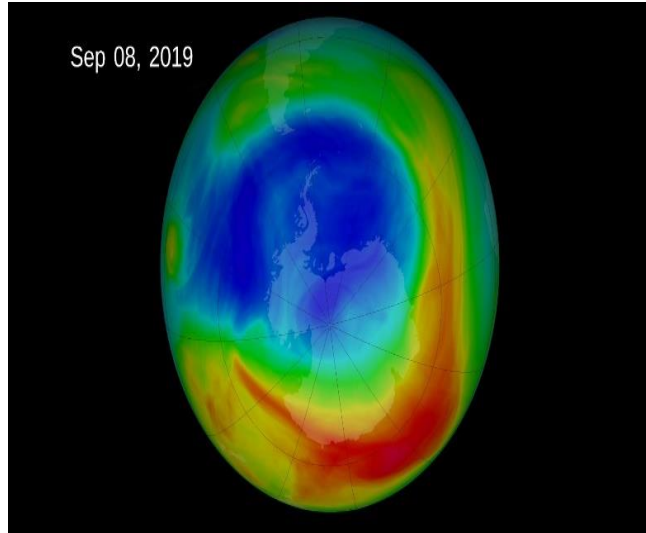


Figure 1.2. The observed maximum ozone hole in Sep 2019 (Nasa, 2019)

Before 2010, people in Turkey were getting hot water by using solar energy system on the roofs of houses and apartments where they were located. This means that solar energy is only used for one purpose in those years. However, in the following years, including 2010, studies on obtaining electricity using solar energy started and the first facility started to serve in 2014. In 2017, it was found that the power obtained from solar energy increased 50 times compared to previous years. Although the duration of enlightenment of our country and the radiation values from the sun are very large, the amount of power obtained from solar energy remains at a very small level with a value of 4,01% compared to other total amounts of power produced. Turkey is late in respect of obtaining electricity by using solar energy. But it is estimated that this low percentage value will be increased by making more production.

Considering the potential of solar energy, Turkey is lucky when compared to other countries due to its geographical location. The total average sunbathing time calculated for Turkey is 2740 hours per year and 7,5 hours per day. Daily sunbathing times decrease from summer to winter and increase again from winter to summer. The efficient solar capacity is 110 days for Turkey (Akusta, 2019). The General Directorate of Renewable Energy prepares a monthly solar energy potential atlas in order to show the distribution of solar energy from the daily values obtained for 12 months. Monthly sunbathing periods of Turkey for the year 2019 are shown in Fig. 1.3.

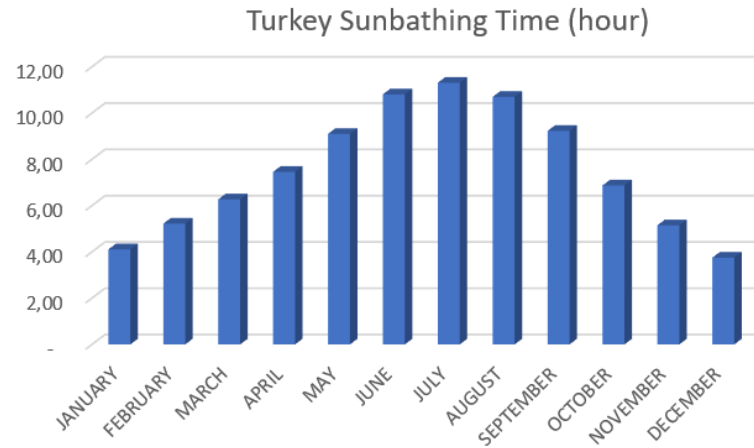


Figure 1.3. Solar energy distribution of Turkey in 2019 (data info: EİGM, 2019)

Given the atlas of the potential of solar energy in Turkey given in Fig. 1.4, it is seen that the potential of sunbathing increases from North to South. The least radiation is observed in the Black Sea region where the number of cloudy days is greater and, in contrast, the number of sunny days is less. Solar radiation levels are medium in Aegean and Marmara Regions, while maximum in Southeastern Anatolia and Mediterranean Regions. In addition, while the southeastern and Mediterranean regions benefit from solar energy efficiently for 12 months of the year, other regions benefit efficiently for approximately 8,5 months (Akusta, 2019).

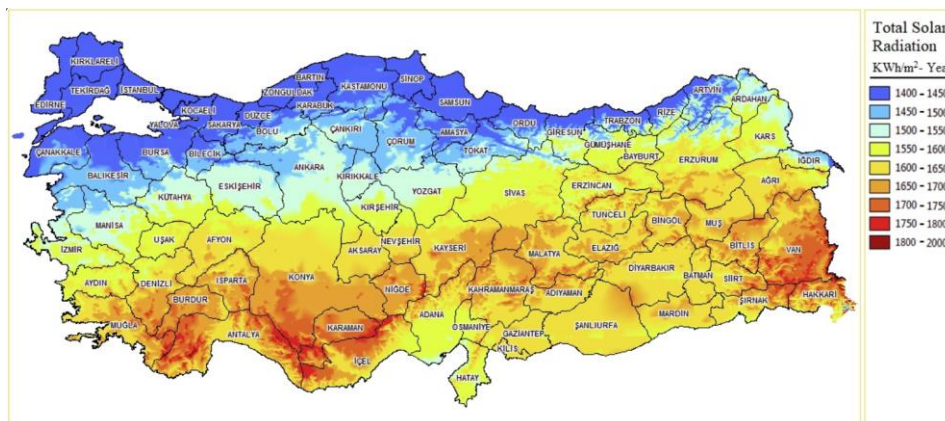


Figure 1.4. Solar energy potential atlas of Turkey (EİGM, 2019)

1.1. Solar Concentrators

Systems that concentrate the rays coming from the sun into a single point or region are called solar concentrating systems, and thus the temperature of the concentrated zone is increased. This concentrating system is performed in two ways as point and linear. Linear solar concentrating systems are combined parabolic concentrators, parabolic trough concentrators, planar concentrators with plane reflectors, linear-fresnel intensifiers, while parabolic dish concentrators and solar towers are point solar concentrators. Some of them are shown in Fig. 1.5.

In this study, parabolic trough solar collector which is main topic of the thesis will be investigated in detail.

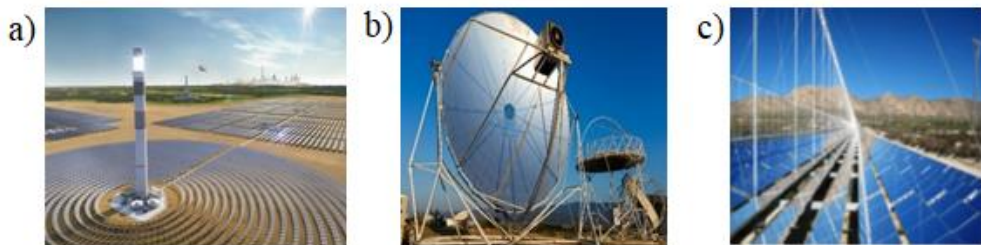


Figure 1.5. Solar collectors: Solar tower (a)(CR, 2020); parabolic dish (b) (DLR, 2011); and linear fresnel collectors (c) (Heller, 2017)

1.2. PTSC

PTSC's are in the first place when compared to other solar concentrator systems (Şanlı, 2010). Thanks for this system it is possible to reach high temperatures. PTSC system basically composed of a parabolic trough shaped surface (mirror) which reflects and concentrates direct solar radiation coming from the Sun to the receiver or absorber tube located in the focal line of the parabola and glass cover on this, tracking mechanism, HTF passing through absorber pipe and bearing structures carrying the system. The detailed information about all these components will be given in chapter 3. Typical PTSC is shown in Fig. 1.6.

The working principle of PTSC is briefly, first, the solar radiation coming from the sun hits the parabolic shape reflective surface. This parabolic mirror concentrates the sun rays to the absorber tube locating in the focal line of parabola and extends through parabola. Thus,

heat energy is transferred from absorber tube to fluid passing in it and temperature of fluid is increased.



Figure 1.6. PTSC (Sbp, 2012)

The pros and cons of PTSC are as follows (Solorio et al., 2020):

- Low environmental emissions during working,
- Lower maintenance and working costs,
- Long life span
- Utilizing inexhaustable solar energy as resource,
- Requiring large installation area because of diffuse solar radiation,
- High initial capital goods (investment) and medium
- Long term recovery
- Intermittance of the solar resource (be unavailable on cloudy days- nights)

It is possible to produce electricity and steam by this fluid whose temperature boosted. When the oil is utilized as heat transfer fluid, steam or electricity is generated. In this process, heated oil coming from the parabolic system transfers its heat energy to the water whose temperature is lower. This energy transfer process is realized in the heat exchanger and thus water is evaporated. Afterwards, electricity is generated by sending this water, which is in steam phase, to the steam turbine. It is shown in Fig. 1.7. On the other hand, when water is utilized as heat transfer fluid, steam is obtained by condenser, then it is sent to steam turbine to produce electricity. No heat exchanger is needed in this process (Şanlı, 2010). It is shown in Fig. 1.8.

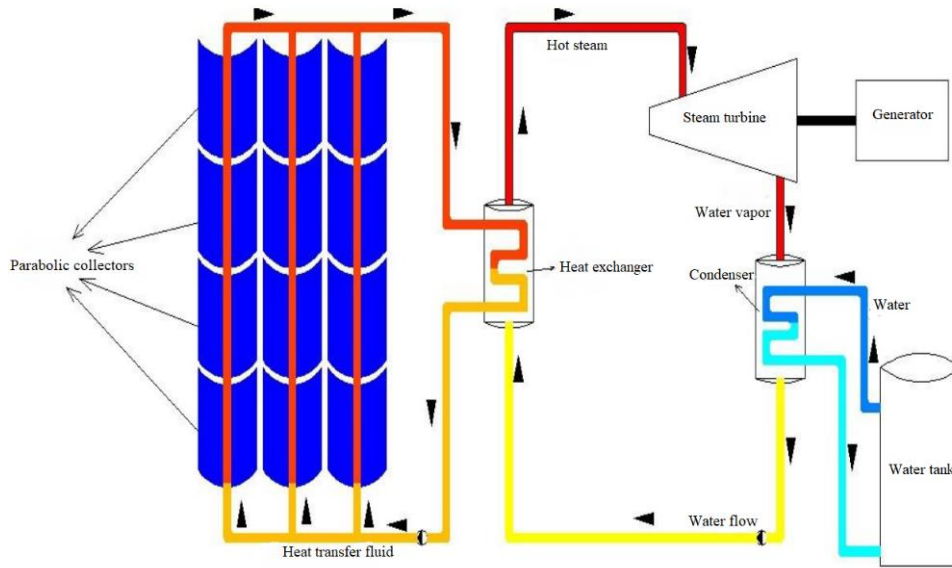


Figure 1.7. Schematic illustration of PTSC when oil is used as HTF (Şanlı, 2010)

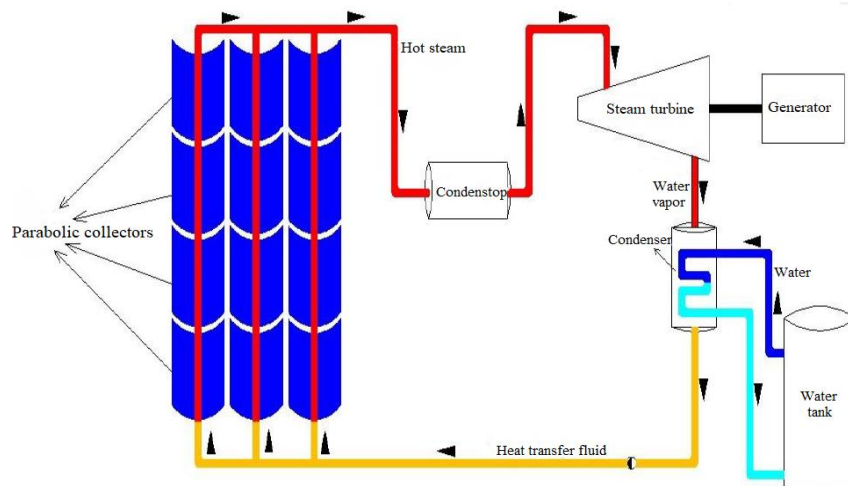


Figure 1.8. Schematic illustration of PTSC when water is used as HTF (Şanlı, 2010)

The purpose of the parabolic trough system is to transmit the energy obtained from the sun to the heat transfer fluid with minimum loss. Detailed information of each component of PTSC will be given in chapter 3.

1.3. Industrial Usage Area of PTSC

PTSC are employed in diverse branch of industries and it is classified into three as shown in Fig. 1.9. The accumulated heat is employed in cooling and heating applications in industry and commercial sectors. However, PVs are still developing.

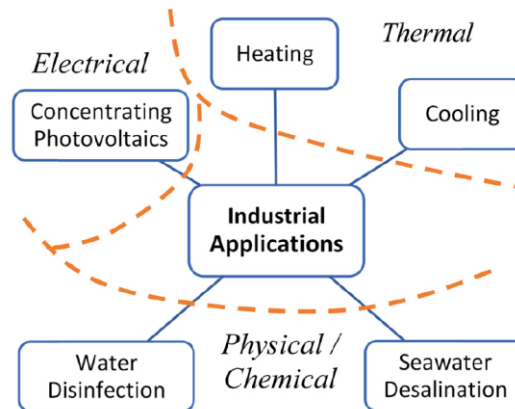


Figure 1.9. Industrial implementation classification (Solorio et al., 2020)

If it is needed to give information about a few of them, in the heating process of industry, the energy is transferred to HTF by solar collector. The main purpose of PTSC is heating the working fluid. Heating implementations may be classified into two depending upon the temperature gained by the HTF. Temperatures up to max 100 °C are for low-temperature implementations, up to 400 °C are for medium-temperature implementations. SG and CSP systems are main execution of medium-temperature PTSC systems. Low-temperature PTSC systems are usually employed in pre-heating and drying processes in industrial, commercial and residential sectors (Solorio et al., 2020). Industrial processes and temperature range of these are listed in Table 1.1.

Table 1.1 Industrial processes and their temperature range (Solorio et al., 2020)

Industry	Process	Temperature (°C)
Dairy	Pressurization	60-80
	Sterilization	100-120
	Drying	12-180
	Bolier feed water	60-90
Bricks and blocks	Curing	60-140

Table 1.1. Industrial processes and their temperature range (continued)

Plastics	Preparation	120-140
	Distillation	140-150
	Seperation	200-220
	Extension	140-160
	Drying	180-200
	Blending	120-140
Chemical	Soaps	200-260
	Synthetic rubber	150-200
	Processing heat	120-180
	Pre-heating water	60-90
Paper	Cooking, drying	60-80
	Boiled feed water	60-90
	Bleaching	130-150
Heating of buildings	-	25-75
Desalination	-	100-250
Power cycles (Rankine)	Vapor generation	300-400
	Phase-change materials	300-375
Others	General steam generation	130-210

CSP is the most suitable execution so as to generate electricity. To carry out this, it employs solar assisted turbines or integrated systems with combined cycles, generally with a thermal storage block. Direct or indirect SG, which are the most rampant method in the world, are employed to generate electricity with PTSC. In these systems, steams are generated to actuate a turbine by direct heating or indirect heating. Direct heating process uses water as HTF of PTSC. Indirect heating uses oil as HTF and this heat is transmitted to water in heat exchanger. Schematic diagram of this direct and indirect SG are shown in Fig. 1.10, Fig. (a) represents CSP plant with direct SG while (b) represents indirect SG united to a combined cycle, and thermal storage block indicated in (a) and (b) boosts the productivity and the capacity factor, thus, it is feasible to produce electricity even if in the night time or cloudy days (Solorio et al., 2020).

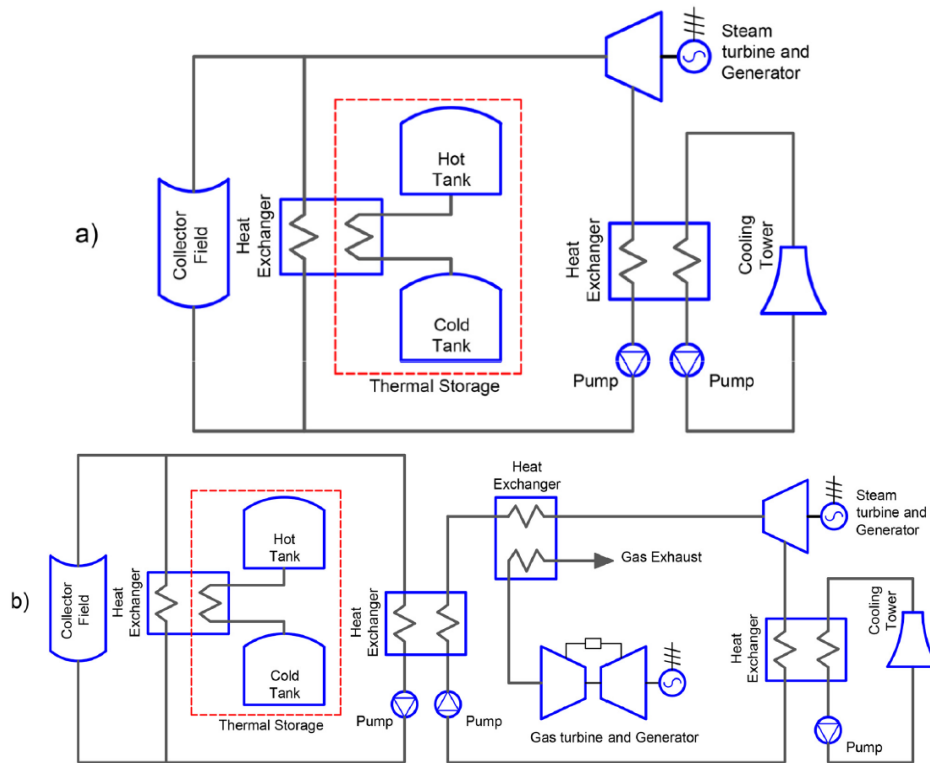


Figure 1.10. CSP diagrams: (a) direct SG, (b) indirect SG united with a combined cycle (Solorio et al., 2020)

Cooling is also one of the application areas of PTSC. Solar cooling means that it employs solar radiation as thermal energy resource so as to cool a fluid, space. There are two basic solar cooling process: Absorption and adsorption. Both of them thermal compressor will be used instead of mechanical compressor. The absorption is widely employed method for solar cooling process by using PTSC. In this method, fluid-fluid mixture (working pair) is utilized as the refrigerant. The fluids that make up the working pair create a forceful solution when stirred at a low temperatures, and also may be set apart when the mixture is heated. The dissolved substance is transformed into a gas and the dissolvent remains in liquid phase when the mixture is heated. Single and double effect cycles are the most widespread processes for absorption cooling. These single and double absorption cycles is shown in Fig. 1.11. Lithium bromide and water ammonia are usually employed as working mixture in solar absorption systems. Solar adsorption cooling is utterly diverse from the solar absorption. Because working mixture of adsorption is solid-fluid combination. Adsorption cycle need to almost no electrical or mechanical input, however needs thermal input from the collector. Adsorption cycle works intermittently, not continuously. The diagram of solar assisted adsorption system is shown in Fig. 1.12. Flat plates and evacuated tubes may be given as examples of the

technologies most commonly used in solar adsorption cooling processes. The most frequently employed adsorbent materials are zeolite, activated carbon and silica gel, and the most frequently employed refrigerants are methanol, ammonia and water. The general advantage of solar cooling is having lower energy depletion when compared to traditional vapor-compressor systems (Solorio et al., 2020).

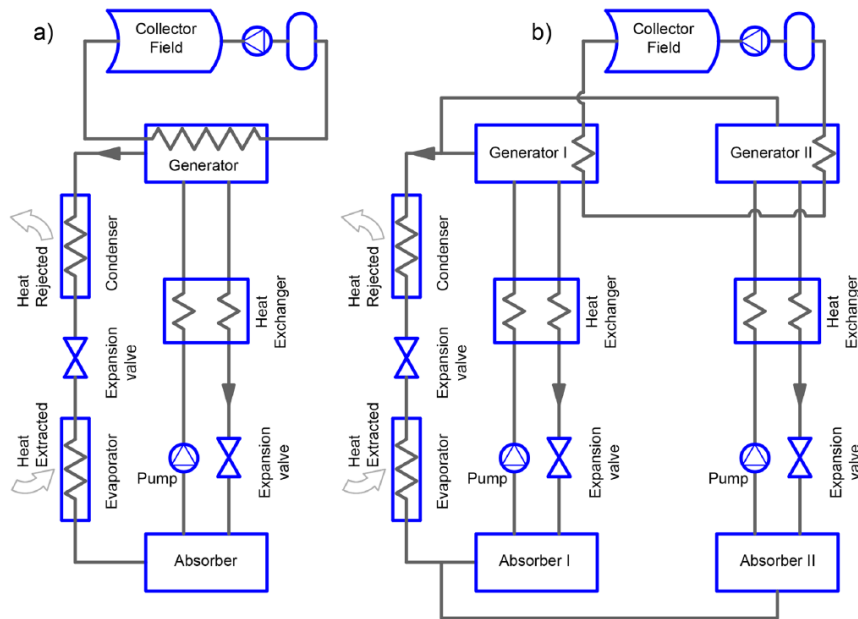


Figure 1.11. Solar absorption: (a) single effect, (b) double effect (Solorio et al., 2020)

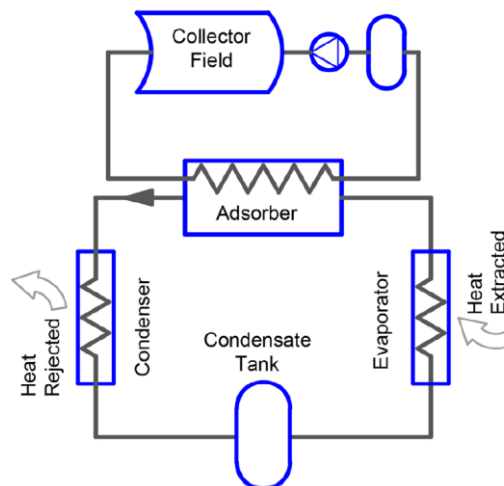


Figure 1.12. Solar adsorption diagram (Solorio et al., 2020)

Another usage area of PTSC is desalination of sea-water. If it is needed to explain the meaning of sea-water desalination, it is a process in which minerals are separated from seawater so as to obtain fresh water. There are many methods employed for separating salts from sea-water in industry (Solorio et al., 2020), and these methods are divided into four as described in Fig. 1.13.

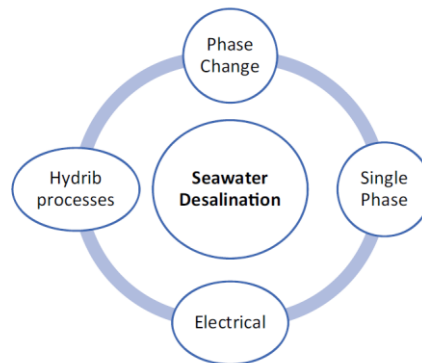


Figure 1.13. Classification of seawater desalination (Solorio et al., 2020)

Thermal processes, in other words phase change, employ thermal energy so as to separate salty water (brine). Multisalt and MED may be shown as the most widely utilized method. Mechanical separation is employed in single phase processes, here, seawater is passed through filter membranes where salts are captured. The most widely employed methods are RO and FO. Electric processes depend upon anionic and cationic ion-exchange effects. In this electrolysis process, anode and cathode membranes are adjusted by turns, then subjected to an electric field, thus, particles are captured throughout the process and dissociated from seawater. Electro-dialysis, ion exchange and capacitive deionization methods are main methods of electrical processes. Phase change is mixed with single phase process like membrane distillation method in hybrid processes. Salty (brine) and fresh water are dissociated through heating seawater in thermal processes and it is shown in Fig. 1.14 (a). Seawater is heated, thus, water is evaporated and water is separated from salt due to seawater has lower boiling point. The water steam then intensifies, leaving fresh water. The requiring electrical energy so as to pressurize the seawater and pump it through the membrane is ensured by rankine cycle (Solorio et al., 2020). It is shown in Fig. 1.14 (b).

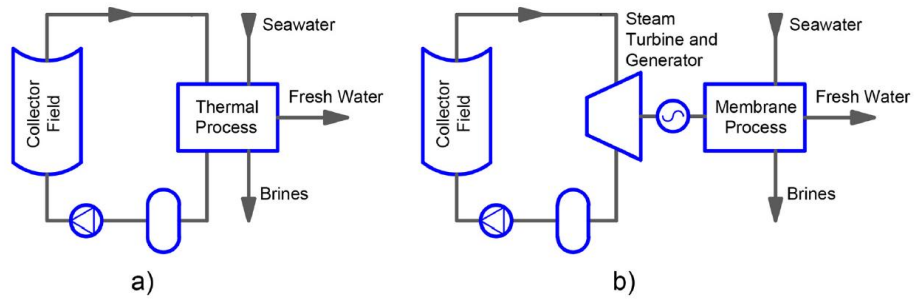


Figure 1.14. Diagram of desalination: (a) phase changing, (b) single phase (Solorio et al., 2020)

Another usage areas of PTSC is SODIS and CPV generation. The solar assisted waste water disinfection diagram is shown in Fig. 1.15.

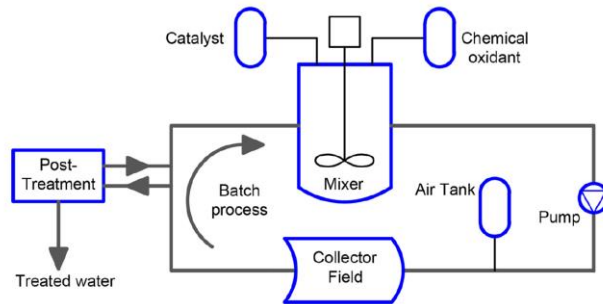


Figure 1.15. Solar assisted wastewater disinfection diagram(Solorio et al., 2020)

The pros and cons of PTSC for water decontamination are as in Table 1.2:

Table 1.2 Pros and cons of PTSC for disinfection processes (Solorio et al., 2020)

Advantages	Disadvantages
Smaller size of reactors	It needs direct solar beam radiation
High volumetric flow (turbulent)	High costs
Better mass transfer	Low water
Low catalyst load	Low water overheating
No vaporization of compounds	Low quantum productivity

1.4. PTSC Applications in Turkey

PTSC is not widely employed in Turkey. Several applications of PTSC are as follows:

- Aydın Adnan Menderes University Central Campus
- Denizli Kızıldere Facility, Pilot Project (Livatyalı, 2011)
- METU Cyprus Campus (Livatyalı, 2011)

2. LITERATURE REVIEW

Yahi et al. (2020) performed modelling and exergetic analysis of PTSC. The detailed study about PTSC taking into account heat exchange mechanisms were done. A novel computation code was developed in Matlab, and analytical model was proposed. Syltherm 800 was utilized as HTF. The results showed that exergy efficiency was directly proportional to the HTF inlet temperature and DNI, inversely proportional to the mass flow rate and ambient temperature.

Abed et al. (2020) studied the corresponding effect of HTF exchange on the thermal and hydraulic performances of PTSC. In study, three types of pure fluids were used; water, Therminol VP-1 and molten salt. After performance of each fluids was appraised, general thermal productivity of PTC system was analyzed. Results verified that changing the working fluid in solar collector increases the overall heat transfer thereby developing thermal productivity.

Vijayan and Rajasekaran (2020) performed the performance assessment of nanofluid on parabolic trough solar collector. The solar collector was enhanced using effortless and locally obtainable materials. In study, aluminum oxide (Al_2O_3) and DI was utilized as HTF in five different concentrations. Experiments were performed at between 8:00-16:00 in everyday to compare the performance of these two fluidics. The results showed that maximum productivity observed at noon was 60.41% for DI, 60,49% for 2,5% concentration of Al_2O_3 at noon, and the productivity improvement was 3,90% than DI.

Bellos and Tzivanidis (2020) studied diverse polynomial expressions for thermal efficiency of PTSC. In study, LS-2 PTC module was investigated with a enhanced numerical model in EES under diverse operating temperatures and solar beam. Then this model was verified utilizing experimental data existing in literature.

Arslan et al. (2019) performed study on the utilizing of PTSC in Isparta Organized Industrial Zone. In study, collector with 67% productivity and 30 m² module length, water as HTF were utilized. Land area, cost analysis and the number of collectors required to reach the desired 10000 MW power were calculated. At the end of study, it were determined that the

number of collector as 500, land area as 200.000 m², total investment of turbine and parabolic system as 30.405.000 TL, annual revenue as 5.570.000 TL.

Alamlı (2019) designed 2m wide, 2m length PTSC, then investigated its efficiency as experimentally and theoretically. Excel program was used to calculate useful energy coming to the solar collector. At the end of study, it was detected that maximum energy and efficiency theoretically were 880 W/collector and 63% maximum energy and efficiency experimentally were 835 W/ collector and 57% respectively.

Kılıç (2019) studied Artificial Neural Network ANN-based optimization of PTSC taking into account Bilecik city conditions. In system, Therminol-VP1 as HTF, melt salt as thermal storage material, five diverse cooling fluidics (R-134a, R-141b, R-600a, R-236ea, R-1234ze) working in ORC cycle were utilized. Diverse temperature and pressure were detected for each fluidics. Then energy, exergy and Net Present Value (NPV) analysis were performed. At the end of optimization, the results showed that energy productivity, exergy and obtainable energy from the system were 32,8%, 41,9% and 186,9 MWh respectively. In addition to this, NPV value of the PTSC was found positive, that means system was suitable to the investment.

Bilgin (2019) designed and setup PTSC to calculate useful energy, heat loss, thermal and optical productivity and to measure the temperatures of inlet and outlet. In study, Renolin Therm 320 as HTF, polished aluminum sheet as reflector, Tanpera's TDB 160/10 dual coil boiler tank as heat storage and heat exchanger, K-type thermocouple for the flow measurement, ASTM A160 GR. B seamless carbon steel pipe for piping the oil cycle was utilized. At the end of study, maximum temperature of 65,25 °C at 14:20, maximum productivity of 14,5% at 15:30 was found. Furthermore, transition and turbulent flow was observed in the receiver while temperature was 60 °C.

Quezada-García et al. (2019) worked on reduced-order mathematical model of PTSC in which radial and axial temperature dispersial is obtained to compute heat transfer. Thermal oil, water and nanofluid was utilized as different fluidics. The model was resolved using Phyton software and used OpenGL to create schematic visuality. As a result, higher thermal efficiency was observed in the collector used in nanofluid as 80% and 79% for volume fraction of 0,04 and 0,02 respectively.

Sahoo et al. (2019) performed CFD work on parabolic trough solar collector by changing HTF input temperature and wind speed parameters over the glass cover. Analysis of the collector's receiver performance, environmental temperature distribution on the absorber tube and glass cover was performed by calculating the temperature increase and pressure drop in HTF. It was concluded that the environmental temperature difference is largely depend upon inlet temperature of HTF.

Dündar (2019) studied the mathematical modelling of the parabolic concentrating collector-reflective surface. In the study, an unknown curve in the perpendicular coordinate plane, the physical properties of sunlight, the geometry of the system were used, the nonlinear differential equation was derived and solved, the equation of the parabolic curve was found analytically.

İşler (2018) studied energy production analysis and implementations of PTSC and solar power tower. In study, PTSC and solar towers with central receiver were examined in detail, implementations of these systems were realized as hybrid and alone for Bilecik region. SAM program was utilized to perform solar power tower- PTSC analysis separately and then annual producible amount of energy when these systems were utilized as hybrid were determined. On SAM program, Average insolation time as 2320 hours, annual global horizontal solar radiation as 1361,45 kWh/m², direct radiation as 920 W/m² were calculated. According to SAM results, it was detected that Bilecik had crucial solar energy potential, and total efficiency was calculated as 18% when this two systems were run together.

Ullah and Min (2018) studied performance evaluation of dual-axis tracking system of parabolic trough solar collector. The solar collector with 24 concentration ratio was improved and impacts of single and dual axis monitoring modes on the optical performance were scrutinized, thermal performance of collector was determined 0,813% experimentally and annual average value was 14,3% The results demonstrated that annual average value was higher than 14,3% and 40,9% East-West and North-South tracking modes respectively.

Prakash and Rai (2018) tried to boost the performance and heat transfer features of PTSC using Taguchi method. Water was selected as working fluid and Cu, Al, GI selected as material of absorber while experimental examination performing. Mass flow rate, absorber tube and its material was taken into account during the study. The results of experiments was optimized using MINITAB 17. The results showed that when Cu was utilized as a material

useful heat was maximum at mass flow rate of 0,001756 kg/sec, at diameter of absorber tube of 0,026 m. Furthermore, it is found that outlet temperature of water was maximum at diameter of absorber of 0,030 m.

Singh and Mishra (2018) studied performance analysis of PTSC combined supercritical SCO_2 and ORC. In study, energy and exergy analysis was performed. SCO_2 and ORC was utilized to obtain power. R134a, R1234yf, R407c, R1234ze and R245fa was used as organic working fluid for ORC. It was observed that R407c combined cycle maximum exergetic productivity of 78,07 at 0,95 kW/m^2 , had maximum thermal productivity of 43,49% at 0,95 kW/m^2 . It was deduced that this combined cycle had a 3740 kW maximum output while minimum depletion ratio was 0,2583.

Kolekar and Patil (2018) studied the performance analysis of PTSC utilizing diverse volume concentration of Al_2O_3 nano-fluid with water. It was aimed to boost thermal productivity of system. Increasing in thermal performance of the system was observed from 63,52% to 73,12% when 0,5% of Al_2O_3 nano-fluid dissolved in water. Based on this, it was concluded that nanofluid boosted the thermal performance of PTSC at around 10%.

Mohd et al. (2017) performed designing, constructing and performance assessment of PTSC for hot water generation. In experimental setup, Acrylic Mirror was utilized as reflecting mirror in 2 m long, 1,22 m wide, 0,32 mm thickness, and absorber pipe in 2,12 m length was placed to system. Performance of the system was investigated one full day in April. At 12:30 PM, maximum solar intensity, maximum outlet temperature were obtained as 1200 W/m^2 and 59,9 °C respectively. As a result, it was understood that the PTSC was better alternative to diminish the water heating cost.

Kumar et al. (2017) investigated performance assessment of PTSC adhering to mathematical analysis of diverse parameters. Mathematical expressions was improved using C++ program to simulate the consequence of performance appraisal. According to results of simulation; heat removal factor, alteration of efficiency was studied. Outlet fluid temperature was examined as a function of mass flow rate for constant value of radiative and thermal loss parameters, and effects of this parameters for modification of the diverse of outlet and inlet fluid temperatures versus dimensionless insolation.

Murtuza et al. (2017) studied the performance of a designed 5m length PTSC. Working fluid and heat collecting element were selected as water and stainless steel respectively. The

experiments were performed at various flow rates of 0,4; 0,8; 1,2 LPM, then Reynolds number corresponding to these was calculated. The better outlet temperature was obtained March to May. The experimental results showed that liquid flow was laminar while February to May exhibited good outlet and surface temperature when compared with other months.

Ihsan et al. (2016) evaluated the performance of PTSC using diverse heat transfer fluids. In study, water and SAE 20 W50 engine oil was utilized as circulating fluid, then new and only slightly PTSC enhanced to carry out the experiment. It was concluded that performance productivity of solar collector using water had higher than SAE 20 W50 engine oil.

Liang et al. (2017) analyzed annual performance of PTSC. In study, a transient heat transfer model was created. With a homemade code, the dynamic performance of solar collector was simulated for three distinct solar tracking systems in diverse climatic zones, considering the building thermal design and solar power distribution in China. As a result, it was understood that the difference in annual collector productivity for different climates was indiscernible.

Boukelia et al. (2016) studied the performance simulation of PTSC, and used two different fluidics as thermic oil–molten solar salt. The performance evaluation was done in June and December. In these months, maximum total performance of system was observed as 67% (June) and %48 (Dec) for thermic oil, and 63% (June) and 44% (Dec) for molten solar salt. It was concluded that thermic oil performs more than molten solar salt.

Kumbhar et al. (2016) performed the performance of PTSC unified with thermal energy storing system. At the end of study, it is deduced that implementing latent thermal energy storing system to PTSC boosts the system productivity by 17% at mass flow rate of 0,0044 kg/sec, and higher temperature incrementation was observed at this mass flow rate. Furthermore, this storage system gave the needed performance though at low solar radiation intensiveness after sunset.

Çakıcı (2016) studied thermal modelling of a geothermal powered supercritical ORC combined with PTSC. In study, detailed thermal models were enhanced for PTSC and heat exchanger. The performance assessment of the system was carried out utilizing each components of ORC and PTSC. The equations that make up the thermal model was solved in EES. The results of modelling were compared with data obtained from geothermal power plant. Then, the verification were performed for modeling. Later, effects of including PTSC to

the system on various parameters was examined. At the end of these parametric studies, operating parameters and working fluid exhibiting the best performance were detected for combined system.

Bhutka et al. (2016) studied modelling of solar thermal power plants utilizing PTSC. In study, design of 1 MW operational power plant located at Gurgaon was changed and redesigned marginally using PTSC. The results obtained were compared with 50 MW power plant at Rajatshan and 1 MW power plant at Gurgaon. As a result it was seen that result of comparison intimately matched with 3,1% deviation for Gurgaon while 3,6% for Rajatshan plants respectively.

Ersöz (2016) studied design, construction of PTSC for torrefaction process and determining optimum operating conditions for diverse biomass. In study, Three types of biomass (cotton shank, pine chips and chicken waste), two types of reactor (glass and metal), two diverse selective coating (matte selective paint and copper selective surface) were utilized. Characteristic of biocoal obtained from these biomass were assessed. At the end, the optical productivity were found as 0,73, metal reactor with copper selective surface was the most effective receiver when compared with others.

Hayta (2015) examined thermal performance network of PTSC theoretically and experimentally. Numeric calculations were carried out using EES. Experimental tests were realized in summer season in Gaziantep. Renolin therm 320 was used as working fluid and productivity tests were performed at different temperature changing & flow. At the end of tests, optical productivity of PTSC network was obtained at around 55% while thermal productivity 56%.

Ramesh et al. (2015) designed and manufactured PTSC for water heater, then investigated the performance analysis of the system. Copper was utilized as receiver tube material The study was carried out at 1, 2, 9, 11 and 13 of March. At the end of experimental study, it was observed high temperature as 103 °C, lowest temperature as 40 °C, high thermal efficiency as 98% in sunny day, thermal efficiency in mid-noon as 63%, highest heat gain in sunny day as 1500 W and lowest heat gain in rainy day as 450 W.

Behar et al. (2015) developed a new PTSC model and validated it, and compared experimental data with theoretical results obtained from EES. Vacuum tube HCE, Syltherm 800 oil HTF, and cermet coating were utilized in the study. They concluded that their model

predicted the thermal efficiency more accurately than EES. The differences were calculated as 0,64% for model, 1,11% for EES.

Akba (2014) carried out the parametric study, transient simulations and enhancing the mathematical modelling of PTSC field with two tank molten salt thermal energy storage. Model was built in TRNSYS and utilizing Matlab new valf, thermal energy control algorithm was included to the system. Optimal length of PTSC was calculated to demonstrate the relevance between DNI and collector length. At the end of parametric study, the situation with maximum solar fraction was chosen, and general behaviour was observed. Impact of thermal energy storing to the energy obtained from collector field was argued. Afterwards, alteration in optimal thermal power plant dimensions of thermal energy storing was monitored.

Bakır (2014) studied designing, manufacturing and performance of PTSC for preparing hot water. In study, the collector was manufactured taking into account Karabük weather condition. During 7 days, the performance of the system was observed at 40, 50, 60, 70, 80, 90 and 100 degrees respectively. At the end of experiment, 66,8% of thermal efficiency was obtained at noon and 100 °C. Furthermore, max average thermal efficiency was obtained as 61,3% at 100 °C. It was deduced that energy efficiency and water outlet temperature was directly proportional to the set temperature values, and total mass of water accumulated in tank was inversely proportional to set temperature values.

Ghoneim (2014) improved a numerical model to investigate various effect of characteristic properties and working conditions on the performance of PTSC in Kuwait. In this model, the equations of convective heat transfer losses was examined and new equations derived and utilized. Environmental effect of solar heating and cooling systems was examined considering Kuwait climate conditions. Obtained results showed that convection loss among the absorber tube and support elements was highest according to radiation and conduction.

Ercoşkun (2013) manufactured PTSC and carried out experiment in Tarsus to observe thermal performance of the system in different date. A reflector that has 103 x 200 cm² surface area and 3 mm thick was utilized in experiment. According to experimental results it was detected that daily average productivity value of 32%, the highest productivity value was reached at 11:00 and 13:00 for these days. The highest and lowest productivity of the system was observed as 47,1% in 24 August, 36,5% at noon respectively, Furthermore, the lowest efficiency value remained above average efficiency.

Ghasemi et al. (2013) examined heat transfer characteristics of parabolic trough solar collector with two segmental rings numerically and impact of remoteness amongst porous this two segmental rings was investigated. In study, Therminol 66 was selected as HTF and model was figured out by RNG k- ϵ turbulent model using CFD. Results of numerical simulation showed that the utilization of two segmental rings in tubular solar absorber boosted the heat transfer feature of PTSC

Şimşek (2012) carried out PTSC designing, manufacturing, testing, and the use of heating in rural region. In experiment, three types of working fluid was utilized: purified water, mixture of purified water with 50% volume concentration of Antifreeze (ethylene glycol), mixture of purified water with 20% mass concentration of NaCl. The experiments were made for 18 days between 10:00-15:00 in sunny days of July 2011. At the end of study, experimental results obtained were compared with theoretical calculations.

Cicibiyık (2012) studied parabolic trough solar collector. Glass cover, reflective surface and absorbent tube of the system were designed for thermal experiments. Optical and thermal efficiency, useful energy transferred to the heat transfer fluid were calculated. With this useful energy, electricity generation simulation in ORC, exergy and thermodynamic analysis of ORC were performed. 1st and 2nd law of efficiency was found as 9% and 45% respectively As a result of the experiment, the average optical, average thermal efficiency, glass cover optical efficiency of the system was calculated as 20%, 85% and 25% respectively. Furthermore, net power output of steam turbine was calculated 50 W.

Akkoç (2012) examined collectors combined with parabolic concentrators. The aim of this study is to design a collector and then perform the mathematical model, experiment, performance analysis and simulation studies of the system and try to verify the mathematical model by comparing the obtained data with the simulation values. It was concluded that the system works correctly, but the optical efficiency and mathematical model should be developed.

Şanlı (2010) studied the theoretical examination of PTSC that utilized steam and steam turbine for electricity generation. In study, absorber tube, glass cover, reflective part and solar tracking mechanism of the system were investigated in detail. Parabolic system was designed theoretically, and tests were performed based 2009-2010 solar data in Denizli. It was deduced

from test results that the efficiency of the system up to steam turbine was 67% and the required capacity of steam turbine to the system was between 300-500 kW.

2.1. Objective of Thesis and Outlines

A thesis study is going to be performed to determine the overall efficiency of PTSC located in Aydın Adnan Menderes University Central Campus and constructed within the scope of the EU Project to meet electrical energy, domestic hot water, and chilled water needs of ADU Hospital, the optical and thermal losses, the parameters that affect the performance, and to verify the applied analysis processes. To obtain experimental data, calculations will be made according to measurements in the solar field located in central campus. Energy analysis will be made based on the DNI coming to the collectors in the solar field, inlet temperature of HTF, wind speed, ambient temperature, and angle of incidence. The necessary data will be defined to the EES program and the theoretical results obtained are compared with the experimental results and the percentage error values are determined. By evaluating the results and making new comments, the purpose of the thesis is achieved and it is considered that an important contribution has been made.

The outline of the thesis: In 3rd chapter, detailed information about PTSC, thermal and optical modeling of collector, method of performance analysis with EES, description of ADU Solar Field, are presented. In 4th chapter, comparison of theoretical and experimental data, and annual performance of the field are presented. In 5th chapter, discussion about the graphics obtained from EES and actual data are presented. In 6th chapter, result studies and recommendation for the future studies are presented.

3. MATERIAL AND METHOD

3.1. Material

In this part, detailed information about components PTSC, optical model and geometry of PTSC will be given.

3.1.1. Components of PTSC

The PTSC basically consists of mirror reflectors, HCE, absorber tube and HTF passing inside it, supporting structures, and control-tracking system. All these components will be investigated in detailed under this title.

3.1.1.1. Mirror Reflectors

The mirrors used in parabolic trough collectors reflect the rays coming from the sun to the absorber/ receiver tube and concentrate there. These mirrors are manufactured from layers of highly reflective materials such as aluminum or silver and protective material layers to prevent wear and corrosion. Silvered glass mirror, anodized sheet aluminum, aluminized polymer and silvered polymer films are the most use as a material (Salazar, 2018). When compared with others, it is most encountered with silvered glass mirror in parabolic systems (Günther et al., 2011). Ideal solar reflector must include the following features (Solar Energy Research Institute, 1985):

- High optical performance (i.e. reflectance, transmittance, specularity, geometrical configuration etc.),
- Low maintenance (i.e. dust free),
- Low initial cost,
- Long life.

There are several factors that affects the optical performance of mirrors. This effect may be due to the atmosphere surrounding the system and manufacturing; Moreover, the performance of mirror can be affected during normal operation. Thermal performance of the

collector decreases as well. The wholeness of the mirror can be disrupted due to impurity, corrosion and wearing, therefore protecting mirrors against these needs suitable coatings. In order to obtain high thermal performance, a suitable coating should be selected according to the desired properties of the reflective surface (Salazar, 2018).

The main element expected from a mirror material is that it has high reflectivity. The fraction of the incident radiation reflected by surface is defined as reflectivity of a surface, and it is a number. Usually, the reflectivity is not same for diverse wavelengths. Therefore, it has to be determined for a given specific wavelength or wavelength range. Reflection is divided into two as specular reflection and diffuse reflection. If the light comes from a single incoming direction and this light is reflected into a single outgoing direction, then this is called specular reflection. On the contrary, if the incoming light is reflected in a broad range of directions, this is called diffuse reflection. In concentrated solar power pursuance, only specular reflectivity is aforementioned (Günther et al., 2011).

On the other hand, geometrical errors occurs in the solar collector while the mirror is manufacturing and the system working. Shape error, slope error, receiver deviation error, specularity error, tracking deviation, frame deformation can be shown as the foremost errors. Shape error forecasts eccentricity of the focal line of receiver because of deflections and alignment of mirror incorrectly. Slope error gauges the deflection of the sun rays because of lightly fluctuation presented in mirror shape. The absorber is not utterly aligned to the focal line, therefore this incorrect alignment is gauged by the receiver deviation error. The error because of defective reflection of mirror (not ideal materials) represents specularity error. Tracking error occurs due to solar collector is sometimes imperfectly pointing to the sun. Finally, self-weight of collector, wind and torsional loads may affect the geometry of collector during actuation; These are cause deformation of the frame of the collector (Salazar, 2018). All these errors are shown in Fig. 3.1.

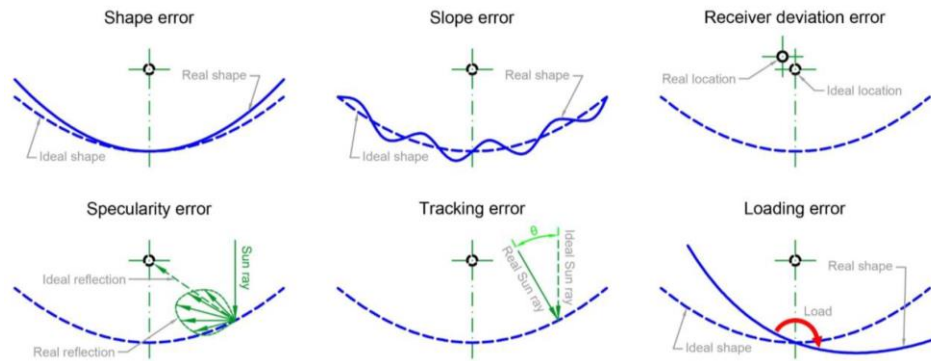


Figure 3.1. Geometrical errors in mirrors (Salazar, 2018)

It was mentioned before that the most encountered and used mirror in parabolic trough reflection system consisted of silver coated glass mirrors. This mirror also is used in the PTSC that will be studied for this thesis. Silver coated parabolic mirror has been started to be used since parabolic trough power plants were built in 1980s and experiences has been obtained (Günther et al., 2011). If it is needed to mention the advantages of glass used in parabolic mirror; it provides high solar transmittance, low cost, smooth surface, physical strength, abrasion resistance, impermeability, resistance to soiling, ease of cleaning, and inertness. When compared with other mirrors, silver and glass composed of those features are preferred because of their highly reflectance, good specularity, durability and resistance to deformity from loads. But glass is relatively heavy and brittle. Therefore, it needs gigantic structural support (i.e. stronger and stiffer). Mirrors made up of silver must be preserved against chemical and physical deterioration of the silver. Among all materials which can be used for solar reflectors, solar weighted spectral reflectance value of only silver and glass is higher than 0,90 (Solar Energy Research Institute, 1985). This glass used for the facets of mirror is normally fabricated with the float glass method. In this method, the molten glass flows continuously over a liquid tin bath, and thus, the very high smoothness of the produced glass is guaranteed (Günther et al., 2011). The silvered glass used in ADU Solar Field is shown in Fig. 3.2 as example.



Figure 3.2. Silvered mirror reflectors of PTSC at ADU Solar Field

3.1.1.2. Receiver Tube or HCE

The typical receiver of PTSC consists of two concentric pipes; an inner steel pipe that contains the working fluid or HTF and outer glass tube (cover) surrounding this steel pipe to reduce heat losses. The glass tube is made up of low-iron borosilicate glass, whose transmissivity is at least 0,96, to enhance its permeability for solar radiation. The outer surface of the steel pipe has optically selective surface. Properties of this surface are high solar absorptivity and low emittance for thermally produced infrared radiation. To obtain a higher solar transmittance and improve yearly performance of solar collector, the glass tube must be catered with an antireflective coating. Receivers of PTSC can be categorized into two as evacuated and non-evacuated. Evacuated receivers are generally employed for temperatures higher than 300 °C, since they have a high vacuum ability (10^{-5} mbar) among the steel pipe and the glass cover. Therefore, while the collector working at higher temperatures, thermal losses is decreased and overall productivity of PTSC is boosted. Non evacuated receivers are utilized for the implementations with an operating temperature below 300 °C since thermal losses are unimportant at these temperatures. Evacuated receivers are welded while non evacuated receivers are generally connected by means of exclusive threaded clogged joints (Moya, 2012).

Even though non evacuated receivers consist of an inner steel pipe and a glass cover, there is no air among the steel pipe and glass cover; glass to metal welds. SCs employed for non-evacuated receivers are not more complex than those employed for evacuated receivers.

They soak up solar radiation as much as possible, then convey it to receiver pipe. They are implemented to pipe to boost heat flux absorption. The most widely used for coatings are black nickel or black chrome due to their price and simply producing. Because of manufacturing limitation, receiver tube length is generally not larger than 5 m, therefore, they are connected in series taking into account total length of PTSC (Moya, 2012). Evacuated tube receiver is shown in Fig. 3.3.

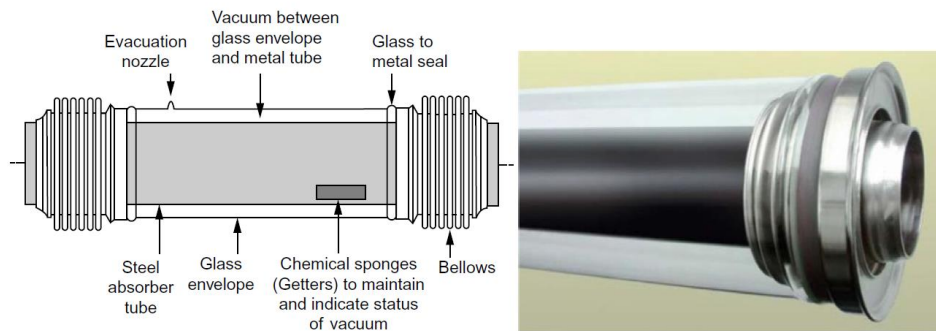


Figure 3.3. Evacuated tube receiver for parabolic trough applications (Heller, 2017)

3.1.1.3. HTF

HTF or working fluid is a indispensable substance that passes inside of the steel pipe available in receiver. Expected features from HTF are high evaporation temperature, low freezing temperature, thermal stability, high heat capacity, high heat conductivity, low viscosity, low investment cost, availability, environmental compatibility, low inflammability, low explosivity. Evaporation temperature and thermal stability identify the maximum working temperature of HTF. Low viscosity plays a major role to reduce pumping energy, and high heat conductivity provides quick heat transfer. Mineral oil, molten salt, and synthetic thermoil are used as HTF in PTSC. However, synthetic thermoil is employed almost all parabolic trough power plants. It is simply called “thermoil”. It consists of biphenyl/diphenyl oxide, and has been started to use for 25 years in PTSC. Therminol 54 is used as HTF in the PTSC that will be evaluated. The pros and cons of synthetic thermoil are as follows (Günther et al., 2011):

- High specific heat capacity, high resist against temperature
- Its maximum working temperature is 400 °C, beyond this limit, thermal cracking occurs,

- Quite expensive
- Periodically replacing
- Environmentally less friendly

3.1.1.4. Supporting Structure

The supporting structure of PTSC carries the mirror reflectors in right position and plays important role in terms of giving stability to troughs, enabling to exact sun tracking. This structure is manufactured from structural materials such as steel or aluminum, and may be categorized into 3 parts as main support, frameworks and brackets. It is shown in Fig. 3.4. Brackets fixes the receiver while frameworks ensures rigidity to mirror reflector in order to preserve its paraboloid shape. When the frameworks are designed correct, misalignment during working is hampered. The most crucial mechanical effects to eschew are torsion and bending of the framework. Self-weight of collector and wind forces are generally cause this torsion and bending. Stiffness of the supporting structure must be high, because any deviation of collector shape affects optical efficiency, and high stiffness enables longer troughs, thus the less pylons and tracking units are employed, this means that cost reduces (Günther et al., 2011; Salazar, 2018).

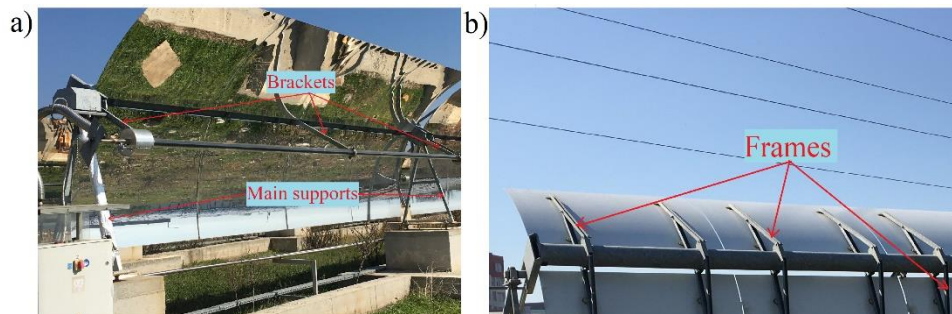


Figure 3.4. Structural sections of PTSC at ADU Solar Field: Brackets, main supports (a), and frames (b)

Furthermore, ball joints (or flexible hoses) are connection element among fix drive part and movable concentrator. They are designed taking into account that they do not introduce extra forces on the structure. and should be leakproof to prevent probable environmental risks. Large amounts of single and multiple plane displacement are soaked up by ball joints with the

inclusion of rotation (Heller, 2017). Both types of assemblies of ADU Solar Field are shown in Fig. 3.5.

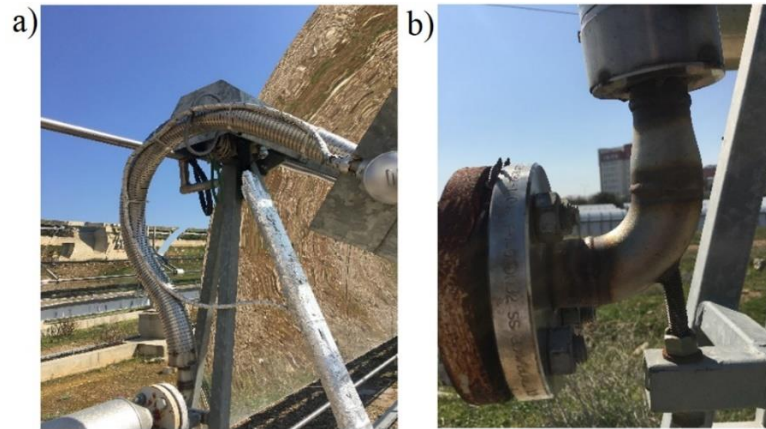


Figure 3.5. Flexible connectors of PTSC at ADU Solar Field: flexible hose (a), ball joints (b)

3.1.1.5. Control and Tracking System

In PTSC, high temperature is obtained by concentrating the radiation coming from the sun to the reflective mirror in the absorbent pipe located at the focal point of the mirror. During the day, the direction and intensity of the solar radiation falling on the collector changes, and the mirror reflector has to receive the sun perpendicular. Therefore, like any collector of a CSP system, PTSC have to follow the Sun for the purpose of obtaining maximum temperature and productivity (i.e. maximize performance). Linear concentrators have one-axis tracking system while point concentrators have two-axis tracking. This means, PTSC has also one-axis tracking system. The condition for the most ideal focusing is the intersection of the aperture surface normal of the collector with the rays direct coming from the sun (Cicibiyık, 2012; Günther et al., 2011).

Solar tracking system may be categorized as passive and active. Passive tracking system utilizes the thermosiphon for the purpose of aligning the collector while active tracking system employs electronic signal converter. Generally, active trackers are used in PTSC because passive trackers can be quite misaligned by wind during working. Active trackers can be examined into three category as open loop, closed loop and hybrid loop. Fig. 3.6 represents how open and closed loop trackers operate. Closed loop trackers employ a feedback control signal transformation for the purpose of aligning the solar collector. The light sensor

mentioned in Fig. 3.6 (a) perceives the misalignment and send out to control system which acts the driver so as to align the collector till the sensor does not give feedback. The main advantages of closed loop trackers is having high tracking sensitivity, however, shadow affects this. It is very difficult to correct the direction of the sun with the control system during long cloudy periods (Salazar, 2018).

On the other hand, open loop tracking system may be categorized as timed and azimuth/altitude. Both of them utilize progressively increasing movements so as to align the solar collector. The difference among them is the algorithm utilized so as to realize the movements. Timed-control open loop tracking systems depend upon periodic movement, while azimuth/altitude control tracking systems utilize astronomical datum subjecting to position and time. The sensitivity of equations employed in algorithms may cause significant misalignment, and this can be counted as disadvantages of these methods. Open and closed loop tracking systems combination is called hybrid loop tracking. Hybrid loop trackers handles the disadvantages of both closed & open loop tracking systems. The fundamental method is so as to align the solar collector employing the open loop algorithm, then fix alignments employing closed loop feedback sensors. Sensors are utilized in the event of high error in algorithm so as to monitor the sun (Salazar, 2018).

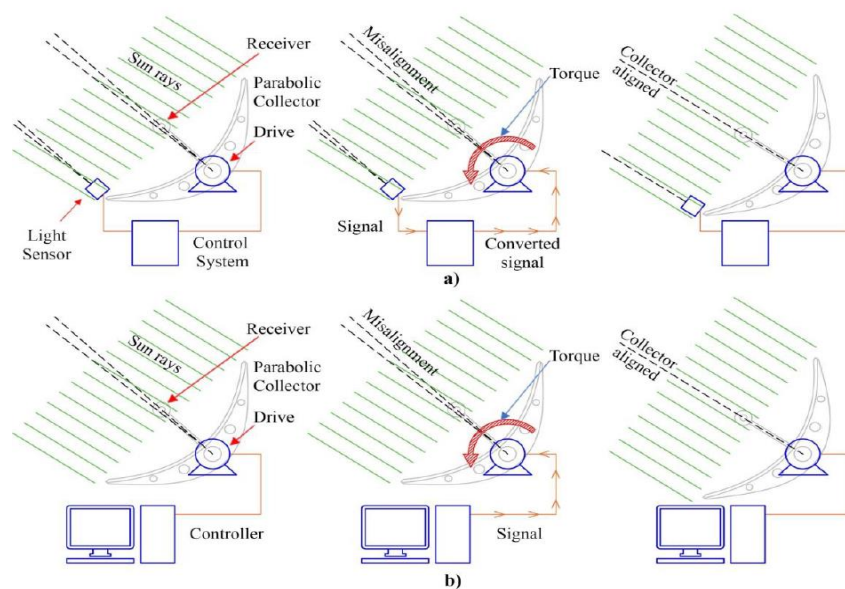


Figure 3.6. Working of active trackers: closed loop (a), open loop (b) (Salazar, 2018)

If it is needed to mention positioning, PTSC may be located as polar tracking, North-South and East-West tracking. But the most common ones are North-South and East-West tracking. Tracking methods are named depending upon direction of rotation of collector's aperture plane. For polar tracking, the rotation axis of the collector points out the pole. In North-South tracking the mirror receiver is placed on East-West direction, therefore, aperture plane of collector rotates starting from North to South and opposite direction of this. The fact that it reduces monitoring energy depletion and has a higher end-effect parameter can be cited as the advantages and disadvantages of a North-South monitoring systems. East-West tracking can be thought of as the vice versa of North-South tracking. The mirror receiver is aligned on North-South direction so as to aperture plane rotates from East to West, and this positioning has lower end effect and high energy depletion (Solorio et al., 2020). Both North-South and East-West positioning are shown in Fig. 3.7. The PTSCs in ADU Solar Field are on the horizontal N-S axis as in Fig. 3.7 (b).

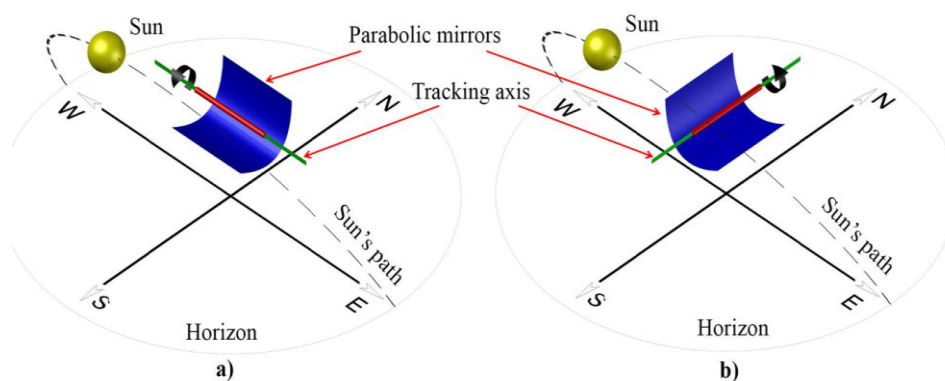


Figure 3.7. Monitoring methods: North-South (a), East-West (b) (Solorio et al., 2020)

3.1.2. Optical Modelling and Geometry of PTSC

In this part information about optical loss calculation of sun rays until it reaches to absorber tube and mathematical modelling of collector will be given.

Rays coming from the sun do not reach the parabolic system with the same value. They first reach the earth and then the heat transfer fluid by giving a certain loss in the atmosphere. The rays that are lost in the atmosphere and come to the system undergo optical loss in the parabolic reflective mirror, glass cover and absorber or receiver pipe and then reach the heat transfer liquid (Şanlı, 2010). It is shown in Fig. 3.8.

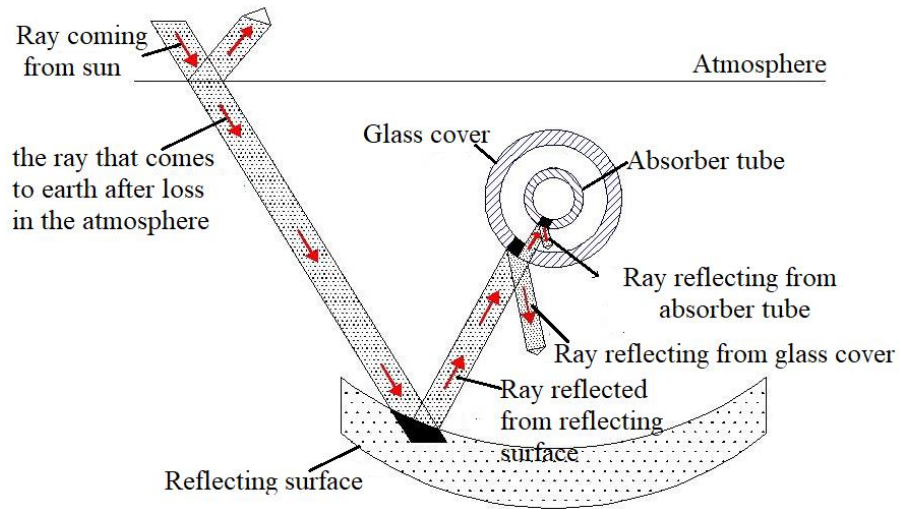


Figure 3.8. Beam transfer illustration of PTSC (Şanlı, 2010)

Sizing process must be performed before starting performance calculation of PTSC. A 2D cross-section view of PTSC is shown in Fig. 3.9 which includes diverse major parameters. The incident radiation on the parabolic shaped mirror or reflector makes an angle φ_r , between the rim and center line of collector. Here reflector radius, r_r , is max. This angle is called rim or edge angle. The equation of the parabola can be shown as follows (Kalogirou, 2014).

$$y^2 = 4fx \quad (3.1)$$

Here f represents the focal length of the parabola in m.

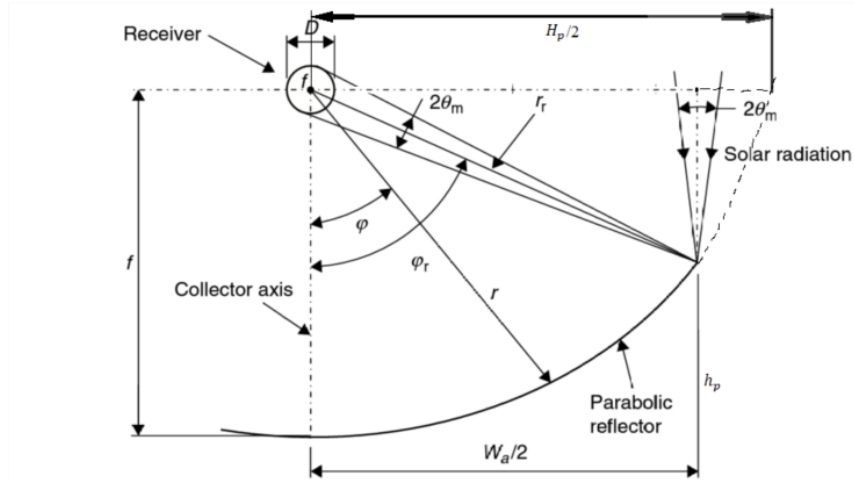


Figure 3.9. 2D cross section view of PTSC with circular absorber (Kalogirou, 2014)

The minimum diameter of receiver tube, D , needed to intercept all the reflected radiation is calculated from Eqn. 3.2 (Kalogirou, 2014).

$$D = 2r_r \sin(\theta_m) \quad (3.2)$$

where θ_m represents half acceptance angle in degree, D and r_r in m, this equation is for specular reflectors of perfect alignment. For parabolic shaped reflector or mirror, the local mirror radius, r , can be calculated from Eqn. 3.3 (Kalogirou, 2014).

$$r = \frac{2f}{1 + \cos(\varphi)} \quad (3.3)$$

where φ represents the angle between the collector axis and the radius, r . Thus maximum mirror radius (r_r) is calculated from Eqn. 3.4 (Kalogirou, 2014).

$$r_r = \frac{2f}{1 + \cos(\varphi_r)} \quad (3.4)$$

where the term rim (φ_r) is rim angle. It can be calculated from Eqn. 3.5. (Coccia et al., 2016):

$$\varphi_r = \tan^{-1} \left[\frac{8 \left(\frac{f}{W_a} \right)}{16 \left(\frac{f}{W_a} \right)^2 - 1} \right] = \sin^{-1} \left(\frac{W_a}{2r_r} \right) \quad (3.5)$$

Magnitude of rim angle defines the material needed for construction of the parabolic surface. Aperture of the parabola, W_a , is defined as the area which receives solar radiation. It is calculated from Eqn. 3.6 (Kalogirou, 2014):

$$W_a = 2r_r \sin(\varphi_r) \quad (3.6)$$

when Eqn. 3.4 is substituted into Eqn. 3.6;

$$W_a = \frac{4f \sin(\varphi_r)}{1 + \cos(\varphi_r)} \quad (3.7)$$

then, equation like in Eqn. 3.8 is obtained.

$$W_a = 4f \tan\left(\frac{\varphi_r}{2}\right) \quad (3.8)$$

Another important parameter of parabolic system is concentration ratio (C) of tubular receiver. It is the ratio of aperture area, A_a , to the receiver tube or HCE surface area, A_{rec} . It can be found from Eqn. 3.9 (Izweik et al., 2016).

$$C = \frac{A_{ap}}{A_{rec}} = \frac{W_a}{\pi D} \quad (3.9)$$

Substituting outer diameter of receiver tube, D , and W_a given in the Eqn 3.2 and 3.8 into 3.9. It reduces:

$$C = \frac{\sin(\varphi_r)}{\pi \sin(\theta_m)} \quad (3.10)$$

For an ideal case, when rim angle is 90° ($\sin(\varphi_r)=1$) maximum concentration ratio occurs, and this maximum concentration ratio can be found using Eqn. 3.11 (Coccia et al., 2016).

$$C_{max} = \frac{1}{\pi \sin(\theta_m)} \quad (3.11)$$

here, using half acceptance angle is 0.267° and it reduces (Coccia et al., 2016):

$$C_{max} = \frac{1}{\pi \sin 0.267} = 68,3 \quad (3.12)$$

The curve length of the reflective surface L_{ref} , is calculated using Eqn. 3.13 (Kalogirou, 2014).

$$L_{ref} = \frac{H_p}{2} \left\{ \sec\left(\frac{\varphi_r}{2}\right) \tan\left(\frac{\varphi_r}{2}\right) + \ln \left[\sec\left(\frac{\varphi_r}{2}\right) + \tan\left(\frac{\varphi_r}{2}\right) \right] \right\} \quad (3.13)$$

where, the term H_p is latus rectum of the parabola (m), it is calculated from Eqn. 3.14 (Izweik et al., 2016). Moreover, H_p is equal to W_a when rim angle $\varphi_r = 90^\circ$.

$$H_p = 4f \tan\left(\frac{\varphi_r}{2}\right) \quad (3.14)$$

3.2. Method

In this part, optical efficiency of collector, thermal modeling of PTSC, description of ADU Solar Field and conduction, convection, radiation heat transfers occurred in PTSC and in other pipes, the methodology of performance analysis of ADU Solar field will be examined in detailed.

3.2.1. Optical Efficiency of the Collector

The ratio of sun rays collected in absorber pipe to sun rays directly coming to collector is called optical efficiency (Cicibiyık, 2012). Optical efficiency of glass envelope is calculated from Eqn. 3.15 (National Renewable Energy Laboratory, 2003).

$$\eta_{ge} = \eta_{shadow} \cdot \eta_{track} \cdot \eta_{geo} \cdot \rho_{mirror} \cdot \eta_{mir,dirt} \cdot \eta_{HCE,dirt} \cdot \eta_{gen} \cdot K \quad (3.15)$$

where the parameters selected are in the Table 3.1.

Table 3.1 Selected parameters for optical efficiency

Parameters	Values
Shadowing factor of HCE (bellows, shielding, supports) (National Renewable Energy Laboratory, 2003)	0,974
Tracking error, η_{track} (National Renewable Energy Laboratory, 2003)	0,994
Geometry effect (mirror alignment), η_{geo} (National Renewable Energy Laboratory, 2003)	0,98
Clean mirror reflectance or cleanliness factor, ρ_{mirror} (National Renewable Energy Laboratory, 2003)	0,95
General error, η_{gen} (National Renewable Energy Laboratory, 2003)	0,96
Mirror reflectance, ρ_m (Wang et al., 2016)	0,935

The term $\eta_{mir,dirt}$ depends reflectivity and cleanliness of mirror, it is calculated from Eqn. 3.16 (National Renewable Energy Laboratory, 2003).

$$\eta_{mir,dirt} = \frac{\rho_m}{\rho_{mirror}} \quad (3.16)$$

According to Eqn. 3.16, $\eta_{mir,dirt}$ becomes 0,984. The term $\eta_{HCE,dirt}$ is calculated from Eqn. 3.17 (National Renewable Energy Laboratory, 2003).

$$\eta_{HCE,dirt} = (1 + \eta_{mir,dirt})/2 \quad (3.17)$$

In this case, dirt factor of HCE becomes 0,992. The term incident angle modifier, K is required for cases at which the solar irradiation is not normal to collector aperture. It is same for each HCE and collector type and depends upon the incidence angle θ , and is calculated from Eqn. 3.18 (Wang et al., 2016).

$$K = \cos(\theta) + 0,00084 \theta - 0,00005369 \theta^2 \quad (3.18)$$

While collector working abnormal, some part of the sun rays reflecting from end of the concentrator can not reach to the absorber, this is called end effect, and this end effect can be diminished by using a longer receiver than parabolic troughs. The aperture area A_e lost to end effect can be found utilizing Eqn. 3.19 (Kalogirou, 2014), and also shown in Fig. 3.10.

$$A_e = fW_a \tan(\theta) \left[1 + \frac{W_a^2}{48f^2} \right] \quad (3.19)$$

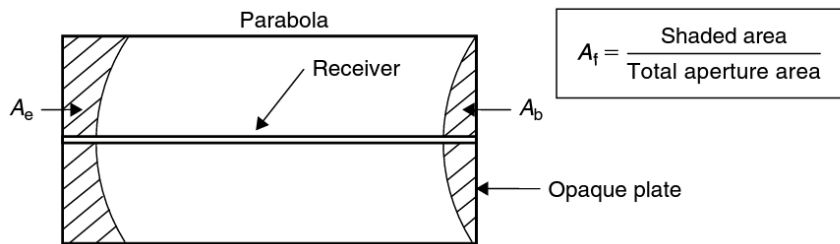


Figure 3.10. End effect and blocking of PTSC (Kalogirou, 2014)

For a plate extending from rim to rim, the lost area, A_b , is calculated from Eqn. 3.20 (Kalogirou, 2014):

$$A_b = \frac{2}{3} W_a h_p \tan(\theta) \quad (3.20)$$

where h_p represents the vertical height of parabola (m), and is calculated from Eqn. 3.21 (Woldemicheal et al., 2012).

$$h_p = \frac{W_a^2}{16f} \quad (3.21)$$

Therefore, total loss in aperture area, A_1 , is calculated by summing up of A_e and A_b without the term $\tan(\theta)$ as in Eqn. 3.22 (Jeter et al., 1983).

$$A_1 = \frac{2}{3}W_a h_p + fW_a \left[1 + \frac{W_a^2}{48f^2} \right] \quad (3.22)$$

and finally geometric factor, A_f , is defined as the ratio of total loss area to the aperture area, it is calculated using Eqn. 3.23 (Kalogirou, 2014).

$$A_f = \frac{A_1}{A_{ap}} \quad (3.23)$$

where A_{ap} represents effective aperture area of collector, and can be found by employing Eqn. 3.24 (Yassen, 2012).

$$A_{ap} = (W_a - D_{co}) \cdot L \quad (3.24)$$

where L represents length of the collector, and D_{co} is outer diameter of glass envelope.

γ is intercept factor, and it is defined as the ratio of solar radiation hitting the glass cover to the solar radiation directed from reflective surface to focusing. Intercept factor value (γ) is generally bigger than 0,9 (Duffie & Beckman, 2013).

Using universal error parameters, intercept factor is calculated from Eqn. 3.25 (Güven & Bannerot, 1986).

$$\gamma = \frac{1 + \cos\varphi_r}{2\sin\varphi_r} \quad (3.25)$$

$$x \int_0^{\varphi_r} \text{Erf} \left\{ \frac{\sin(\varphi_r) [1 + \cos(\varphi)] [1 - 2d^* \sin(\varphi)] - \pi\beta^* [1 + \cos(\varphi_r)]}{\sqrt{2}\pi\sigma^* [1 + \cos(\varphi_r)]} \right\} \\ - \text{Erf} \left\{ -\frac{\sin(\varphi_r) [1 + \cos(\varphi)] [1 + 2d^* \sin(\varphi)] + \pi\beta^* [1 + \cos(\varphi_r)]}{\sqrt{2}\pi\sigma^* [1 + \cos(\varphi_r)]} \right\} \\ \frac{d\varphi}{[1 + \cos(\varphi)]}$$

where

- ✓ $d^* = (d_r)_y/D$, and is the universal non-random error parameter due to receiver mislocation and reflector profile errors,
- ✓ $\beta^* = \beta C$, and is the universal non-random error due to angular errors,
- ✓ d_r is displacement of receiver from focus (m),
- ✓ β is misalignment angle error (degrees) and C is concentration ratio = A_a/A_r ,
- ✓ σ_{sun} is energy distribution standard deviation of the sun's rays at normal incidence and solar noon,
- ✓ σ_{slope} is standard deviation of the normal distribution of local slope errors at normal incidence,
- ✓ σ_{mirror} is diffusivity of the reflective material at normal incidence.
- ✓ $\sigma^* = \sigma_{tot,n} C$, and is the universal random error parameter, $\sigma_{tot,n}$ is random errors and is calculated from Eqn. 3.26 (Güven & Bannerot, 1986).

$$\sigma_{tot,n} = \sqrt{\sigma_{sun}^2 + 4\sigma_{slope}^2 + \sigma_{mirror}^2} \quad (3.26)$$

3.2.2. Thermal Modelling of the PTSC

The performance model of HCE depends upon an energy balance of the solar collector and HCE that contains the DNI on the collector and optical losses of HCE and collector, also useful heat gain inside HTF. In this thesis study 1D thermal modelling is employed due to parabolic trough receivers that will be evaluated are shorter than 100 m. 2D thermal

modelling is required for longer receiver (i.e. >100 m) (National Renewable Energy Laboratory, 2003)

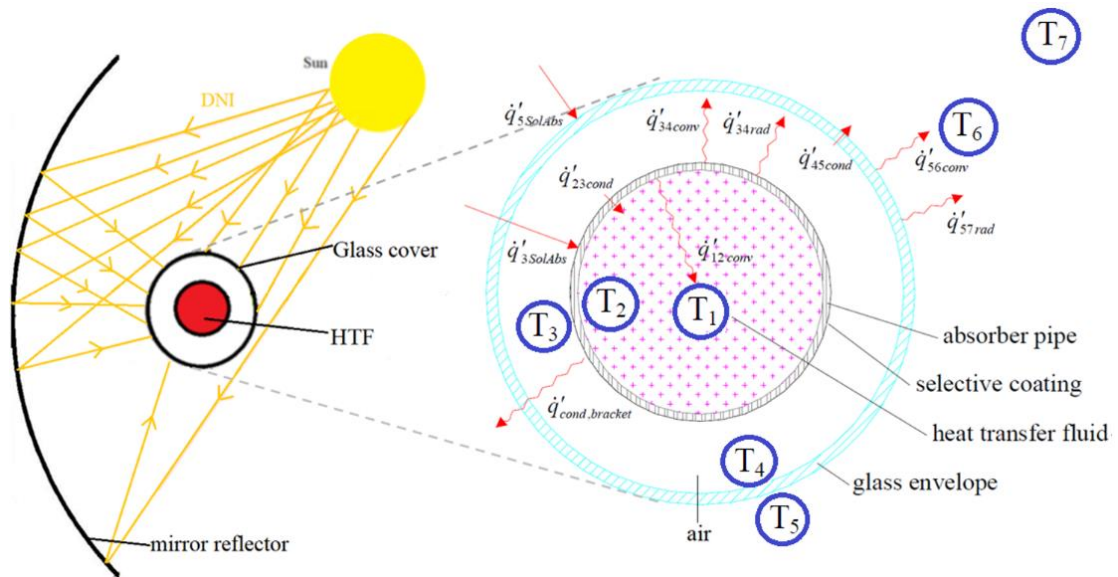


Figure 3.11. Thermal modelling of HCE

Fig. 3.11 represents the 1D thermal modelling of HCE under steady-state condition. The thermal resistance of this modelling is shown in Fig 3.12.

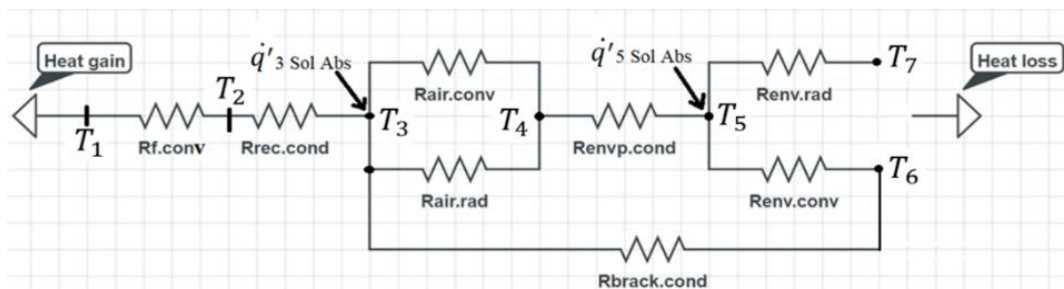


Figure 3.12. Thermal network diagram of HCE

The factors caused thermal loss in PTSC (Şanlı, 2010):

- Environment temperature
- Wind speed
- Fluid properties (pressure, viscosity etc.)
- Magnitude of direct solar radiation coming to collector
- Sizing of collector

- Sizing and properties of glass cover
- Sizing and properties of absorber tube

The heat transfers occurred and temperatures in Fig. 3.11 are as follows:

- \dot{q}'_{12conv} is convection between inner surface of absorber pipe and HTF (W/m)
- \dot{q}'_{23cond} is conduction between outer and inner surfaces of absorber pipe (W/m)
- \dot{q}'_{34conv} is convection between outer surface of absorber pipe and inner surface of glass envelope (W/m)
- \dot{q}'_{34rad} is radiation between outer surface of absorber pipe and inner surface of glass envelope (W/m)
- \dot{q}'_{56conv} is convection between outer surface of glass envelope and ambient (W/m)
- \dot{q}'_{57rad} is radiation between outer surface of glass envelope and sky (W/m)
- \dot{q}'_{45cond} is conduction between outer and inner surfaces of glass envelope (W/m)
- $\dot{q}'_{cond,bracket}$ is conduction between outer surface of absorber pipe and HCE support bracket (W/m)
- $\dot{q}'_{5 Sol Abs}$ is solar irradiation absorption between incident solar irradiation and outer surface of glass envelope (W/m)
- $\dot{q}'_{3 Sol Abs}$ is solar irradiation absorption between incident solar irradiation and outer surface of absorber pipe (W/m)
- T_1 is mean (bulk) temperature of HTF (°C)
- T_2 is inner surface temperature of absorber pipe (°C)
- T_3 is outer surface temperature of absorber pipe (°C)
- T_4 is inner surface temperature of glass envelope (°C)
- T_5 is outer surface temperature of glass envelope (°C)
- T_6 is atmosphere (ambient) temperature (°C)
- T_7 is effective sky temperature (K)

If the energy balance equation is written by applying conservation of energy, the equations are obtained as follows (National Renewable Energy Laboratory, 2003);

$$\dot{q}'_{12conv} = \dot{q}'_{23cond} \quad (3.27)$$

$$\dot{q}'_{3 Sol Abs} = \dot{q}'_{34conv} + \dot{q}'_{34rad} + \dot{q}'_{23cond} + \dot{q}'_{cond,bracket} \quad (3.28)$$

$$\dot{q}'_{34conv} + \dot{q}'_{34rad} = \dot{q}'_{45cond} \quad (3.29)$$

$$\dot{q}'_{45cond} + \dot{q}'_{5 Sol Abs} = \dot{q}'_{56conv} + \dot{q}'_{57rad} \quad (3.30)$$

$$\dot{q}'_{Heat Loss} = \dot{q}'_{56conv} + \dot{q}'_{57rad} + \dot{q}'_{cond,bracket} + \dot{q}'_{other pipes} \quad (3.31)$$

3.2.3. Description of ADU Solar Field

ADU Solar Field consists of 2 areas as large and small. In this thesis study, only large solar field that includes 5 loop and 10 rows will be considered. Each row in large solar field has 12 parabolic trough collector. Therefore, total 120 PTSCs available in the field. Therminol 54 is used as HTF in the field. The placement of PTSC of ADU large solar field located in the direction of West-East is as shown in Fig. 3.13

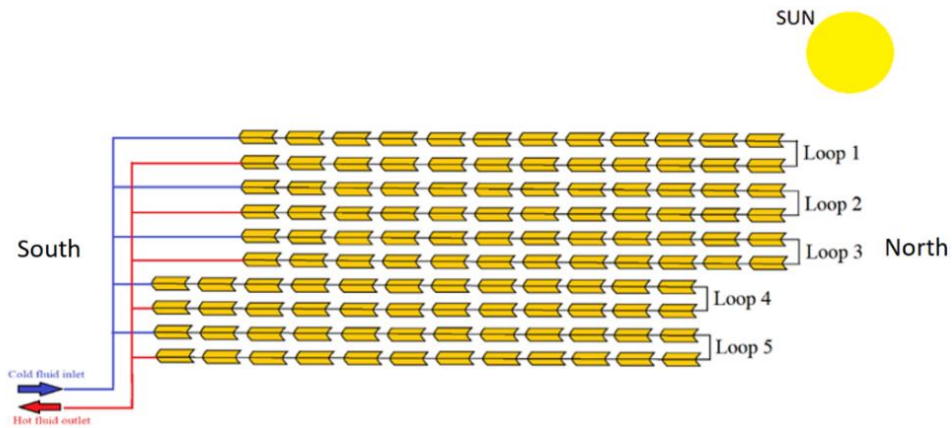


Figure 3.13. Collector placement in ADU Solar Field

The solar field that includes parabolic trough consists of one large field and one small field. Collectors are connected in series throughout a line in solar field. This line is called “row”. Cold Therminol 54 oil enters a collector from one row, and warms up throughout second row. The path in which cold oil warms up throughout these two rows is called “one loop”. The large solar field and its panoramic view are shown in Fig. 3.14 and 3.15 respectively.



Figure 3.14. ADU Solar Field



Figure 3.15. Panoramic view of ADU Solar Field (Yeni Kiroba, 2018)

Therminol 54 HTF can be defined as a synthetic fluid produced to ensure reliable and continuously heat transfer performance over a long service at a recommended bulk temperature of 280 °C. It is designed to be utilized in nonpressurized/low pressure, indirect heating systems and has great pumpability features and supplies processes up to temperatures lower than possible with many other mineral oils. It also ensures dependable, efficient and uniform process heat without the need for high pressures. As it has high boiling point, it helps diminish the volatility and fluid leakage issues related with other fluids. Actual fluid life depends upon the total system design, operation, and this may change by HTF chemistry. The

HTF has no corrosive effect on metals mostly utilized in the construction of heat transfer systems (Eastman, (n.d)). Typical features of the HTF can be seen in Table 3.2.

Table 3.2. Typical features of Therminol 54 (Eastman, (n.d))

Appearance	Clear, yellow liquid
Composition	Synthetic hydrocarbon mixture
Temperature range	-28 °C to 280 °C
Max film temperature	310 °C
Normal boiling point	351 °C
Autoignition temperature	> 330 °C

Specifications of PTSCs in ADU large solar field are listed in Table 3.3:

Table 3.3. Specifications of PTSCs located in ADU Solar Field

Aperture width	2,38 m
Total mirror length of 1 collector	5,92 m
Number of mirror in 1 collector	8
Maximum mirror radius	1,235 m
Total number of mirror	960
Aperture area of whole field	1690,7 m ²
Rim angle	74,48°
Concentration ratio of 1 collector	17,62
Distance between two parallel rows	6,85 m
Focal length	0,78 m
HCE	Net length: 5,86 m Total net length: 703,2 m
Conditions of HCE	Non-vacuumed (annulus is filled with the ambient air)
Atmospheric air pressure	99,128 kPa
HTF	Therminol 54
Equation of parabolic mirror	$y^2 = 3,12 x$

The dimensions of glass envelope and absorber tube are as shown in Fig. 3.16.

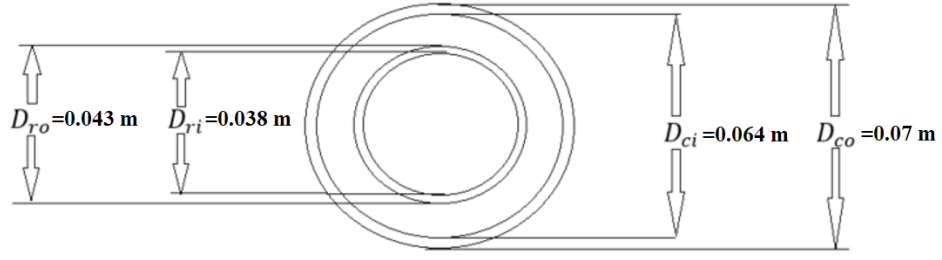


Figure 3.16. Inner and outer diameters of glass cover and absorber pipe

Useful heat is defined as momentary heat energy gained by the HTF while flowing from the inlet to outlet of the receiver tube. Experimental useful heat may be calculated by employing the temperature difference among inlet and outlet surface temperature of absorber tube as in Eqn. 3.32 (Izweik et al., 2016).

$$\dot{Q}_{u,exp} = \dot{m} \cdot c_{HTF} (T_{out} - T_{in}) \quad (3.32)$$

where \dot{m} is the mass flow rate of HTF (kg/s), T_{out} is outlet temperature of absorber tube ($^{\circ}\text{C}$), T_{in} is inlet temperature of absorber tube ($^{\circ}\text{C}$), and c_{HTF} is specific heat of HTF (J/kg- $^{\circ}\text{C}$).

If the energy balance of cylindrical absorber tube is written considering that it is under steady-state condition, solar radiation coming to collector is obtained as in Eqn. 3.33 (Bilgin, 2019).

$$\dot{Q}_s = \dot{Q}_{u,exp} + \dot{Q}_{loss} \quad (3.33)$$

The thermal losses occurred from the absorber pipe to its surroundings are denoted by \dot{Q}_{loss} , and are also equal to the term $\dot{q}'_{Heat\ Loss}$ earlier defined in the energy balance equation. It is calculated from Eqn. 3.34 (Bilgin, 2019).

$$\dot{Q}_{loss} = U_L A_r (T_r - T_{amb}) \quad (3.34)$$

where T_r is mean temperature of receiver tube ($^{\circ}\text{C}$), and the term U_L represents the overall heat loss coefficient which includes all thermal losses from absorber outer surface to environment. So, it can be obtained considering previous equation.

Overall heat transfer coefficient U_o that describes total heat transfer coefficient from HTF inside the absorber pipe to ambient is calculated from Eqn. 3.35 (Kalogirou, 2014).

$$U_o = \left[\frac{1}{U_L} + \frac{D_3}{h_1 D_2} + \frac{D_3 \ln(D_3/D_2)}{2k_{23}} \right]^{-1} \quad (3.35)$$

The collector heat removal factor F_R is defined as the ratio of useful heat gain of the fluid to the gain that would occur if the absorber pipe were at inlet fluid temperature everywhere. It is in the range in between 0 and 1 (Coccia et al., 2016). It is calculated from Eqn. 3.36 (Coccia et al., 2016).

$$F_R = \frac{\dot{m}_{HTF} \cdot c_{pHTF}}{A_{r,int} \cdot U_L} \left[1 - \exp \left(- \frac{A_{r,int} U_L F'}{\dot{m}_{HTF} \cdot c_{pHTF}} \right) \right] \quad (3.36)$$

where A_r is the internal area of absorber (receiver) pipe, the term F' is collector efficiency factor and is the ratio of overall heat transfer coefficient to overall heat loss coefficient, and it is calculated from Eqn. 3.37 (Bilgin, 2019).

$$F' = \frac{1/U_L}{\frac{1}{U_L} + \frac{D_3}{h_1 D_2} + \frac{D_3 \ln(D_3/D_2)}{2k_{23}}} = \frac{U_o}{U_L} \quad (3.37)$$

where k_{23} is thermal conductivity of receiver tube depending coating placed onto absorber tube.

Another important parameter employed in the analysis of solar collector is flow factor F'' . It is the ratio of heat removal factor to the collector efficiency factor (F_R/F') as in Eqn. 3.38 (Elmohlawy et al., 2018).

$$F'' = \frac{F_R}{F'} = \frac{\dot{m}_{HTF} \cdot c_{pHTF}}{A_r U_L F'} \left[1 - \exp \left(- \frac{A_r U_L F'}{\dot{m}_{HTF} \cdot c_{pHTF}} \right) \right] \quad (3.38)$$

The thermal efficiency of solar field may be depended upon DNI or ANI. Here, ANI value is suggested to be considered as it is the true solar energy input to solar field. (National Renewable Energy Laboratory, 2011). The relation between DNI and ANI is shown in Fig. 3.17., and ANI is calculated from Eqn. 3.39 (National Renewable Energy Laboratory, 2011).

$$ANI = DNI \cdot \cos(\theta) \quad (3.39)$$

where θ is angle of incidence.

It was mentioned that the collectors available in ADU Solar Field were on horizontal N-S axis and tracks the sun in the E-W direction, so, θ is calculated from Eqn. 3.40 for this placement (Kalogirou, 2014).

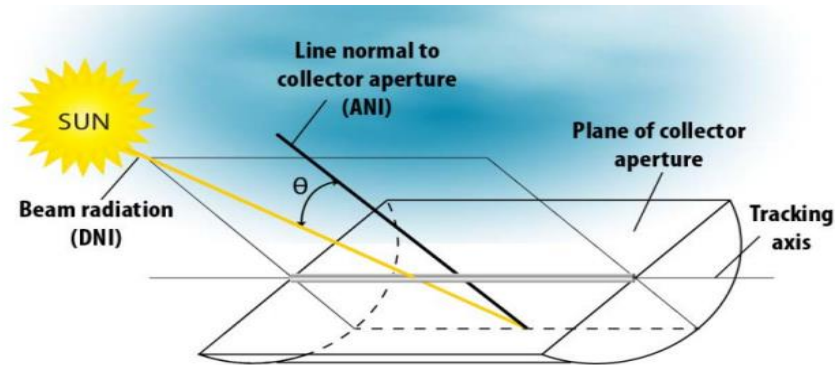


Figure 3.17. PTSC true energy input (National Renewable Energy Laboratory, 2011).

$$\cos(\theta) = \sqrt{\sin^2(\alpha) + \cos^2(\delta)\sin^2(\omega)} \quad (3.40)$$

where α is solar altitude angle, δ is declination angle, ω is hour angle.

The solar altitude angle is defined as the angle between the line to the sun and the horizontal. Zenith angle is the angle between the line to the sun and vertical. Hour angle is the angular displacement of the sun west or east of the local meridian because of rotation of the

earth on its axis. It changes 15° at every hour, and afternoon positive, morning negative. Both α and θ_z are complement each other to 90 degrees (Duffie & Beckman, 2013). It is shown in Fig. 3.18.

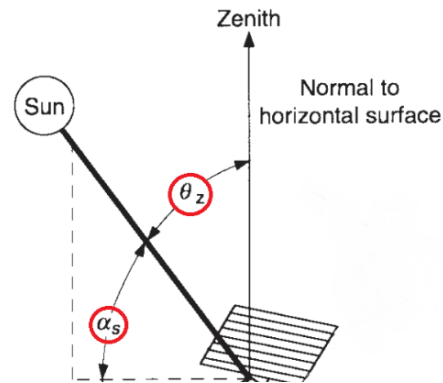


Figure 3.18. Solar angles (Duffie & Beckman, 2013)

The angles α , δ in Eqn. 3.40 can be calculated from Eqn. 3.41 and 3.42 respectively (Kalogirou, 2014).

$$\sin(\alpha) = \cos(\theta_z) = \sin(\phi) \sin(\delta) + \cos(\phi) \cos(\delta) \cos(\omega) \quad (3.41)$$

where ϕ is local latitude, and is north positive, south negative ($+37,85^\circ$ for ADU).

$$\delta = 23,45 \sin \left[\frac{360}{365} (284 + n) \right] \quad (3.42)$$

where n is day of the year, and may be calculated from Table 3.4.

Table 3.4. Day number for each month (Duffie & Beckman, 2013)

Months	Day of Month
January	n
February	31 + n
March	59 + n
April	90 + n
May	120 + n

Table 3.4. Day number for each month (continued)

June	151 + n
July	181 + n
August	212 + n
September	243 + n
October	273 + n
November	304 + n
December	334 + n

According to Eqn. 3.39, total true solar energy coming to whole solar field may be calculated from Eq 3.43 (Elmohlawy et al., 2018).

$$Q_{total,sf} = ANI \cdot A_{sf} \quad (3.43)$$

where A_{sf} is area of solar field (m^2) and it is found from Eqn. 3.44 (Elmohlawy et al., 2018).

$$A_{sf} = W_a \cdot L \cdot M \cdot N \quad (3.44)$$

where W_a is aperture width of collector (m), L is total collector length in one row (m), M is number of rows of collectors in series, and N is number of parallel lines

3.2.4. Heat Transfers Occurred in PTSC

In this part, all conduction, convection, radiation heat transfers occurred in PTSC will be considered.

3.2.4.1. Heat Transfer Between the HTF and the Absorber Pipe

If the Newton's law of cooling is utilized, the convective heat transfer from the inner surface of the absorber pipe to the HTF (W/m) can be calculated from Eqn. 3.45, and convective heat transfer coefficient of HTF h_1 , depends upon the flow type of HTF (turbulent or laminar) and calculated considering Nusselt number as in Eqn. 3.46 (National Renewable Energy Laboratory, 2003).

$$\dot{q}'_{12conv} = h_1 \pi D_2 (T_2 - T_1) \quad (3.45)$$

where h_1 is convective heat transfer coefficient of HTF at T_1 (W/m²-K), and is calculated from Eqn. 3.46 (National Renewable Energy Laboratory, 2003).

$$h_1 = Nu_{D2} \frac{k_1}{D_2} \quad (3.46)$$

Other terms in Eqn. 3.45 are; D_2 is inner diameter of the absorber pipe (m), T_1 is mean (i.e bulk) temperature of the HTF (°C), T_2 is inside temperature of absorber pipe (°C), Nu_{D2} is Nusselt number based on D_2 , and k_1 is thermal conductivity of the HTF at T_1 (W/m-K)

Nusselt number must be calculated considering the flow type of HTF. At typical working conditions, the flow in the absorber pipe is turbulent flow. On the other hand, when the days are cloud (off-solar hours) or while assessing the absorber pipe heat losses on a test platform, the HTF may be in transitional or laminar flow due to the viscosity of the HTF at lower temperatures. If the flow is turbulent or transitional, then the term Nusselt number in Eqn. 3.46 is calculated from Gnielinski correlation as in Eqn. 3.47 (National Renewable Energy Laboratory, 2003).

$$Nu_{D2} = \frac{\frac{f_2}{8} (Re_{D2} - 1000) Pr_1}{1 + 12,7 \sqrt{\frac{f_2}{8}} (Pr_1^{\frac{2}{3}} - 1)} \left(\frac{Pr_1}{Pr_2} \right)^{0,11} \quad (3.47)$$

$$f_2 = (1,82 \log_{10}(Re_{D2}) - 1,64)^{-2} \quad (3.48)$$

where f_2 is friction factor for the inner surface of absorber pipe, Pr_1 is Prandtl number appraised at the HTF temperature T_1 , and Pr_2 is Prandtl number appraised at the absorber inner surface temperature T_2 .

This correlation is valid for $0,5 < Pr_1 < 2000$; $0,5 < Pr_2 < 2000$ and $2300 < Re_{D2} < 5.10^6$. Moreover, this correlation calculates the transitional flow case for Reynolds number in range 2300 and 4000. Except for Pr_2 , all fluid features are assessed at the average HTF temperature, T_1 . In Eqn. 3.47 and Eqn. 3.48. both T_1 and T_2 are not depend upon the angular

and longitudinal HCE directions. For a laminar pipe flow type, Reynolds number is lower than 2300, the Nusselt number will be 4,36. Hydraulic diameter D_h equals to inner diameter of absorber pipe for both laminar and turbulent pipe flow as it can be seen in Eqn. 3.49. Pipe flow values are appraised presuming constant heat flux (National Renewable Energy Laboratory, 2003).

$$D_h = \frac{4A_{cs}}{P_w} = \frac{4\pi D_2^2/4}{\pi D_2} = D_2 \quad (3.49)$$

where D_2 is inner absorber diameter (m), A_{cs} is flow cross-sectional area (m^2), and P_w is wetted perimeter (m). Convective resistance of HTF can be calculated from Eqn. 3.50 (Bialobrzewski, 2007).

$$R_{12.conv} = \frac{1}{h_1 A_2} \quad (3.50)$$

here, A_2 represents the inner surface area of absorber pipe (m^2) $\pi D_2 L$.

3.2.4.2. Heat Transfer Through the Absorber Wall

Fourier's law of conduction through a hollow cylinder describes the conduction heat transfer between the inner and outer surfaces of absorber pipe. This conductive heat transfer (W/m) is calculated from Eqn. 3.51 (National Renewable Energy Laboratory, 2003).

$$\dot{q}'_{23cond} = \frac{2\pi k_{23}(T_2 - T_3)}{\ln(D_3/D_2)} \quad (3.51)$$

where

- k_{23} is thermal conductivity of absorber pipe at average absorber temperature $(T_2 + T_3)/2$ (W/m-K), this k value is constant and depends upon the absorber material type as well,
- T_2 is inner surface temperature of absorber pipe (K),

- T_3 is outer surface temperature of absorber pipe (K),
- D_2 is inner diameter of absorber pipe (m),
- D_3 is outer diameter of absorber pipe (m).

The thermal conductivity depends upon absorber material type. In this study stainless steel 304L was used as absorber material. So, according to this material type the k value is calculated from Eqn. 3.52 (National Renewable Energy Laboratory, 2003).

$$k_{23} = (0,013)T_{23} + 15,2 \quad (3.52)$$

Conductive heat resistance of absorber or receiver wall can be found employing Eqn. 3.53 (Bialobrzeski, 2007).

$$R_{rec.cond} = \frac{\ln \left[\frac{D_3}{D_2} \right]}{2\pi L k_{23}} \quad (3.53)$$

where D_3 is outer diameter of absorber pipe (m), D_2 is inner diameter of absorber pipe (m), and L is axial length of receiver tube (m).

3.2.4.3. Heat Transfers from the Absorber Pipe to the Glass Envelope

Convection and radiation heat transfer occurs between the absorber pipe and glass envelope. Sure, this convection heat transfer depends upon the status of annulus (i.e evacuated or non-evacuated). The PTSC that will be studied in this thesis includes air in annulus, pressure $> \sim 1$ torr, (i.e non-evacuated). Therefore heat transfer mechanism occurs by natural (free) convection. The thermal losses from the absorber to envelope are convection (only occurs in non-evacuated tube case) and radiation. This convection loss (W/m) is calculated from Eqn. 3.54 (National Renewable Energy Laboratory, 2003).

$$\dot{q}'_{34conv} = \frac{2,425 k_{34}(T_3 - T_4)(Pr_{34} \cdot Ra_{D3} / (0,861 + Pr_{34}))^{0,25}}{(1 + (D_3/D_4)^{0,6})^{1,125}} \quad (3.54)$$

$$Ra_{D3} = \frac{g \beta (T_3 - T_4) D_3^3}{\alpha_{34} \cdot \nu_{34}} \quad (3.55)$$

where

- k_{34} is thermal conductance of air at T_{34} ,
- T_3 is outer surface temperature of absorber ($^{\circ}\text{C}$),
- T_4 is inner surface temperature of glass envelope ($^{\circ}\text{C}$),
- D_3 is outer diameter of absorber (m),
- D_4 is inner diameter of glass envelope (m),
- T_{34} is average temperature $(T_3 + T_4)/2$ ($^{\circ}\text{C}$),
- Pr_{34} is Prandtl number at T_{34} ,
- Ra_{D3} is Rayleigh number at D_3 ,
- α is thermal diffusivity of air at T_{34} (m^2/s) and is calculated from Eq. 3.56 (National Renewable Energy Laboratory, 2003).
- ν is kinematic viscosity of air at T_{34} (m^2/s) and is calculated from Eq 3.57 (National Renewable Energy Laboratory, 2003).
- β is volumetric thermal expansion coefficient (1/K), for an ideal gas, it is calculated from Eqn. 3.58 (National Renewable Energy Laboratory, 2003).

$$\alpha_{34} = \frac{k_{34}}{\rho_{34} \cdot Cp_{34}} \quad (3.56)$$

$$\nu_{34} = \frac{\mu_{34}}{\rho_{34}} \quad (3.57)$$

$$\beta = \frac{1}{T_{avg}} \quad (3.58)$$

Radiation heat transfer occurred between the absorber outer surface and glass envelope inner surface (W/m) can be calculated from Eqn. 3.59 (National Renewable Energy Laboratory, 2003).

$$\dot{q}'_{34rad} = \frac{\sigma\pi D_3(T_3^4 - T_4^4)}{\left[\frac{1}{\varepsilon_3} + \frac{(1/\varepsilon_4) D_3}{\varepsilon_4 D_4}\right]} \quad (3.59)$$

where

- σ is Stefan-Boltzmann constant ($\text{W/m}^2\text{-K}^4$),
- D_3 is outer diameter of absorber (m),
- D_4 is inner diameter of glass envelope (m),
- T_3 is outer surface temperature of absorber (K),
- T_4 is inner surface temperature of glass envelope (K),
- ε_3 is absorber selective coating emissivity,
- ε_4 is glass envelope emissivity.

Absorptance and emittance of glass envelope are constant and are not depended upon the temperature and types of selective coatings. $\alpha = 0,02$ $\varepsilon = 0,86$. The transmittance of glass tube, absorptance and emittance of selective coating depend upon the coating type. In this study, Luz Cermet is selected as selective coating. The cross section of HCE is shown in Fig. 3.19. Envelope transmittance and coating absorptance of Luz Cermet are 0,935 and 0,92 respectively. Emittance of Luz Cermet coating is calculated from Eq 3.60. If ε_3 value is below 0,05 then it is taken as 0,05 (National Renewable Energy Laboratory, 2003).

$$\varepsilon_3 = 0,000327(T_3 + 273,15) - 0,065971 \quad (3.60)$$

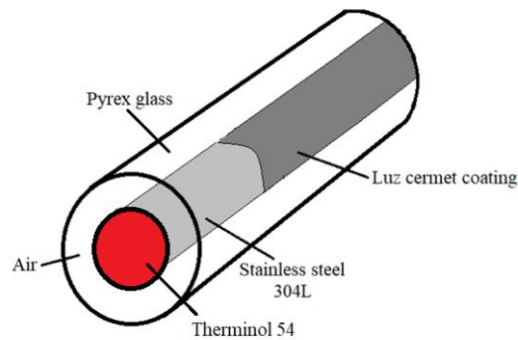


Figure 3.19. The cross section of HCE (not scaled)

Radiation resistance and convection resistance between outer surface of absorber pipe and inner surface of glass envelope, radiation heat transfer coefficient are calculated from Eqns. 3.61, 3.62 and 3.63 respectively (Bialobrzeski, 2007).

$$R_{air,conv} = \frac{1}{h_{in}A_{ro}} \quad (3.61)$$

$$R_{air,rad} = \frac{1}{h_{rad,a-ge} A_{ro}} \quad (3.62)$$

$$h_{rad,a-ge} = \frac{\sigma \varepsilon_{abs} \varepsilon_{glass} (T_3^2 + T_4^2)(T_3 + T_4)}{\varepsilon_{glass} + \varepsilon_{abs} \frac{(1 - \varepsilon_{glass})(D_3/2)}{(D_4/2)}} \quad (3.63)$$

where

- A_{ro} is outer surface area of absorber pipe (m^2) $\pi D_3 L$,
- ε_{abs} is emissivity of absorber coating,
- ε_{glass} is emissivity of glass envelope (Pyrex glass),
- T_3 is outer temperature of receiver ($^{\circ}C$),
- T_4 is inner temperature of glass envelope ($^{\circ}C$),
- D_3 is outer absorber diameter (m),
- D_4 is inner glass envelope diameter (m),
- h_{in} is convective heat transfer coefficient between absorber tube and glass envelope ($W/m^2 \text{ } ^{\circ}C$).

The h_{in} value is calculated by employing effective thermal conductivity method as given in Eqn. 3.64 (Bellos & Tzivanidis, 2018).

$$h_{in} = \frac{2 \cdot k_{eff}}{D_3 \cdot \ln \left[\frac{D_4}{D_3} \right]} \quad (3.64)$$

It was earlier mentioned that the receiver annulus was not under vacuumed. In this case, the effective thermal conductivity k_{eff} , can be calculated from Eqn. 3.65 (Coccia et al., 2016).

$$\frac{k_{eff}}{k_{air}} = (0,386) \cdot \left[\frac{Pr_{air}}{0,861 + Pr_{air}} \right] \cdot [F_{cyl} \cdot Ra_{air}] \quad (3.65)$$

where

- k_{air} is thermal conductivity of air at mean temperature $(T_3 + T_4)/2$,
- Pr_{air} is Prandtl number of air at mean temperature $(T_3 + T_4)/2$,
- Ra_{air} is Rayleigh number of air at mean temperature $(T_3 + T_4)/2$, and at characteristic length $(D_4 - D_3)/2$,
- F_{cyl} is form factor or geometric factor for concentric cylinders

F_{cyl} is calculated employing Eqn. 3.66 (Coccia et al., 2016), and Ra_{air} is calculated from Eqn. 3.67 (Alfellag, 2014).

$$F_{cyl} = \frac{[\ln(D_4/D_3)]^4}{[(D_4 - D_3)/2]^3 \cdot [D_4^{-0,6} + D_3^{-0,6}]^5} \quad (3.66)$$

$$Ra_{air} = \frac{g \beta (T_3 - T_4) [(D_4 - D_3)/2]^3}{\nu_{34} \alpha_{34}} \quad (3.67)$$

Eqn. 3.65 is valid for $0,7 \leq Pr_{air} \leq 6000$ and $100 < F_{cyl} Ra_{air} < 10^7$, and if this multiplication is lower than 100, then convection is neglected, and thus $k_{eff} = k_{air}$. Furthermore, k_{eff} can not be less than k_{air} (Coccia et al., 2016).

3.2.4.4. Heat Transfer Through the Glass Envelope

Conduction heat transfer occurred between the inner and outer surfaces of glass envelope (W/m) can be calculated employing same equation described in Eqn. 3.51 (National Renewable Energy Laboratory, 2003).

$$\dot{q}'_{45cond} = \frac{2\pi k_{45}(T_4 - T_5)}{\ln(D_5/D_4)} \quad (3.68)$$

where

- k_{45} is thermal conductivity of glass envelope at the average glass envelope temperature $(T_4 + T_5) / 2$,
- T_4 is inner surface temperature of glass envelope (K),
- T_5 is outer surface temperature of glass envelope (K),
- D_4 is inner diameter of glass envelope (m),
- D_5 is outer diameter of glass envelope (m).

Here the glass cover is selected as Pyrex glass with a thermal conductance value of $k_{45} = 1,04$ (National Renewable Energy Laboratory, 2003). Conductive resistance between inner and outer surface of glass envelope can be calculated from Eqn. 3.69 (Bialobrzeski, 2007).

$$R_{env,cond} = \frac{\ln\left[\frac{D_5}{D_4}\right]}{2\pi L k_{45}} \quad (3.69)$$

where D_5 is inner diameter of glass envelope (m), D_4 is outer diameter of glass envelope (m), and L is axial length of receiver tube (m).

3.2.4.5. Heat Transfer from Glass Envelope to the Atmosphere

Convection and radiation heat transfer occurs among the outer surface of glass envelope and ambient. Convection heat transfer will be either forced or natural depending upon whether there is wind. Radiation heat transfer occurs because of temperature difference among the glass envelope and sky. Here, convection heat transfer is the largest source of heat loss if there is a wind. In this case, evaluation will be performed taking into account wind case, and the convection heat transfer will be forced. To calculate radiation heat transfer, glass envelope is presumed to be a small convex gray object in a large blackbody cavity (i.e sky). As a result, total heat transfer between glass envelope outer surface and ambient (W/m), term

h_{out} can be calculated from Eqns. 3.70 and 3.71 (National Renewable Energy Laboratory, 2003).

$$\dot{q}'_{56conv} + \dot{q}'_{57rad} = h_{out}\pi D_5(T_5 - T_6) + D_5\sigma\pi\varepsilon_5(T_5^4 - T_7^4) \quad (3.70)$$

$$h_{out} = \frac{k_{56}}{D_5}Nu_{D5} \quad (3.71)$$

where

- T_6 is ambient temperature ($^{\circ}\text{C}$),
- σ is Stefan- Boltzmann constant ($5,67 \times 10^{-8} \text{ W/m}^2\text{K}^4$),
- ε_5 is emittance of glass envelope outer surface,
- T_5 is outer cover (envelope) temperature ($^{\circ}\text{C}$),
- D_5 is glass envelope outer diameter (m),
- h_{out} is convection heat transfer coefficient between the cover (glass envelope) and ambient at $(T_5 - T_6) / 2$ ($\text{W/m}^2\text{-K}$),
- k_{56} is thermal conductance of air at $(T_5 - T_6) / 2$ (W/m-K),
- Nu_{D5} is average Nusselt number based on the glass envelope outer diameter D_5 ,
- T_7 is effective sky temperature (K).

For the wind case, the term Nu_{D5} in Eqn. 3.71 is calculated from Zhukauskas' correlation as in Eqn. 3.72 (National Renewable Energy Laboratory, 2003)., and C, m, n values are read from Table 3.5.

$$Nu_{D5} = C Re_{D5}^m Pr_6^n \left(\frac{Pr_6}{Pr_5} \right)^{0,25} \quad (3.72)$$

with

Table 3.5 C and m coefficients corresponding Re numbers range
(National Renewable Energy Laboratory, 2003)

Re_D	C	m
1-40	0,75	0,4

Table 3.5 C and m coefficients corresponding Re numbers range (continued)

40-1000	0,51	0,5
1000-200000	0,26	0,6
200000-1000000	0,076	0,7

and $n = 0,37$ for $Pr_6 \leq 10$; $n = 0,36$ for $Pr_6 > 10$. Eq 3.72 is valid for $0,7 < Pr_6 < 500$, and $1 < Re_{D5} < 10^6$. Here all fluid features are appraised at the atmospheric temperature T_6 , only Pr_5 is appraised at glass envelope outer temperature (National Renewable Energy Laboratory, 2003).

Effective sky temperature T_7 is presumed as 8 °C below ambient as in Eqn. 3.73 (National Renewable Energy Laboratory, 2003).

$$T_7 = T_6 - 8 \quad (3.73)$$

Convective and radiative resistances between glass envelope and ambient environment and radiative heat transfer coefficient are calculated from Eqns. 3.74, 3.75 and 3.76 respectively (Bialobrzeski, 2007).

$$R_{envp,conv} = \frac{1}{h_{out}A_{co}} \quad (3.74)$$

$$R_{envp,rad} = \frac{1}{h_{rad,ge-atm}A_{co}} \quad (3.75)$$

$$h_{rad,ge-atm} = \varepsilon_{glass}\sigma(T_5 + T_7)(T_5^2 + T_7^2) \quad (3.76)$$

Solar irradiation absorption between incident solar irradiation and outer surface of glass envelope $\dot{q}'_{5 Sol Abs}$, and solar irradiation per receiver length \dot{q}'_{si} are calculated from Eqns. 3.77 and 3.78 (National Renewable Energy Laboratory, 2003).

$$\dot{q}'_{5 Sol Abs} = \dot{q}'_{si} \cdot \eta_{opt,env} \cdot \alpha_{env} \quad (3.77)$$

$$\dot{q}'_{si} = ANI \cdot A_{ap} \quad (3.78)$$

where the term α_{env} in Eqn. 3.74 is absorptivity of glass envelope, its value is 0,02 (National Renewable Energy Laboratory, 2003).

Solar irradiation absorption between incident solar irradiation and outer surface of absorber pipe, $\dot{q}'_{3 Sol Abs}$ is calculated from Eqn. 3.79 (National Renewable Energy Laboratory, 2003).

$$\dot{q}'_{3 Sol Abs} = \dot{q}'_{si} \cdot \eta_{opt,env} \cdot \tau_{env} \cdot \alpha_{abs} \quad (3.79)$$

where τ_{env} is transmittance value of glass envelope (pyrex glass) 0,935 and α_{abs} is absorptance of absorber, and its value is 0,92 for Luz Cermet coating (National Renewable Energy Laboratory, 2003).

3.2.4.6. Heat Transfer Through the HCE Support Bracket

The HCEs located at the focal line of collector are supported by support brackets which run from the collector structure to absorber pipe as shown in Fig. 3.20. The C-shaped profiles are used in ADU Solar Field. Each of collector has 3 support brackets which are in 0,85 m length, 0,21 m perimeter, and 5 cm wide. Since there are 72 bracket in 1 loop, total 360 brackets are available in whole solar field.



Figure 3.20. Support bracket of HCE at ADU Solar Field

This heat loss through HCE (W) is calculated from Eqn. 3.80 (National Renewable Energy Laboratory, 2003).

$$\dot{q}'_{cond,bracket} = \sqrt{\bar{h}P_b k_b A_{cs,b}} (T_{base} - T_6) \quad (3.80)$$

where

- \bar{h} is average convective coefficient of support bracket (W/m²-K),
- P_b is perimeter of bracket (0,21 m),
- k_b is conduction coefficient (W/m.K),
- $A_{cs,b}$ is minimum cross section area of bracket (m²) (0,1785 m²),
- T_{base} is temperature at the base of bracket (°C),
- T_6 is ambient temperature (°C).

However, since there is no Nu number for C shaped profile, brackets are assumed as circular in 5 cm diameter, and corresponding Nu number can be calculated from Eqn. 3.72. Material of brackets is assumed as AISI 310 Stainless Steel. It is a high chromium nickel austenitic stainless steel that includes high carbon. Moreover, it has good features: great mechanical properties, high oxidation and heat resistances at high temperature. Diverse industrial furnaces, steam boilers, petroleum systems parts, thermocouple protection tubes can be cited as the usage areas of it, and if it is needed to give examples these too: furnace linings, boiler baffles, jet engine burner liners, air craft cabin heaters (The World Material, 2020).

3.2.4.7. Heat Transfers Occurred due to Other Pipes in ADU Solar Field

In this section, heat losses occurred due to other pipes and connecting elements will be considered. Pipes in which Therminol 54 HTF flows inside either in the diameter of DN50 or DN80.

The material of all these pipes is selected as AISI 1040 Carbon Steel. It is a medium carbon steel and protects its high strength at elevated temperature, exhibits great resistance to corrosion cracking, resistant to sea water in both stagnant and flowing case, and to heat. It is

utilized in many areas such as marine engineering, nuclear power plants, furnaces and gas turbines, boiler and pressure vessels, chemical processing plants (BPF, 2017).

The route of Therminol 54 in 1 row will be determined, and total number of pipes and connecting elements through 1 loop and whole field will be mentioned. Their cross sections are as shown in Fig. 3.21. First of all, the HTF passing inside the vertical pipe which is in 4 m length, 40 cm perimeter, and each of loops has 2 vertical pipes (oil in and oil out) as shown in Fig. 3.22. So, there are 10 vertical pipes in whole field. The diameter of inner tubes through which Therminol 54 flows through these vertical pipes is DN50. The needed convective heat transfer coefficient to be calculated the heat transfer from outer surface of the pipes to the ambient may be found from Eqn. 3.81. (Tijani & Roslan, 2014).

$$h_{out} = 4 D_{pipe,outer}^{-0.42} V_6^{0.5} \quad (3.81)$$

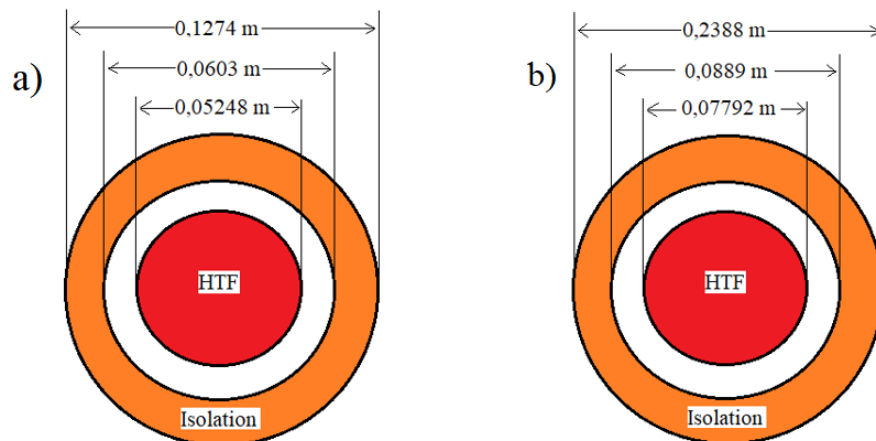


Figure 3.21. The cross section of pipes: DN50 (a) and DN80 (b)

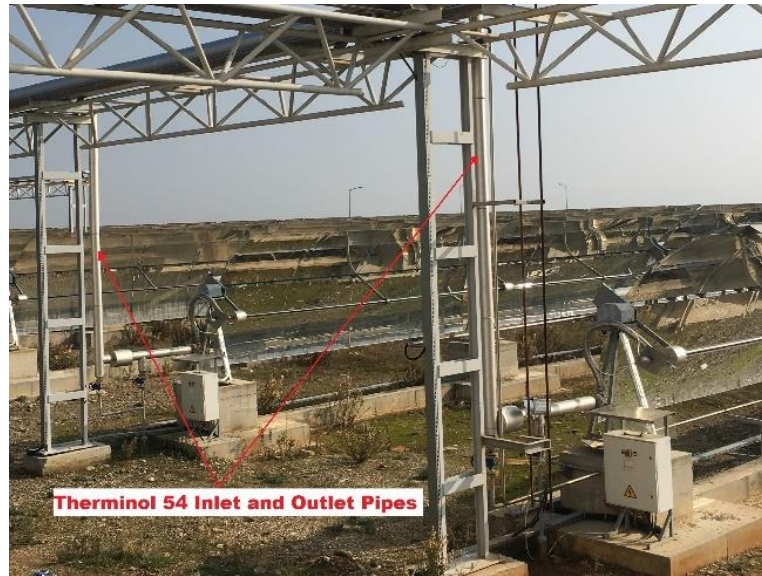


Figure 3.22. The oil inlet and outlet vertical pipes in 1 loop

After passed that vertical pipe, it comes to cylindrical horizontal pipe that is in 26 cm length, and 75 cm in perimeter. There are 2 pipes in 1 loop, so 10 pipes are available in whole field. The pipe inside it has diameter of DN80. The pipes are shown in Fig. 3.23.

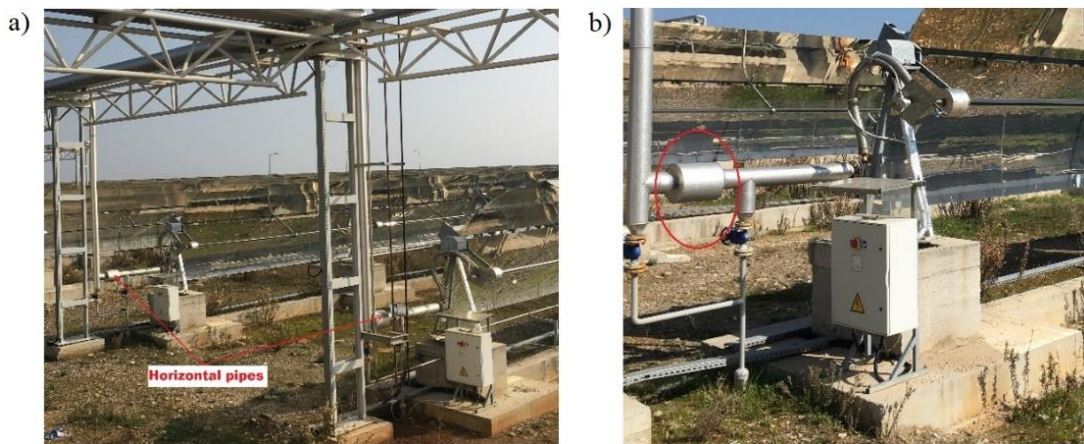


Figure 3.23. Horizontal pipes: Available in 1 loop (a), and close-up image (b)

Then, it comes to the other horizontal pipes which is in 1,16 m length and 40 cm perimeter. There are 2 pipes in 1 loop, so total 10 pipes exist in whole field. This pipe is same with the vertical pipes mentioned before, and has diameter of DN50 pipe inside it. It is shown in Fig. 3.24.



Figure 3.24. Other pipe next to the horizontal pipe

After passed that pipe, the HTF comes to bare pipe before entering the flexible hose pipe as shown in Fig. 3.25(b). It is in 25 cm length, 42,4 mm outer diameter, 2 mm thickness.

There are 2 types of bare elbow pipes as long and short in the field. There are 8 bare-short elbow pipes in 1 loop, so total 40 pipes exist in whole field. They are manufactured from S304L (1.4307) stainless steel material as shown in Fig. 3.25(a).

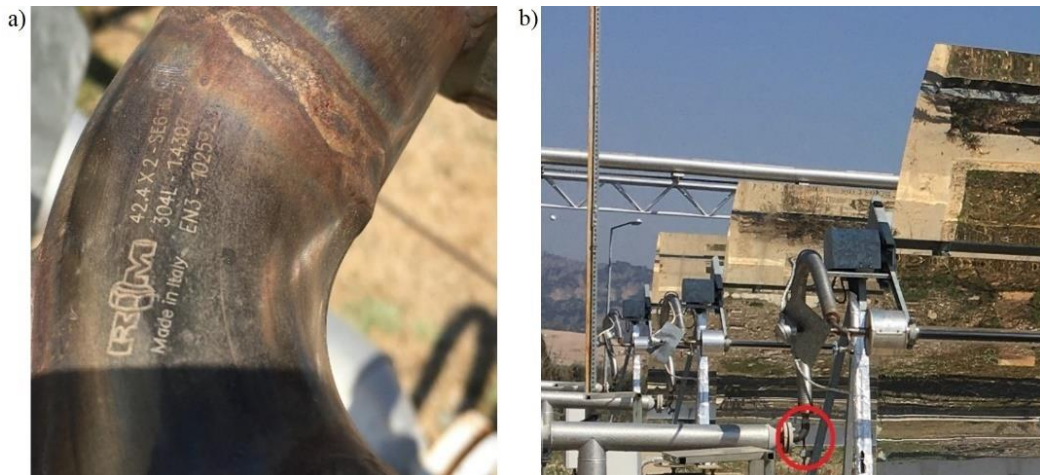


Figure 3.25. Bare-short elbow pipe: 304L material (a) and remote view (b)

Then, it comes to the flexible hose pipe whose perimeter is 23 cm, pipe thickness is 0,5 cm, and length is 1,35 m. There are 4 flex pipe in 1 loop, so total 20 flex pipe in whole field.

Stonewool is employed to isolate these pipes as shown in Fig. 3.26(a), and ISOVER product was selected as insulation material, it is pre-formed stone wool (or rockwool) and

consists of single layered hollow cylinders made up of one or more segments. Thanks to their snap-on configuration, it prevents heat loss in the pipe longitudinally. It includes many advantages such as high level of thermal and acoustic insulation performance, moisture resistance, mechanical resistance, environmentally friendly, non-combustible material and weight, protects its shape during over time. It is utilized for industrial pipework in HVAC (Isover Saint Gobain, (2017); Isover Saint Gobain, (n.d)). Flex pipe in which the HTF flows is shown in Fig. 3.26.

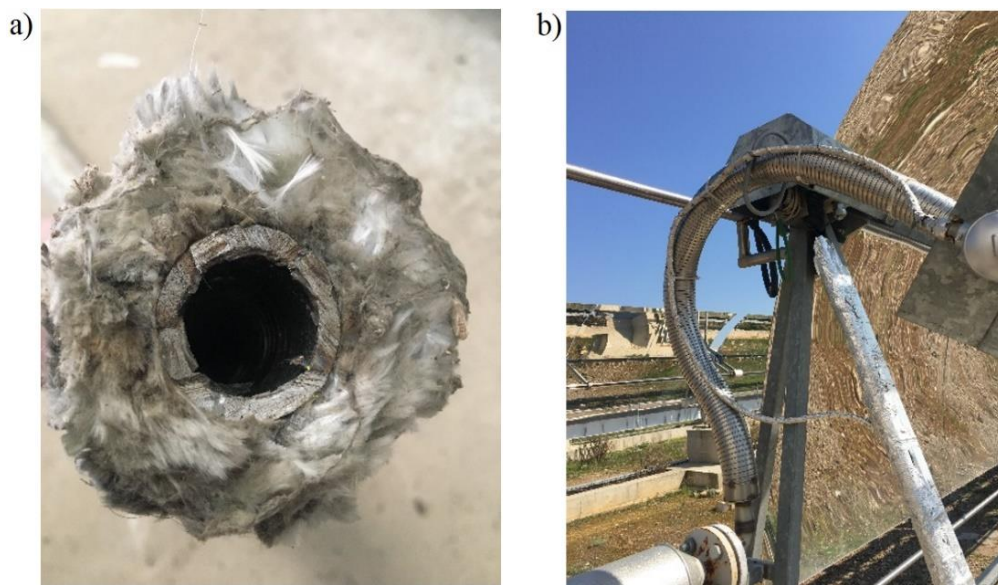


Figure 3.26. Flex pipe: Rockwool inside it (a) and remote view (b)

The last two pipes before the HTF entering the absorber tube are: bare-long elbow pipe whose length is 30 cm, and short cylindrical pipe whose perimeter is 65 cm, length is 20 cm. There are two types of cylindrical pipe as long and short in the field. The HTF firstly passes inside short cylindrical pipe then long pipe. Since there are 24 short cylindrical pipes in 1 loop, total 120 pipes like that in whole field, and since there are 4 bare-long elbow pipes in 1 loop, total 20 pipes exist in whole field. The short cylindrical pipe and bare elbow pipe are shown in Fig. 3.27 and Fig. 3.28 respectively.



Figure 3.27. Short cylindrical pipes



Figure 3.28. Bare-long elbow pipe

After passed that pipe, the HTF enters the absorber tube. The net length of the absorber tube of 1 PTSC, in other words, the length of part exposed to sun rays is 5,86 m. Therefore, total absorber tube length of 1 loop is 140,64 m. When the HTF came to the absorber tube, for 1 PTSC, it encounters with 3 support bracket and annular brackets that exist on the tip of the bracket. Its perimeter and length 28 cm and 6 cm respectively. The material of annular brackets was selected as AISI 310 Stainless Steel as in support bracket. The detailed image is shown in Fig. 3.29.



Figure 3.29. The annular brackets

Then, the HTF passes inside the long-cylindrical pipe whose perimeter and length are 65 cm and 50 cm respectively. Since there are 2 pipes like that in 1 loop, total 10 pipes exist in the whole field. One of them is shown in Fig. 3.30.

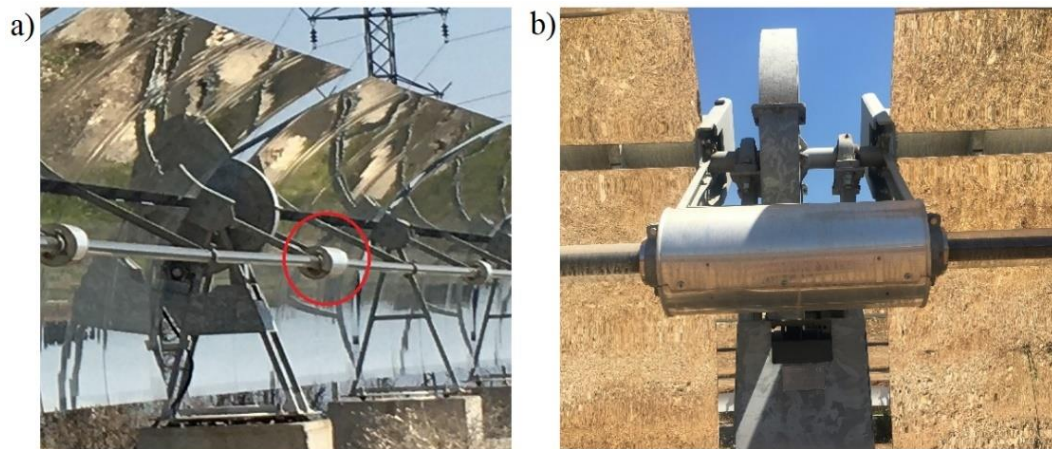


Figure 3.30. Long-cylindrical pipe: Remote view (a) , and close-up view (b)

Then, the HTF comes to isolated-long elbow pipe and the flexible pipe located at the tip of the short cylindrical pipe. It is shown in Fig. 3.31. Since there are 4 isolated-long elbow pipes in 1 loop, total 20 pipes available in the whole field.



Figure 3.31. Isolated-long elbow pipe

After passed inside these pipes, it comes to the T-shaped pipe located after 6 PTSC in 1 row. The pipe has 60 cm in length, 40 cm in perimeter, and includes DN50 pipe inside of it. Since there are 2 T-shaped pipes in 1 loop, total 10 pipe exits in the whole field. It is shown in Fig. 3.32.

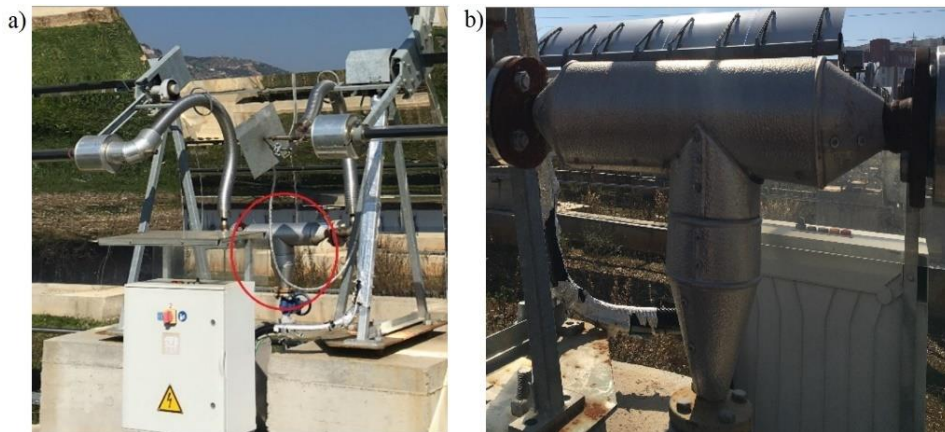


Figure 3.32. The T-shaped pipe: remote view (a), and close-up view (b)

Then, it follows the flexible pipe, isolated-long elbow pipe and short-cylindrical pipe respectively to enter again the absorber tube. At the end of 1 row, it encounters with J-shaped pipe located between two parallel rows. It is shown in Fig. 3.33(a). The elbow pipe is in 60 cm length, the flat pipe is 6,85 m, and the pipe located at the tip of flat pipe and shown in Fig. 3.33(b) is 1,40 m. It was assumed as if it had been added to the tip of J-shaped pipe. So, total length of pipe is 8,85 m. Since there are 5 loops in the whole field, total 5 pipes available. Moreover, they include DN50 pipes inside of them.

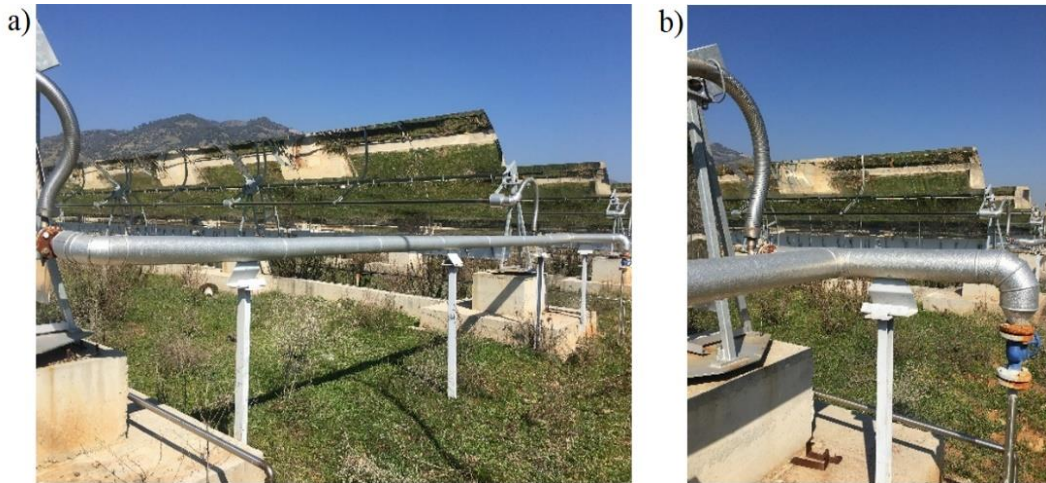


Figure 3.33. Pipe between two parallel rows: J-shaped pipe (a), and pipe at the end of it (b)

Thus, the HTF passes through 1 row, and continues with the second row. It again passes inside the same pipes for other row, thus, completes 1 loop. The 5 same processes are realized for the whole field. There are the pipes in which hot and cold HTF passes in the field, and heat transfers occur in these pipes as well. The pipes above are same with the horizontal cylindrical pipes. The pipes between two parallel rows and other side pipes are shown in Fig. 3.34. They include the DN80 pipes, and the material of them was selected as AISI 1040 Carbon Steel.

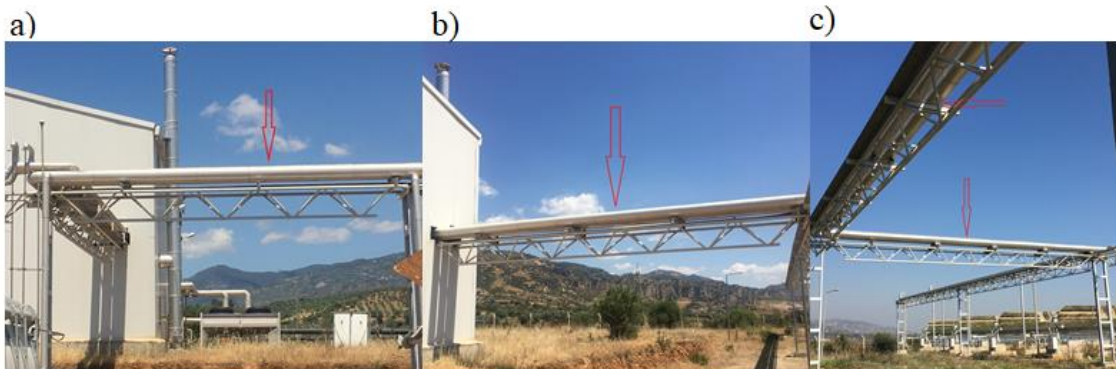


Figure 3.34. Pipes above: between two rows (a), side pipes coming to building (b), and other side pipes coming from other rows (c)

3.2.5. Performance Analysis of ADU Solar Field with EES

Assumptions and simplifications while performance analysis carrying out are as follows (National Renewable Energy Laboratory, 2003):

- The PTSC is assumed to be in steady-state conditions,
- Flowing of Therminol 54 is uniform,
- The model is a 1-D model (i.e temperature increment along the length of the PTSC is negligible),
- The sky is a blackbody, and 8 degrees below than environment temperature,
- Heat losses due to the joint elements and main support structure are negligible,
- T_{1ave} is the bulk temperature,
- Wind direction is normal to the axis of HCE,
- HCE is long isothermal horizontal cylinders,
- $\dot{q}'_{3 Sol Abs}$ and $\dot{q}'_{5 Sol Abs}$ may be treated as heat flux,
- Optical properties are same for all HCE, uniform,
- Annulus gas pressure is same with the ambient pressure,
- Optical properties are not depend upon the temperature, except emittance of selective coating located on absorber tube,
- Selective coating is Luz Cermet,
- Glass envelope is made up of Pyrex glass and is opaque,
- Absorber and glass envelope surfaces are formed from long concentric isothermal cylinders,
- Incident angle modifier (K) does not change from HCE to HCE,
- The end-loss effect and the shadow effect due to absorber tube are negligible,
- The C-shaped support bracket is assumed as 5 cm in diameter cylinder,
- Convection perimeter for support bracket is the perimeter of C-shaped profile,
- Conduction cross sectional area is the area C-shaped support (0,21*0,85) connection tabs from the frames to the absorber connection bracket,
- That bracket is estimated as an infinite fin,
- The thermal-physical properties of Therminol 54 could change over time,
- Base temperature of bracket, T_{base} , is assumed 10 degrees below than outer surface of absorber pipe, T_3 , and average temperature is presumed as $(T_{base} + T_{amb})/3$,
- The contact resistance from absorber pipe to annular bracket is negligible.
- The radiation heat transfers due to other pipes are negligible,
- The isolation material for all pipes is ISOVER stonewool,

- The material of other all pipes is AISI 1040 Carbon Steel,
- The material of support brackets and annular brackets is AISI 310 Stainless Steel.

EES Professional was utilized in this thesis study. First of all, lookup tables are created for Therminol 54, AISI 310, ISOVER Stonewool, AISI 1040 and Air. Thus, thanks to that table, the values corresponding to a given temperature like specific heat (c_p), density (ρ), thermal conductivity (k) etc. may be obtained. The method of creating new lookup table window is shown in Fig. 3.35.

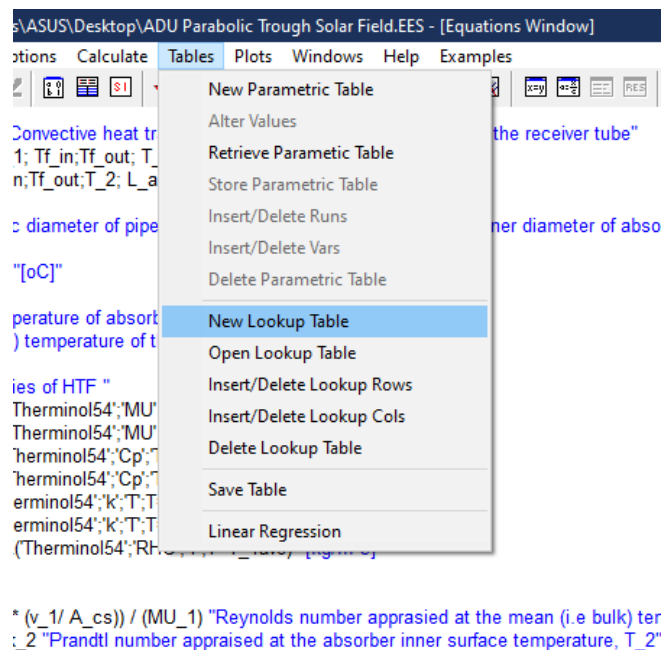


Figure 3.35. Creating lookup table

The number of rows and columns are adjusted, then, features of each column like units, titles were defined as shown in Fig. 3.36. All numerical values were entered to lookup table by applying that method.

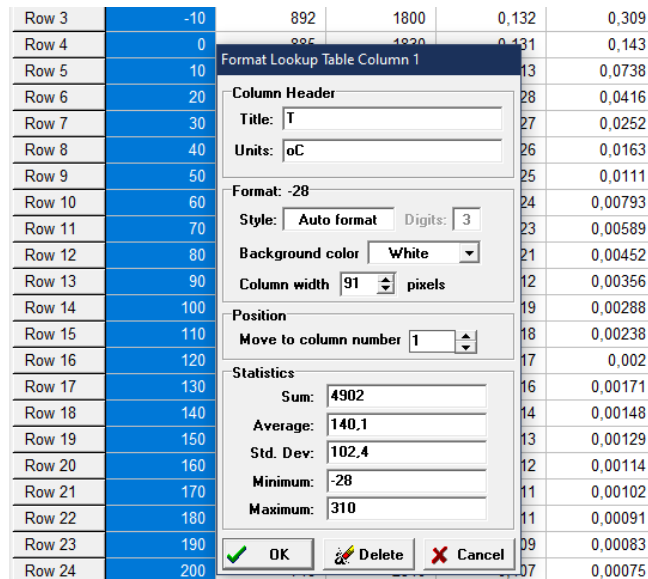


Figure 3.36. Properties defined to lookup table

Constant parameters like aperture width (m), HTF flow rate (m^3/h), and wind speed (m/s), inner and outer diameters of glass envelope and absorber pipe (m), total mirror length (m), atmospheric pressure of ADU Solar Field (kPa), and glass envelope annulus pressure (kPa) etc. were defined to EES. Every 10,5 m from sea level upwards, the atmospheric pressure drops 1 mmHg (Wikipedia, 2006). Therefore, the pressure of ADU Solar Field is 99,12583553 kPa. Some main variable input parameters like angle of incidence (degree), DNI (W/m^2), ambient temperature ($^{\circ}\text{C}$), and HTF inlet temperature ($^{\circ}\text{C}$) are also defined as shown in Fig. 3.37.

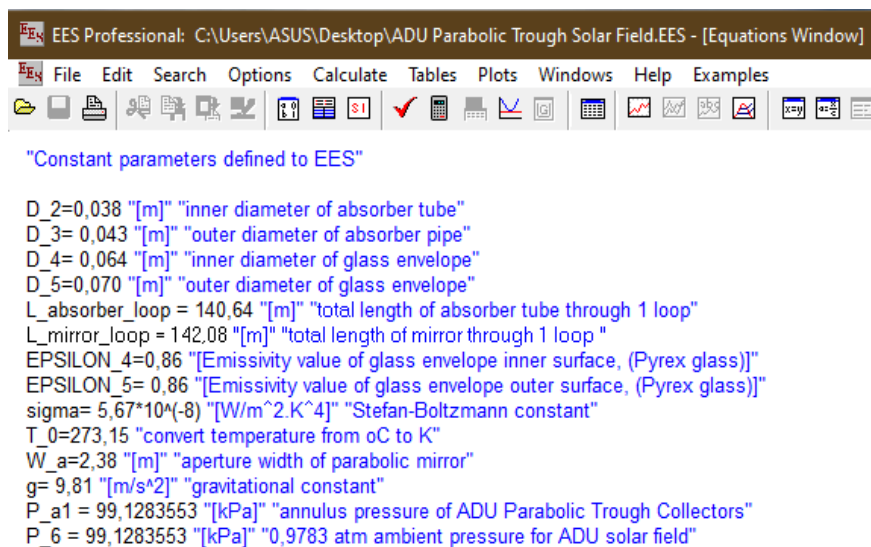


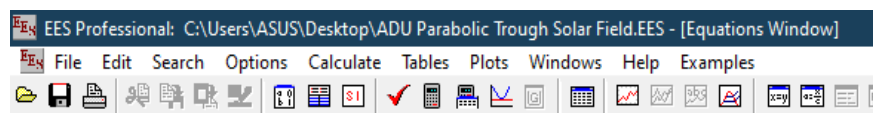
Figure 3.37. Defining of constant parameters

Then, appropriate EES codes for conduction, convection, radiation heat transfers, and the energy balance equations for whole solar field are written. Afterwards, the equations are iterated to see the outlet temperature of the HTF ($T_{f_{out}}$) and all other amount of heat transfers.

Then, one more lookup table is created to enter all input values that correspond to different hours of different days (DNI, $T_{f_{in}}$, T_{amb} , angle of incidence θ , HTF flow rate V_1 , wind speed V_6) as shown in Fig.. and each different inputs are read from this lookup table as shown in Fig. 3.38.

	1	2	3	4	5	6	7
	DNI	$T_{f_{in}}$	$T_{f_{out,real}}$	θ	Flow Rate	Wind Speed	Ambient Temp.
	[W/m ²]	[oC]	[oC]	[Degree]	[m ³ /h]	[m/s]	[oC]
Row 1	529,7	110,5	111,5	5,27	26,09	1	32
Row 2	709,4	102,6	120,7	10,47	26,32	0,9	32,6
Row 3	850,8	107,3	126,5	13,78	26,46	0,4	33,1
Row 4	948,1	112,9	133,2	14,92	26,6	0,6	35
Row 5	433,2	88,93	97,9	13,78	26,5	1,1	34,1
Row 6	791	60,12	60,91	10,47	25,82	1,7	33
Row 7	937,2	107,6	126,4	5,27	26,33	1,8	32
Row 8	779,7	121	144,2	1,44	26,64	1,4	30,5
Row 9	547,7	112,7	130,3	9,28	26,55	1,4	29,1
Row 10	349,6	104,1	117	17,92	26,45	0,9	27,6
Row 11	167,6	88,75	95,28	26,99	26,28	0,3	25,7
Row 12	27,74	65,86	64,52	36,17	25,88	0,1	25,2

Figure 3.38. An example image of variable data input



```

"Variable parameters"
DNI = LookUp("9 JUNE 2020";TableRun#;1) "[W/m^2]" "Direct Normal Irradiation"
Tf_in = LookUp("9 JUNE 2020";TableRun#;2) "[W/m^2]" "[oC]" "inlet temperature of Therminol 54"
THETA = LookUp("9 JUNE 2020";TableRun#;3) "[W/m^2]" "[degree]" "Angle of Incidence"
v_1 = LookUp("9 JUNE 2020";TableRun#;4) /18000 "[m^3/s]" "HTF velocity of 1 loop"
v_6 = LookUp("9 JUNE 2020";TableRun#;5) "[W/m^2]" "[oC]" "inlet temperature of Therminol 54"
T_amb = LookUp("9 JUNE 2020";TableRun#;6) "[W/m^2]" "[oC]" "inlet temperature of Therminol 54"

T_1ave = (Tf_in+Tf_out) /2
Cp_1 = INTERPOLATE(Therminol54;'Cp';T;T=T_1ave) "[J/kg-K]"
RHO_1 = INTERPOLATE(Therminol54;'RHO';T;T=T_1ave) "[kg/m^3]"

q_12conv = v_1*5*RHO_1*Cp_1*(Tf_out-Tf_in)

```

Figure 3.39. Defining variable parameters

Then, New Parametric Table is created to calculate automatically the $T_{f_{out}}$, optical and thermal efficiency, and other heat transfers as shown in Fig 3.40(a). After this process, the parametric table is solved to calculate heat transfers and efficiencies as shown in Fig 3.40(b).

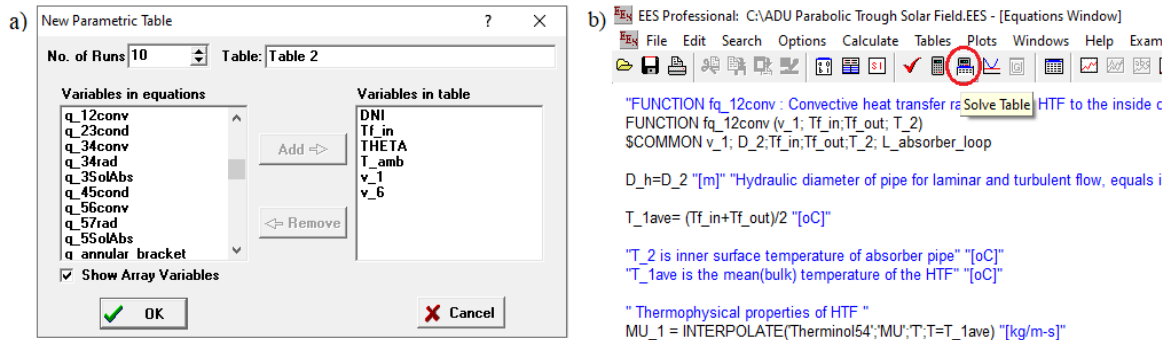


Figure 3.40. EES windows: Creating new parametric table (a), and solving table (b)

Thus, all calculations are completed, and now, all solutions can be displayed.

Run	DNI [W/m ²]	T _{f_in} [oC]	T _{f_out} [oC]	η _{Col} [%]	η _{OptEff,env} [%]	q _{12conv} [W]	q _{heat,loss} [W]	T _{1ave}	q _{5SolAbs} [W]	q _{3SolAbs}	q _{solar,field}
Run 1	529.7	110.5	141	45.14	0.8302	402526	273057	125.7	14808	636897	891806
Run 2	709.4	102.6	147.6	50.88	0.8199	600101	274127	125.1	19340	831823	1,179E+06
Run 3	850.8	107.3	163.5	54.34	0.8085	759172	256394	135.4	22592	971679	1,397E+06
Run 4	948.1	112.9	173.1	52.97	0.8038	820411	300659	143	24899	1,071E+06	1,549E+06
Run 5	433.2	88.93	113.8	46.12	0.8085	328056	195074	101.4	11503	494765	711385
Run 6	791	60.12	118.6	56.75	0.8199	746362	219637	89.34	21566	927552	1,315E+06
Run 7	937.2	107.6	167.1	50.77	0.8302	800985	385190	137.3	26199	1,127E+06	1,578E+06
Run 8	779.7	121	166.5	47.19	0.832	621865	376325	143.8	21928	943140	1,318E+06
Run 9	547.7	112.7	140.9	41.65	0.8231	380580	308907	126.8	15043	647008	913855
Run 10	349.6	104.1	118.2	33.38	0.7892	187725	222856	111.2	8877	381806	562444
Run 11	167.6	88.75	92.69	20.32	0.7271	51312	121365	90.72	3672	157912	252477
Run 12	27.74	65.86	63.9	0	0.638	-24451	50688	64.88	483.1	20778	37862

Figure 3.41. Displaying results

4. RESULTS

In this chapter, experimental and theoretical investigation of ADU Solar Field and model validation are presented. The theoretically and experimentally performance analysis of the field was carried out in EES program considering different days and different hours of certain summer months in which parabolic trough collectors operated full day. The analysis was also conducted for 2020 year, but February, March, July, and December could not be taken into account because of malfunction. One day in months in which the collector operated full day and in steady-state condition was taken into account so as to determine average annual performance of the field. DNI, HTF flow rate, wind speed, angle of incidence, ambient temperature, real inlet temperature of HTF was employed. Average thermal efficiency, heat gain, heat loss and outlet temperature comparisons between experimental and modeled results were plotted.

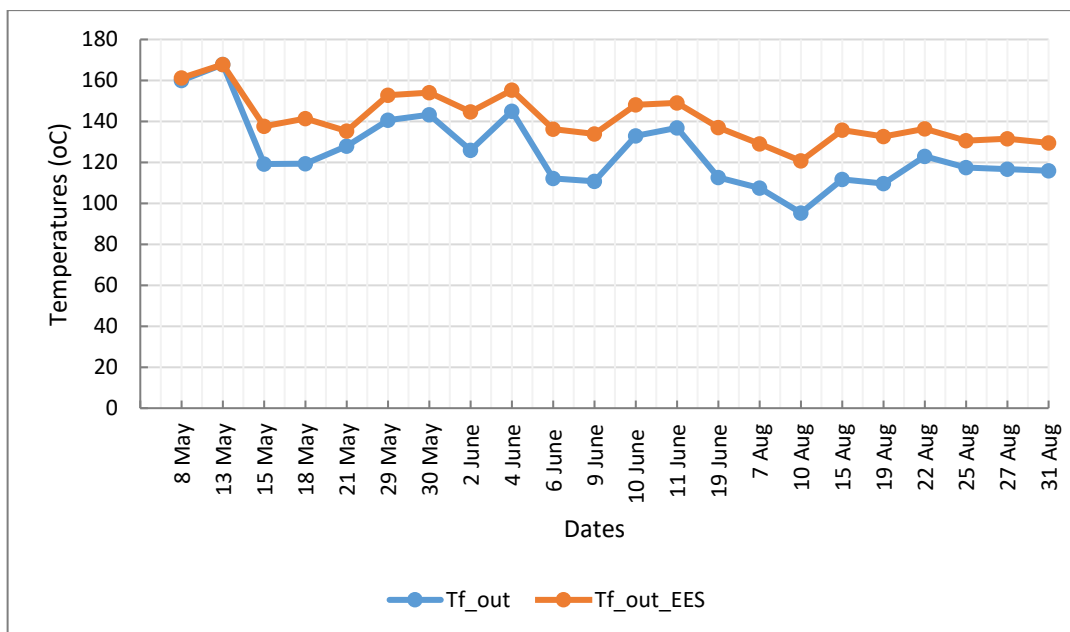


Figure 4.1. Variation of average outlet temperatures with respect to date

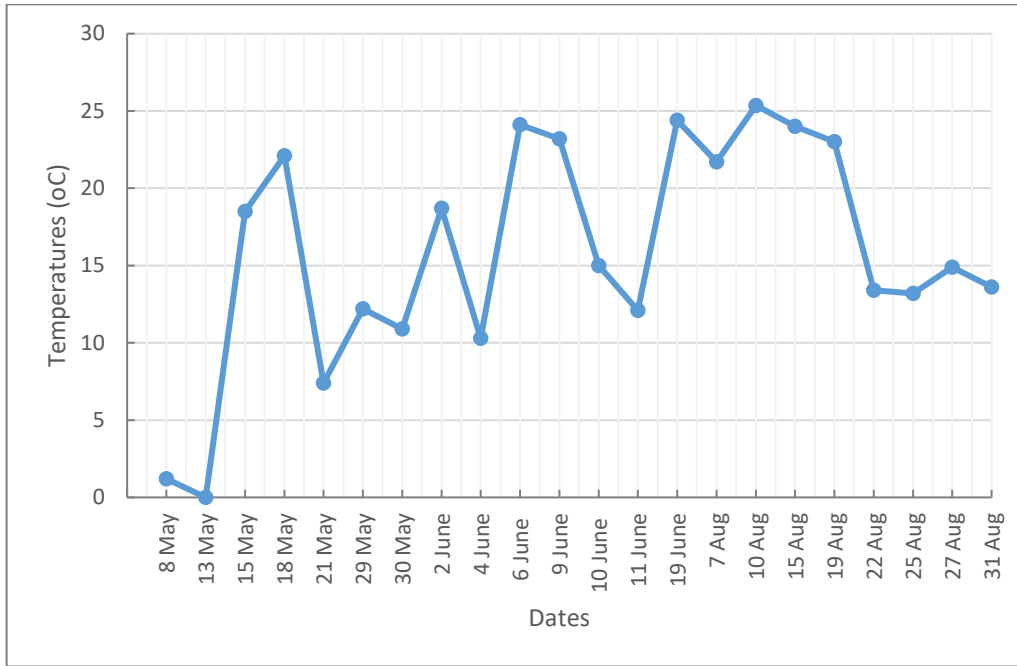


Figure 4.2. Variation of modeled and experimental average outlet temperature difference (ΔT)

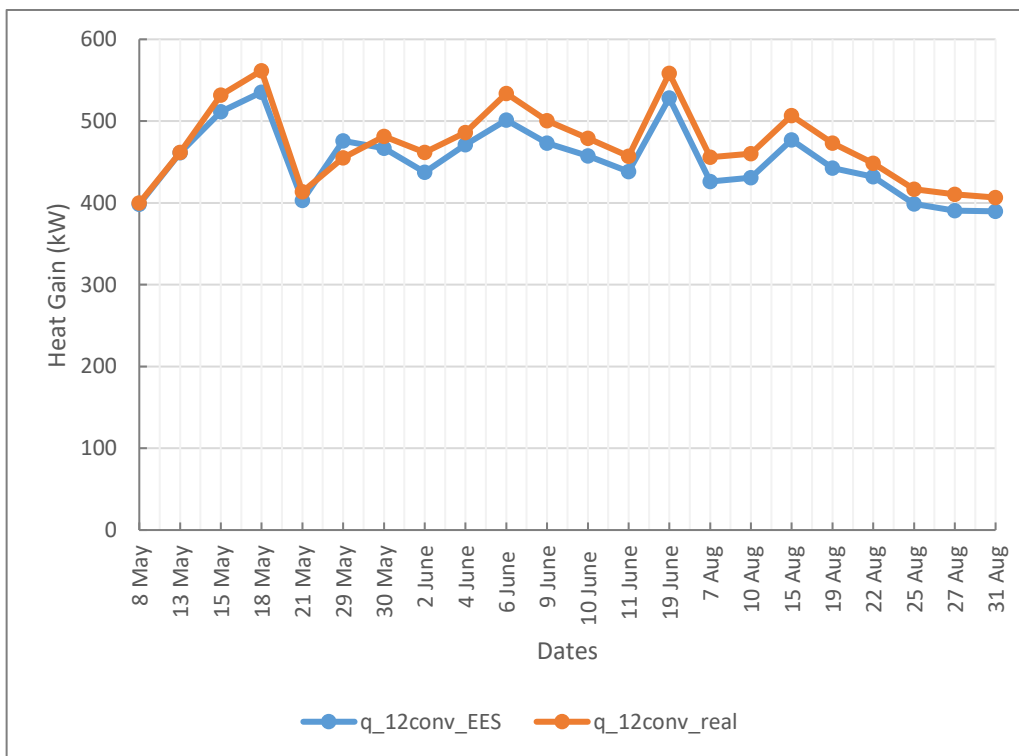


Figure 4.3. Variation of average collected energy with respect to date

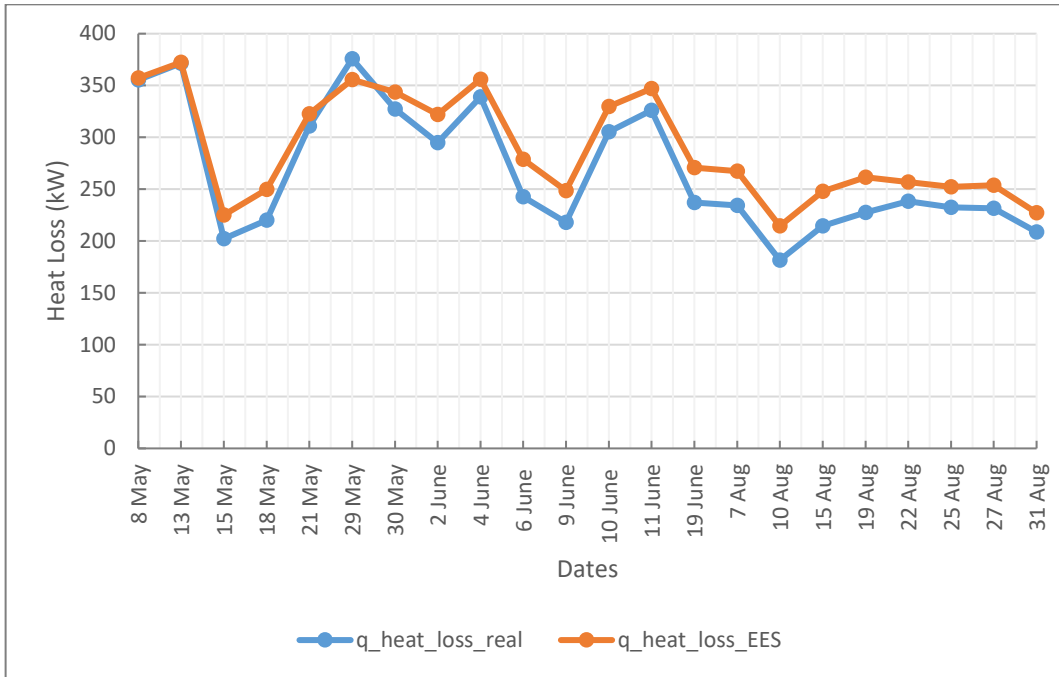


Figure 4.4. Variation of average heat loss with respect to date

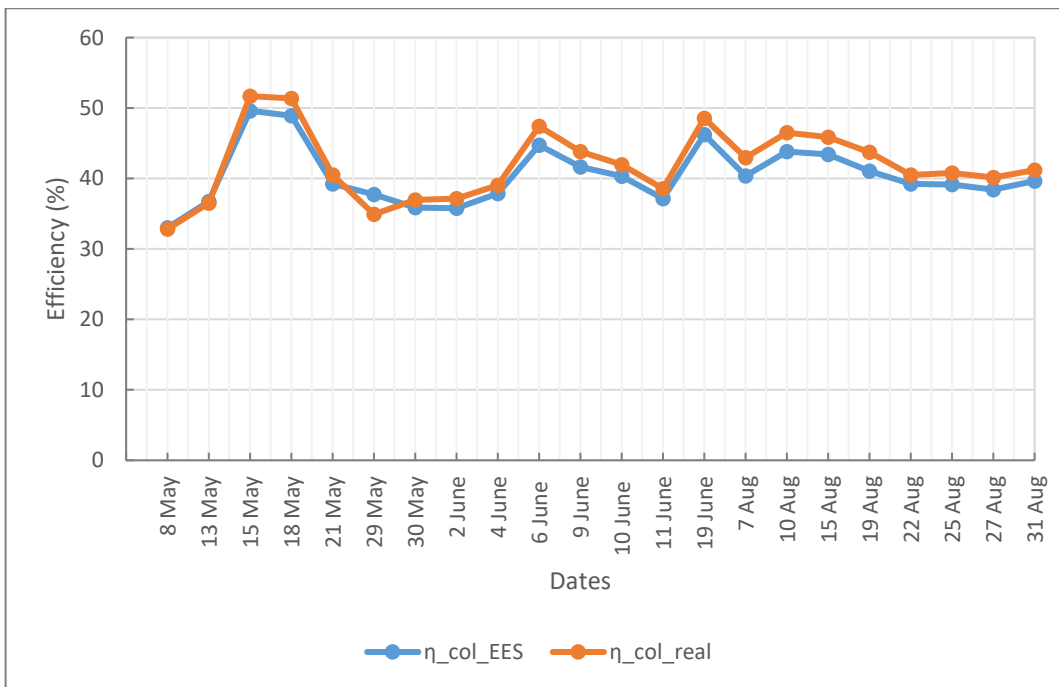


Figure 4.5. Variation of average thermal efficiency with respect to date

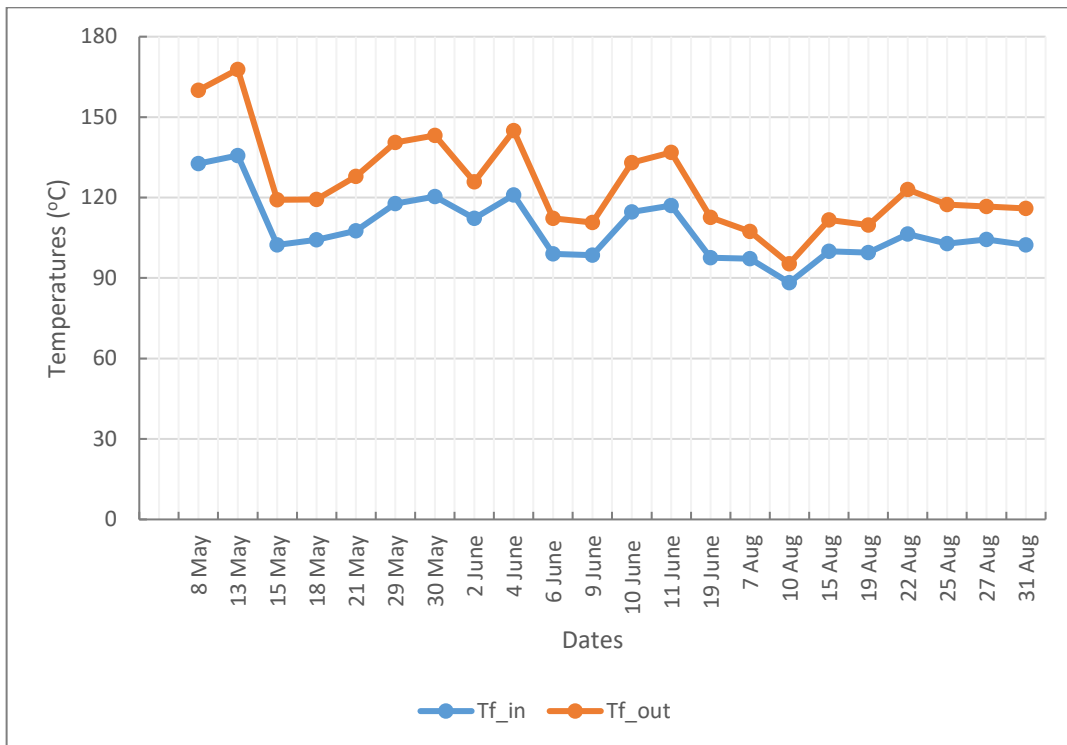


Figure 4.6. Variation of experimental inlet and outlet temperatures

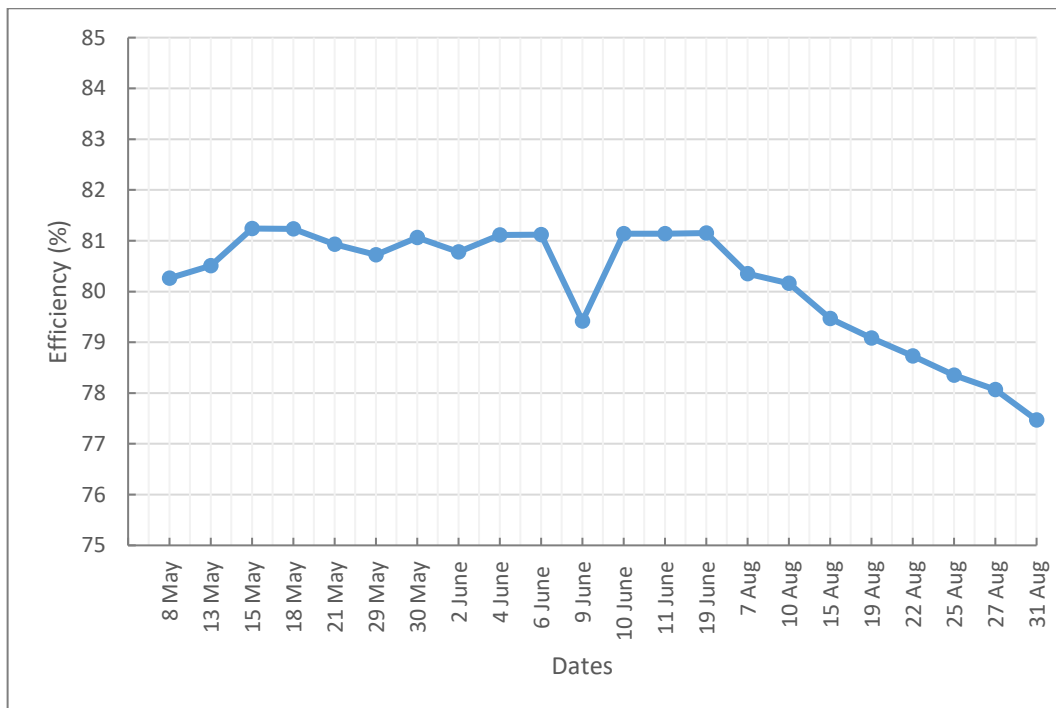


Figure 4.7. Variation of optical efficiency with respect to date

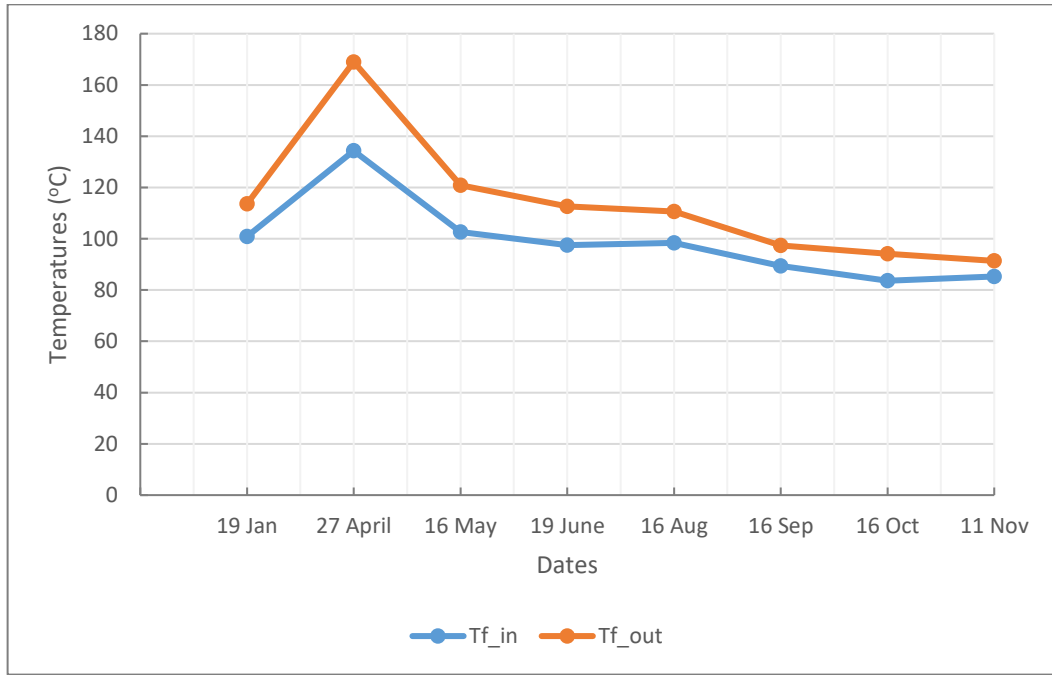


Figure 4.8. Variation of inlet and outlet of annual average temperatures

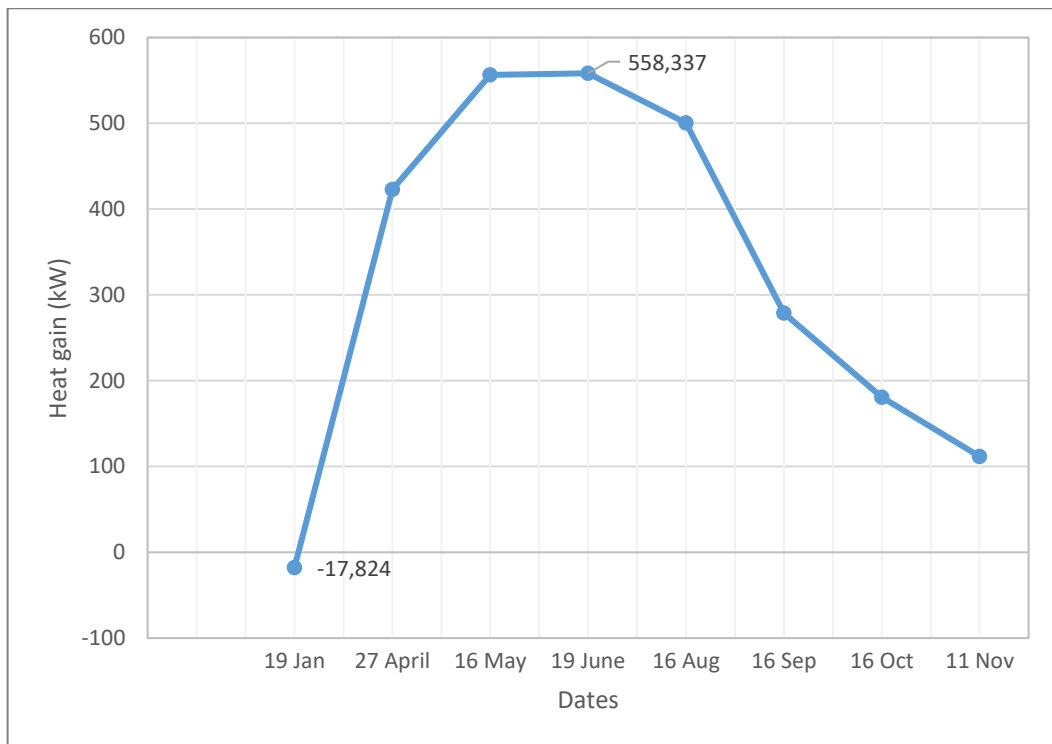


Figure 4.9. Variation of average annual heat gain

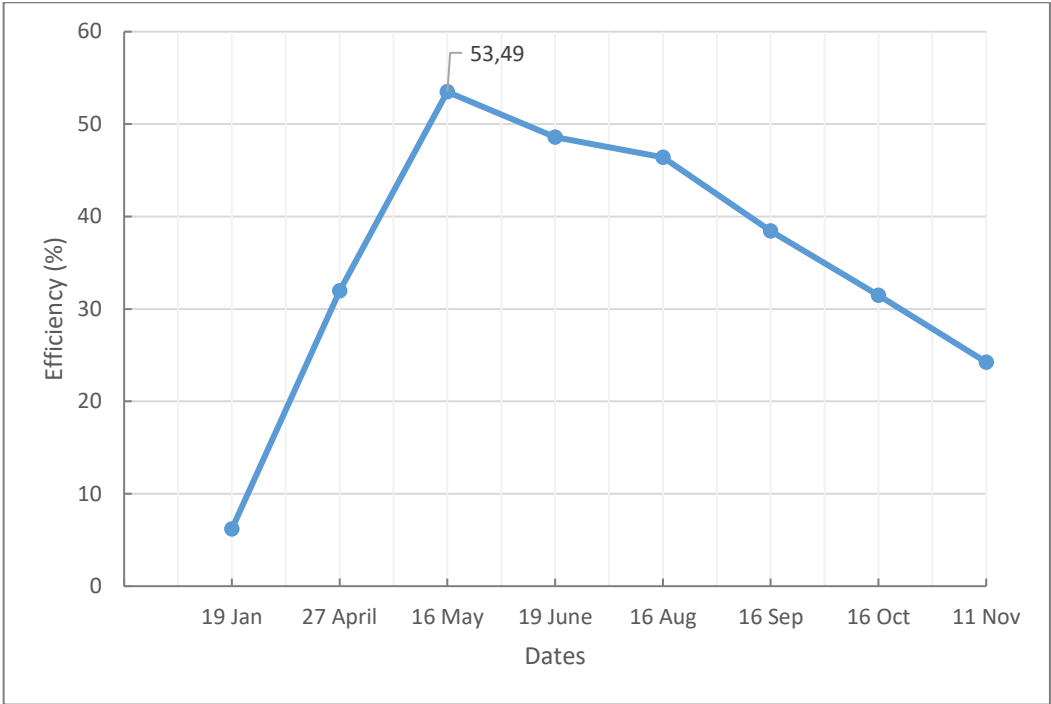


Figure 4.10. Variation of average annual thermal efficiency

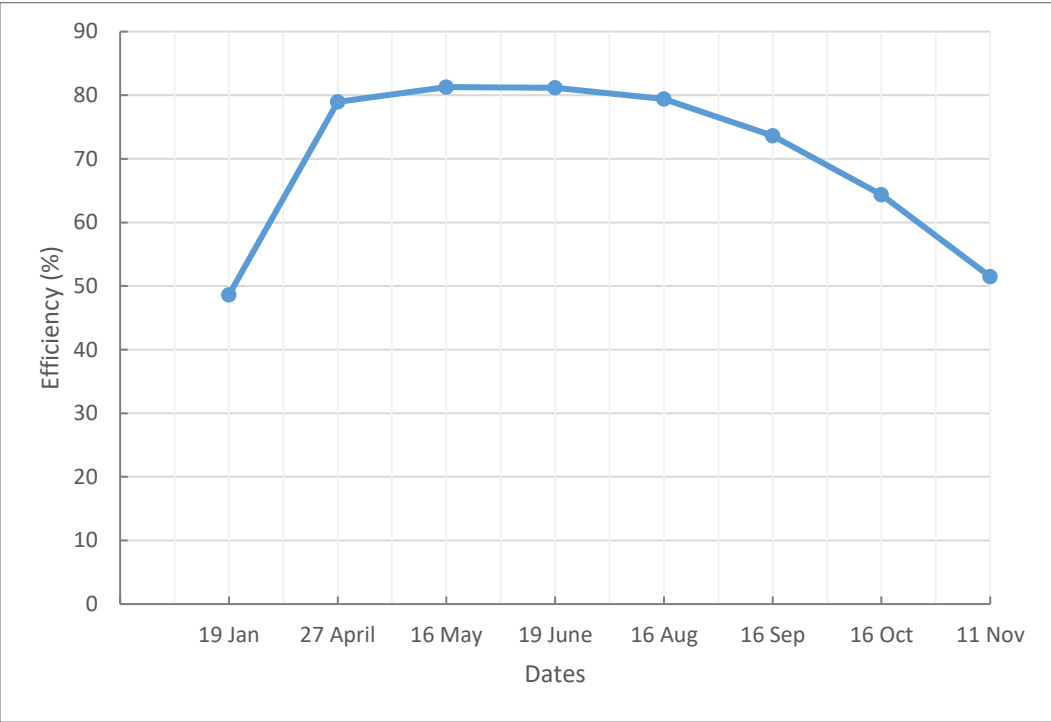


Figure 4.11. Variation of average annual optical efficiency

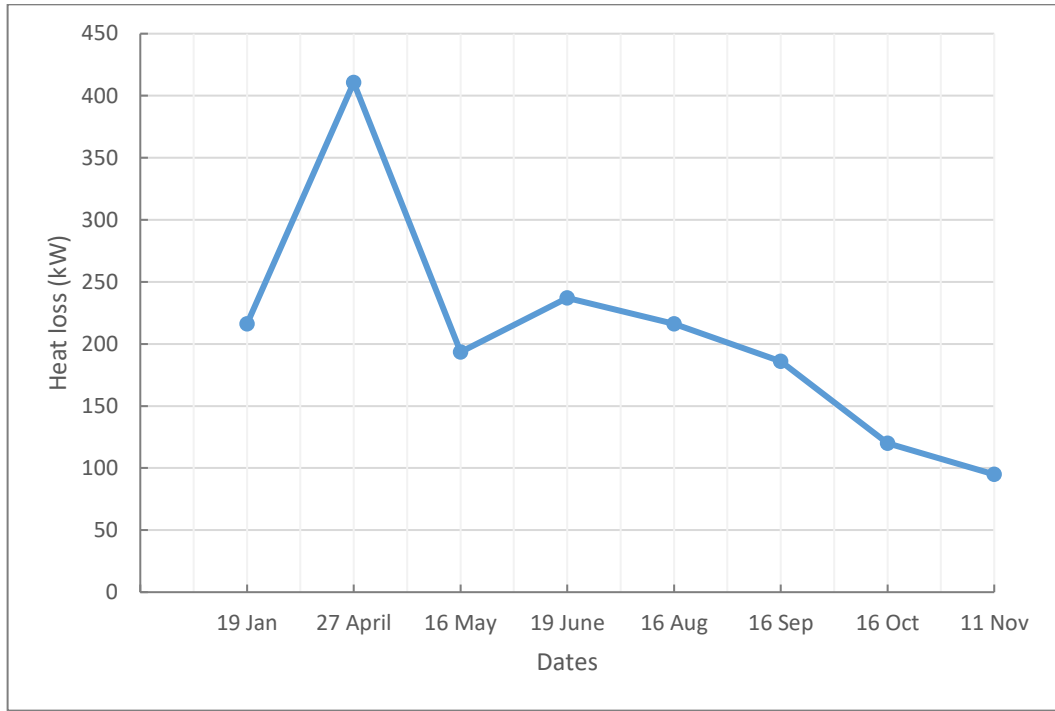


Figure 4.12. Variation of average annual heat loss

5. DISCUSSIONS

Figure 4.1. explains the comparison of average outlet temperature difference between EES modeling and experimental results. It is understood from the figure that maximum outlet temperatures for theoretical and experimental results were observed in the 13 May with the value of 167,8 °C for both. The highest DNI value was measured on this date, the DNI and low wind speed affected the results. When other days are examined, it is seen that maximum divergence were obtained on 10 August with 25,36 °C temperature difference. On the other hand, minimum average outlet temperatures of theoretical and experimental results were also observed in 10 August with the value of 120,7 °C and 95,34 °C respectively. Generally, it was deduced that theoretical results converged to experimental results with the average error of 11,62%.

Figure 4.2. explains the average temperature difference between theoretical and experimental results. It is understood from the figure that minimum delta T occurred in 13 May with the difference and error of 0, and maximum delta T occurred on 10 August with the 25,36 °C difference and 21,01% error. It is also seen that the fluctuations because of temperature difference considerably decreased towards end of the August. When examined generally, it was deduced that average temperature difference occurred with the value of 15,88 °C.

Figure 4.3. shows the comparison of average collected energy (heat gain) between theoretical and experimental results. As it is seen in the figure, the results obtained on 13 May are very close of each other with the difference of approximately value of 0,5 kW, and error of 0,11%. On the other hand, the great divergence was obtained on 7 August. The DNI values were measured quietly low when compared, so, the solar energy input to solar field was low and this was affected the collector outlet temperature. The peak value for actual heat gain was obtained on 18 May with the value of 561,68 kW, and vice versa minimum actual heat gain was seen on 8 May with the value of 399,78 kW. On the other hand, the maximum and minimum heat gains were obtained for EES on 18 May with the value of 535,32 kW, and on 8 May with the value of 398,5 kW respectively. According to EES 452,12 kW average heat gain was calculated. The solar field was gained in reality average 470,89 kW energy. In

general, great difference was not determined between them, and they are almost close to each other for all other days, average error was calculated as 4,54%, and this is good result.

Figure 4.4. explains the comparison average heat loss between model and real data with respect to dates. As it is seen in figure, the best convergence was obtained with the error of 0,19% on 13 May again. The peak value in reality was seen on 29 May with the approximate value of 376 kW. In real, heat loss started with the value of 181,5 kW and climbed up to 375 kW. The minimum heat loss for experimental was seen on 15 May with the approximate value of 202,2 kW. The great divergence was obtained on 10 August with the difference value of 32,896 kW and error of 15,34%. According to EES, the solar field reached its peak and minimum value on 13 May with the value of 372,26 kW and on 10 August with the value of 214,45 kW respectively. Generally, it was deduced that the solar field was lost in reality average 267,95 kW heat, and average error was determined as 8,51% and that is good result.

Figure 4.5. shows the comparison of average thermal efficiency between theoretical and experimental results with respect to date. The best convergence was obtained on 8 May with the error of 0,58%, and vice versa the great divergence was seen on 29 May with the error of 7,53%. The solar field actually reached its maximum and minimum values in 15 May with the value of 51,69%, and on 8 May with the value of 32,82% respectively. High angle of incidence, low ambient temperature, low heat gain and high heat loss rate can be shown in between the reasons of this low efficiency. According to EES, the maximum and minimum efficiencies were obtained on 15 May with the value of 49,61% and on 8 May with the value of 33,01% respectively. Generally, great divergence was not determined between theoretical and experimental results, actual average thermal efficiency was calculated as 41,96%. It was concluded that theoretical results converged to experimental results with the average error value of 4,38%.

Figure 4.6. explains variation of average real inlet and outlet temperature distribution with respect to date. When the diagram was considered, it is seen that the average maximum difference was on 13 May. Normally, it is expected that the approximate temperature difference between inlet and outlet is 25-30 °C. From the diagram, it is understood that the solar field achieved this for this date. The oil started warming up with the lowest value of 88,27 °C and reached its maximum value of 167,8 °C during the summer months. The least delta T value was observed on 10 August with the value of 7,07. It is thought that the reason

of this low delta due to low DNI value and measurement error. Generally, it was recorded that the HTF entered the field with the approximate average value of 108,3 °C and abandoned the field with the value of 125,1 °C.

Figure 4.7. shows the average variation optical efficiency of the solar field with respect to date. As it is obviously seen in the figure, solar field reached its maximum efficiency on 15 May with the value of 81,24%, and the lowest efficiency on 31 August with the value of 77,47%. High angle of incidence that affects the incidence angle modifier caused this decline. When the diagram generally examined, it is seen that the efficiency started to continuously diminish after 19 June. The average efficiency of glass envelope was calculated as 80,16%. Thus, the evaluation of summer months was completed. In the following parts, the annual evaluation of the solar field will be done.

Figure 4.8. explains the variation of inlet and outlet of annual average temperatures with respect to months. It is seen from the figure that the temperatures difference continuously decreased after April. The field reached its peak outlet value on this date with 169 °C. The least outlet value was measured as 85,27 °C in November due to lowest DNI measured and high angle of incidence. On the other hand, the minimum and peak values of inlet temperature was observed in November with the value of 85,27 °C and April with the value of 134,3 °C respectively. It is also seen that the inlet value continuously decreased after April. Generally, it was deduced that the HTF enters the system with the average value of 99,01 °C, and leaves the system with the average value of 113,7 °C.

Figure 4.9. shows the variation of average annual heat gain. Firstly, it is seen that average heat gain is negative in January due to inside surface temperature of absorber tube is less than the average temperature of the HTF. So, the solar field could not reach any heat gain during this day. Sure, this negative value affected the average annual heat gain value of the solar field. Secondly, it is deduced that the heat gain continuously increased until June, and reached its peak value in June with the approximate value of 558,3 kW, after this point, it again continuously decreased until November with the value of 111,74 kW. Generally, when the data were evaluated, the solar field gained 323,93 kW average heat annually.

Figure 4.10. explains the variation of average annual thermal efficiency. It is seen from the figure that thermal efficiency had the lowest value 6,19% in January, and continuously increased until May, and reached its peak value here with the value of 53,49%. After this

point, it started to continuously decrease until November at which 24,22% value. Generally, it was concluded that the solar field annually operated with the average thermal productivity of 35,1%.

Figure 4.11. shows the variation of average annual optical efficiency. It is seen from the figure the efficiency of the solar field was lowest in January with the value of 48,59% due to high angle of incidence and incidence angle modifier. The peak value was obtained in May with the value of 81,28%, and after this point, it started continuously decrease until November at which 51,48% value. Generally, it was deduced that the solar field exhibited average annual optical performance of 69,85%.

Figure 4.12 explains the variation of average annual heat loss. As it is obviously seen in the figure, the maximum heat loss occurred in April with the value of 410,6 kW, and the least value occurred in November at which 94,8 kW. Fluctuations were observed until June, however, the heat loss continuously diminished after June until November. Generally, the solar field lost average annual 209,3 kW heat.

6. CONCLUSION AND RECOMMENDATIONS

Factors such as the gradually decrease of fossil resources and the increase in population in the developing world have led to an increase in the needs of countries for renewable energy sources and the search for them has begun to increase. Inexhaustible solar energy has an important place among renewable energy sources and is easily accessible. When examined in terms of solar energy potential of Turkey, it has a very important place and in general, it is seen that the necessary importance is not given to solar energy and solar collectors. The usage area of solar energy must be expanded in our country, and depending upon imported energy must be reduced. There are pilot executions of PTSC in our country, as mentioned in introduction part of the thesis, and part of the energy requirement can be met at the end of establishing this collectors in Mediterranean and Southeastern Anatolia whose solar energy potentials are highest in Turkey.

In this thesis study, PTSC which is one of the renewable energy systems has been investigated, and performance analysis carried out. EES program has been utilized for this analysis, simulation studies have been performed for ADU large solar field located in Aydın region. In analysis, the data wind speed, ambient temperature, DNI, angle of incidence belong to 2020 have been used as input parameters, and theoretical results obtained from EES has been compared with experimental results. Generally, average the heat gain, average heat loss, average optical and thermal productivities of the solar field have been evaluated for summer months and annually, and average errors for each of them have been calculated.

According to the outlet temperature data obtained from EES and experimental results, it has been concluded that the theoretical calculations have converged to experimental results with the average error of 11,62%.

According to values calculated with EES, it has been deduced that the average heat gain of the solar field was 452,11 kW for summer months, and 315,61 kW for annual. Average actual heat gain for summer months and annual have been calculated as 470,89 kW and 323,93 kW respectively. It has also been concluded that the average error of heat gain for summer months is 4,54%, and this is an excellent agreement. According to outlet temperature results of EES and experimental data, it has been concluded that theoretical results have

converged to experimental results with the average error of 11,62%. The average value of delta T has been calculated as 15,88 °C.

Average actual and theoretical heat losses for summer months have been calculated as 267,95 kW and 289,12 kW respectively. Average heat loss error for summer months has been found as 8,51%, and this is a good result. Average annual heat loss has been calculated as 209,3 kW.

Average actual and theoretical thermal productivities for summer months have been calculated as 41,96% and approximate 40,45%. Errors has been calculated for each date, and average error has been found as 4,38%. When the optical performance of PTSC is considered, the system has exhibited an average optical productivity of 80,16% for summer months, and 69,85% for annual. The new performance analysis studies with PTSC the end loss effect occurred due to length of absorber tube and shading effect of the collector can be taken into account, and 2D analysis of the field may be realized. Moreover, the studies of increasing the thermal efficiency of the system should be carried out, and thus, the usage area of useful energy will be large and efficient.

REFERENCES

- Abed, N., Afgan, I., Cioncolini, A., Iacovides, H., & Nasser, A. (2020). Assessment and Evaluation of the Thermal Performance of Various Working Fluids in Parabolic Trough Collectors of Solar Thermal Power Plants under Non-Uniform Heat Flux Distribution Conditions. *Journal of Energies*, 13(15), 1–27. <https://doi.org/10.3390/en13153776>
- Akba, T. (2014). *Modelling, Transient Simulations and Parametric Studies of Parabolic Trough Collectors With Thermal Energy Storage*. M. Sc. Thesis, Middle East Technical University Graduate School of Natural and Applied Sciences, Ankara.
- Akkoç, S. (2012). *Birleşik Parabolik Yoğunlaştırıcı Güneş Kollektörleri ile Su Isıtma Sisteminin Matematiksel Modeli, Simülasyonu ve Performans Analizi*. Yüksek Lisans Tezi, Başkent Üniversitesi Fen Bilimleri Enstitüsü, Ankara.
- Akusta, E. (2019). *Yenilenebilir Enerji, Büyüme ve Çevre İlişkisi: Türkiye Örneği*. Yüksek Lisans Tezi, Kırklareli Üniversitesi Sosyal Bilimler Enstitüsü, Kırklareli.
- Alamılı, A. S. (2019). *Design and Axperimental Investigation of the Parabolic Trough Solar Collector*. M. Sc. Thesis, Erciyes University Graduate School of Natural and Applied Sciences, Kayseri.
- Alfellağ, M. A. A. (2014). *Modeling and Experimental Investigation of Parabolic Trough Solar Collector*. M.Sc. Thesis, Embry-Riddle Aeronautical University College of Engineering, Florida.
- Atlioğlu, A. (1991). *Parabolik Yansıtıcı Güneş Kollektörlerinde Kullanılan Yansıtıcı Malzemeler ve Özellikleri*. Yüksek Lisans Tezi, Gazi Üniversitesi Fen Bilimleri Enstitüsü, Ankara.
- Bakır, A. A. (2014). *Parabolik Oluklu Güneş Kollektörlerinin Tasarımı, İmalatı ve Deneysel Analizi*. Yüksek Lisans Tezi, Karabük Üniversitesi Fen Bilimleri Enstitüsü, Karabük.
- Behar, O., Khellaf, A., & Mohammedi, K. (2015). A Novel Parabolic Trough Solar Collector Model-Validation With Experimental Data and Comparison to Engineering Equation Solver (EES). *Journal of Energy Conversion and Management*. 106(2015), 268-281, <http://dx.doi.org/10.1016/j.enconman.2015.09.045>

- Bellos, E., & Tzivanidis, C. (2018). Enhancing the Performance of Evacuated and Non-Evacuated Parabolic Trough Collectors Using Twisted Tape Inserts, Perforated Plate Inserts and Internally Finned Absorber. *Journal of Energies*, 11(5), 1–28. <https://doi.org/10.3390/en11051129>
- Bellos, E., & Tzivanidis, C. (2020). Polynomial Expressions for the Thermal Efficiency of the Parabolic Trough Solar Collector. *Applied Sciences*, 10(19), 6901. <https://doi.org/10.3390/app10196901>
- Bhutka, J., Gajjar, J., & Harinarayana, T. (2016). Modelling of Solar Thermal Power Plant Using Parabolic Trough Collector. *Journal of Power and Energy Engineering*, 04(08), 9–25. <https://doi.org/10.4236/jpee.2016.48002>
- Bialobrzeski, R. W. (2007). *Optimization of a SEGS Solar Field For Cost Effective Power Output*. M.Sc. Thesis, Georgia Institute of Technology, Atlanta USA.
- Bilgin, E. O. (2019). *Design and Implementation of a Parabolic Trough Solar Collector*. M. Sc. Thesis, Boğaziçi University Institute of Graduate Studies in Science and Engineering , İstanbul.
- Boukelia, T., Mecibah, M., & Laouafi, A. (2016). Performance simulation of parabolic trough solar collector using two fluids (thermic oil and molten salt). *Journal of Fundamental and Applied Sciences*, 8(2), 600–626. <https://doi.org/10.4314/jfas.v8i2.28>
- BPF. (2017). *Boldport Fasteners (BPF): Compherensive Fastening Solutions, Medium Carbon Steel, AISI 1040*. Accessed from: <https://boltport.com/materials/medium-carbon-steel/aisi-1040/> Accessed Date: 04.05.2021
- Cicibıyık, C. (2012). *Parabolik Oluk Tipi Güneş Kollektörleri ile Enerji Üretimi*. Yüksek Lisans Tezi, Gazi Üniversitesi Fen Bilimleri Enstitüsü, Ankara.
- Coccia, G., Nicola, G. D., & Hidalgo, A. (2016). *Parabolic Trough Collector Prototypes for Low-Temperature Process Heat*. Switzerland: Springer International Publishing.
- CR. (2020). *Construction Review Online (CR): World's Tallest Concentrated Solar Power Tower Installed*. Accessed from: <https://constructionreviewonline.com/news/worlds-tallest-concentrated-solar-power-tower-installed/>. Access Date: 30.11.2020

- Çakıcı, D. M. (2016). *Thermal Modeling of a Geothermal Powered Organic Rankine Cycle Integrated With Parabolic Trough Solar Collector*. M. Sc. Thesis, Dokuz Eylül University Graduate School of Natural and Applied Sciences, İzmir.
- Çengel, Y.A., Ghajar, A.J. (2014). *Heat and Mass Transfer: Fundamentals & Applications* (5th Ed). USA: McGraw-Hill Education.
- Demirci, M. (2015). *Güneş Termik Santrallerinde Kullanılan Bir Parabolik Güneş Kollektörünün Termal Hidrolik Analizi*. Yüksek Lisans Tezi, Gazi Üniversitesi Fen Bilimleri Enstitüsü, Ankara.
- DLR. (2011). *Deutsches Zentrum für Luft- und Raumfahrt: Dish-Sterling System*. Accessed from: https://www.dlr.de/content/en/images/2011/4/dish-sterling-system_3750.html. Access Date: 30.11.2020
- Duffie, J. A., & Beckman, W. A. (2013). *Solar engineering of thermal processes*. (4th Ed). New Jersey, USA: John Wiley & Sons.
- Dündar, S. (2019). Parabolik yoğunlaştırıcı toplayıcı-yansıtıcı yüzeyin matematiksel modellenmesi. *Dicle Üniversitesi Mühendislik Fakültesi Dergisi (DÜMF)*, 10(1), 131–138. <https://doi.org/10.24012/dumf.397018>
- Eastman. (n.d). *Therminol 54 Heat Transfer Fluid* (Publication No: TF-5353B) Eastman Chemical Company, Kingsport, USA.
- EİGM. (2019). *Enerji İşleri Genel Müdürlüğü: Güneş Enerjisi Potansiyel Atlası (GEPA)*. Accessed from: <https://gepa.enerji.gov.tr/MyCalculator/>. Access Date: 23.10.2020.
- Elmohlawy, A. E., Kazanjan, B. I., & Ochkov, V. F. (2018, June 13-14). *Modeling and Performance Prediction of Solar Parabolic Trough Collector for Hybrid Thermal Power Generation Plant Under Different Weather Conditions* [Conference presentation]. American Institute of Physics (AIP) Conference Proceedings 17th Conference of Power System Engineering, Thermodynamics and Fluid Mechanics, Pilsen, Czech Republic.
- Engineering Toolbox. (2019). *Stainless Steel AISI 310- Properties*. Accessed from: https://www.engineeringtoolbox.com/stainless-steel-310-properties-d_2167.html Accessed date: 08.03.2021

- Ercoşkun, G. T. (2013). *Parabolik oluk tipi güneş toplayicisi tasarımı ve deneysel incelenmesi*. Yüksek Lisans Tezi, Mersin Üniversitesi Fen Bilimleri Enstitüsü, Mersin.
- Ersöz, Ö. (2016). *Biyokömürleştirme için Parabolik Güneş Yoğunlaştırıcı Sistem Tasarımı, Kurulumu ve Farklı Biyokütle Kaynakları İçin Optimum İşletme Koşullarının Belirlenmesi*. Doktora Tezi, Ege Üniversitesi Fen Bilimleri Enstitüsü, İzmir.
- Ghasemi, S. E., Ranjbar, A. A., & Ramiar, A. (2013). Three-dimensional Numerical Analysis Of Heat Transfer Characteristics Of Solar Parabolic Collector With Two Segmental Rings. *Journal of Mathematics and Computer Science*, 07(02), 89–100. <https://doi.org/10.22436/jmcs.07.02.02>
- Ghoneim, A. (2014). Performance Analysis of Parabolic Trough Collector in Hot Climate. *British Journal of Applied Science & Technology*, 4(14), 2038–2058. <https://doi.org/10.9734/bjast/2014/8772>
- Günther, M., Joemann, M., & Csambor, S. (2011). *Advanced CSP Teaching Materials: Chapter 5: Parabolic Trough Technology*, enerMENA, DLR, Accessed from: [http://edge.rit.edu/edge/P15484/public/Detailed Design Documents/Solar Trough Preliminary analysis references/Parabolic Trough Technology.pdf](http://edge.rit.edu/edge/P15484/public/Detailed_Design_Documents/Solar_Trough_Preliminary_analysis_references/Parabolic_Trough_Technology.pdf) Access Date: 01.12.2020
- Güven, H. M., & Bannerot, R. B. (1986). Derivation of Universal Error Parameters for Comprehensive Optical Analysis of Parabolic. *Journal of Solar Energy Engineering*, 108(November 1986), 275–281. <https://doi.org/10.1115/1.3268106>
- Hayta, H. (2015). *Theoretical and Experimental Investigation on Thermal Performance of a Parabolic Trough Solar Collector Array*. M. Sc. Thesis, University of Gaziantep Graduate School of Natural & Applied Sciences, Gaziantep.
- Heller, P. (2017). Introduction to CSP Systems and Performance. Peter Heller (Ed.), In *The Performance of Concentrated Solar Power (CSP) Systems: Analysis, Measurement and Assessment: Design and Components of CSP Technologies* (p. 11,15,17). Duxford, UK: Woodhead Publishing.

- Ihsan, S. I., Safian, M. A. I. M., Taufek, M. A. M., & Mohiuddin, A. K. M. (2016, July 25-27). *Improvement Design of Parabolic Trough*. [Conference presentation]. International Conference on Mechanical, Automotive and Aerospace Engineering, Kuala Lumpur, Malaysia.
- Isover Saint Gobain. (2017). *Technical Report: Technical Insulations, Information for Designers and Assembly Companies*. (Publication no:-) Smrčkova, Czechia.
- Isover Saint Gobain. (n.d). *Technical Insulation Materials: Stone Wool: Everything You Need to Know*. Accessed from: <https://www.isover-technical-insulation.com/stone-wool>
Access date: 26.05.2021.
- Izweik, H. T., Ahmed, A. M., & Albusefi, A. A. (2016). Design , Construction , and Experimental Testing of a Parabolic Trough Collector for Process Heat Applications. *International Journal of Innovative Research in Science, Engineering and Technology (IJIRSET)*, 5(9), 15890–15900. <https://doi.org/10.15680/IJIRSET.2016.0509001>
- İşler, G. (2018). *Parabolik Oluk Kollektörleri ve Merkezi Alıcılı Güneş Kuleleri ile Enerji Üretim Analizi ve Uygulaması*. Yüksek Lisans Tezi, Bilecik Şeyh Edebali Üniversitesi Fen Bilimleri Enstitüsü, Bilecik.
- Jeter, S. M., Jarrar, D. I., & Moustafa, S. A. (1983). Geometrical Effects on the Performance of Trough Collectors. *Journal of Solar Energy*, 30(2), 1–5. [https://doi.org/10.1016/0038-092X\(83\)90201-3](https://doi.org/10.1016/0038-092X(83)90201-3)
- Kalogirou, S. A. (2014). *Solar energy engineering: Processes and systems (2nd Ed)*. Oxford UK: Academic Press Elseiver Inc.
- Kılıç, D. (2019). *Parabolik Oluk Tipi Güneş Toplayıcı Güç Santralinin Ysa Tabanlı Optimizasyonu : Bilecik Uygulaması Parabolik Oluk Tipi Güneş Toplayıcı Güç Santralinin Ysa Tabanlı Optimizasyonu*. Yüksek Lisans Tezi, Bilecik Şeyh Edebali Üniversitesi Fen Bilimleri Enstitüsü, Bilecik.
- Kolekar, M. S. T., & Patil, M. P. S. (2018). Performance Analysis Of Solar Parabolic Trough Collector System For Different Concentration Of Al₂O₃ With Water As Base Fluid. *International Research Journal of Engineering and Technology (IRJET)*, 5(7), 2472–2479.

- Kumar, P., Nayak, Y. K., Sinha, U. K., & Kumar, N. (2017). Performance Analysis of Parabolic Trough Collector. *International Journal of Engineering and Technology*, 9(2), 386–394. <https://doi.org/10.21817/ijet/2017/v9i1/170902317>
- Kumbhar, N. A., Shinde, S. R., & Shinde, V. S. (2016). Performance investigation of parabolic trough solar collector integrated with thermal energy storage system. *International Journal of Current Engineering and Technology*, 5(5), 424–430. <https://doi.org/10.14741/ijcet/22774106/spl.5.6.2016.79>
- Liang, H., Zheng, C., Zheng, W., You, S., & Zhang, H. (2017). Analysis of Annual Performance of a Parabolic Trough Solar Collector. *Energy Procedia*, 105, 888–894. <https://doi.org/10.1016/j.egypro.2017.03.407>
- Livatyalı, H. (2011). *Yoğunlaştırılmış Güneş Enerjisi Teknolojileri*. Accessed from: https://www1.mmo.org.tr/resimler/dosya_ekler/c21ec3eb17542d5_ek.pdf
Accessed date: 11.12.2020
- MatWeb. (n.d). *Material Property Data: AISI 1040 Steel, as rolled*. Accessed from: <http://www.matweb.com/search/DataSheet.aspx?MatGUID=c8ada14779744d008a6c3e80f035c5d5&ckck=1> Accessed date: 03.05.2021
- Mohd, S., Arsalan, Y., Singh, D. P., & Singh, A. (2017). Performance Evaluation of Solar Parabolic Trough Collector with Acrylic Mirror Sheet as a Reflector. *International Journal of Research in Engineering and Social Sciences*, 07(06), 1–7.
- Moya, E. Z. (2012). Parabolic-Trough Concentrating Solar Power (CSP). Concentrating Solar Power (CSP) Systems. Parabolic-Trough Concentrating Solar Power (CSP), In Keith Lovegrove and Wes Stein. (Eds), *Concentrating Solar Power Technology: Principles, Developments and Applications* (pp. 208-210), Oxford: Woodhead Publishing Series in Energy.
- Murtuza, S. A., Byregowda, H. V., H, M. M. A., & Imran, M. (2017). Experimental and simulation studies of parabolic trough collector design for obtaining solar energy. *Journal of Resource-Efficient Technologies*, 3(4), 414–421. <https://doi.org/10.1016/j.refit.2017.03.003>

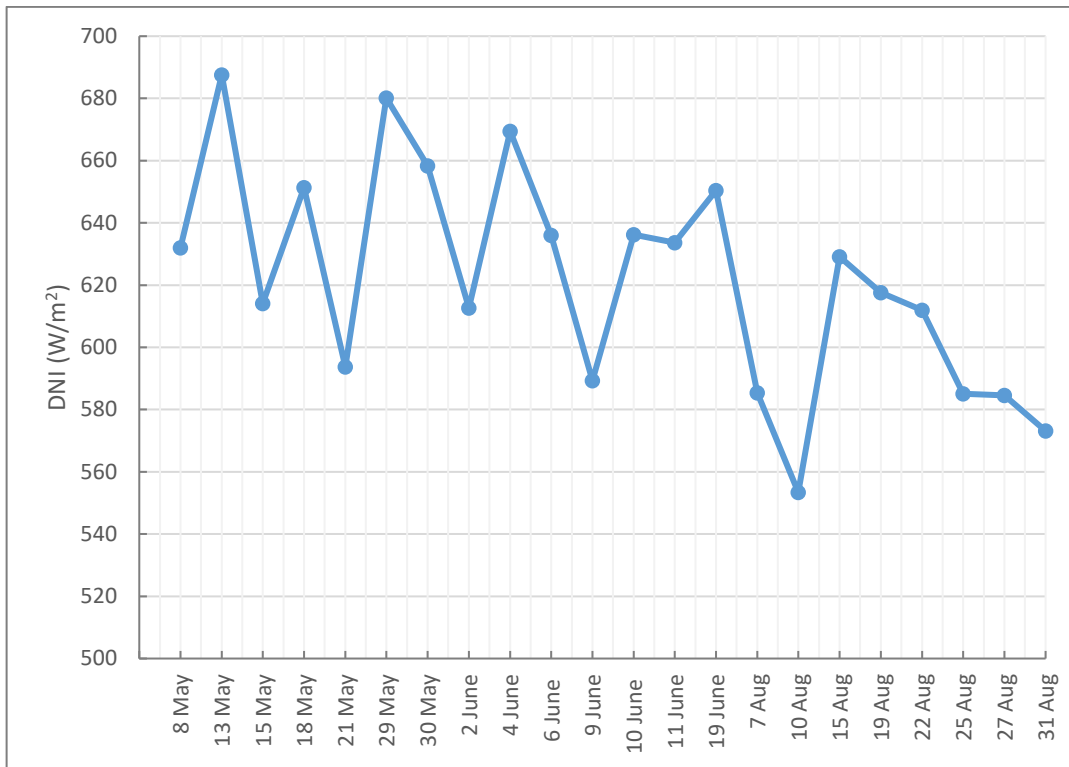
- National Renewable Energy Laboratory. (2003). *Technical Report: Heat Transfer Analysis and Modeling of a Parabolic Trough Solar Receiver Implemented in Engineering Equation Solver (Publication No. TP-550-34169)*. Colorado, USA.
- National Renewable Energy Laboratory. (2011). *Utility-Scale Parabolic Trough Solar Systems: Performance Acceptance Test Guidelines (Publication No: SR-5500-48895)*. Colorado, USA
- Nasa. (2019). *2019 Ozone Hole is the Smallest on Record Since Its Discovery*. Accessed from: <https://www.nasa.gov/feature/goddard/2019/2019-ozone-hole-is-the-smallest-on-record-since-its-discovery>. Access Date: 22.10.2020
- Prakash, E. V., & Rai, A. K. (2018). Performance Optimization of Solar PTC Using Taguchi Method. *International Journal of Mechanical Engineering and Technology (IJMET)*, 9(2), 523–529.
- Quezada-García, S., Sánchez-Mora, H., Polo-Labarríos, M. A., & Cázares-Ramírez, R. I. (2019). Modeling and simulation to determine the thermal efficiency of a parabolic solar trough collector system. *Case Studies in Thermal Engineering*, 16(August). <https://doi.org/10.1016/j.csite.2019.100523>
- Ramesh, J., Kumar, J. K., & Subbareddy, E. . (2015). Design , Fabrication and Performance Analysis of a Parabolic Trough Solar Collector Water. *International Journal of Innovative Research in Science, Engineering and Technology (IJIRSET)*, 4(7), 6038–6043. <https://doi.org/10.15680/IJIRSET.2015.0407122>
- Sahoo, Sudhansu S.Ray, S., Tripathy, A. K., & Singh, S. (2019). Effect of inlet temperature of heat transfer fluid and wind velocity on the performance of parabolic trough solar collector receiver: A computational study. *International Journal of Heat and Technology*, 37(1), 48–58. <https://doi.org/10.18280/ijht.370106>
- Salazar, P. D. T. (2018). *Thermo-Hydraulic Performance Modeling of Thermal Energy Systems Using Parabolic Trough Solar Collectors*. Ph.D Thesis, Tecnológico De Monterrey School of Engineering and Sciences, Monterrey Nuevo Leon.
- Sbp. (2012). *Schlaich Bergermann Partner: Projects: Ultimate Trough Test Loop*. Accessed from: <https://www.sbp.de/en/project/ultimate-trough-testloop/>. Accessed date: 11.12.2020

- Singh, H., & Mishra, R. S. (2018). Performance analysis of solar parabolic trough collectors driven combined supercritical CO₂ and organic Rankine cycle. *Engineering Science and Technology, an International Journal*, 21(3), 451–464. <https://doi.org/10.1016/j.jestch.2018.03.015>
- Solar Energy Research Institute. (1985). *Silver/Glass Mirrors for Solar Thermal Systems*. (Publication No: SP-271-2293). U.S Department of Energy, Colorado, USA.
- Solorio, C. I. R., Salazar, P. D. T., & Nigam, K. D. P., (2020). Parabolic Trough Solar Collectors : A General Overview of Technology , Industrial Applications , Energy Market , Modeling , and Standards. *Journal of Green Processing and Synthesis*, 9(1), 595–649. <https://doi.org/10.1515/gps-2020-0059>
- Soylu, B. N. (2019). *Yenilenebilir Enerji Kaynakları ve Konya İlinin Yenilenebilir Enerji Potansiyeli*. Yüksek Lisans Tezi, Selçuk Üniversitesi Sosyal Bilimler Enstitüsü, Konya.
- Şanlı, G. (2010). *Parabolik Oluk Tipi Güneş Kollektörlerinin Teorik Olarak İncelenmesi*. Yüksek Lisans Tezi, Pamukkale Üniversitesi Fen Bilimleri Enstitüsü, Denizli.
- Şimşek, Ö. (2012). *Parabolik Güneş Kollektörü Tasarımı, İmalatı, Test Edilmesi ve Kırsal Bölgelerde Isıtma Kullanım Alanı Fizibilitesi*. Yüksek Lisans Tezi, Gazi Üniversitesi Fen Bilimleri Enstitüsü, Ankara.
- The World Material. (2020). *US ASTM AISI and SAE Standarts: AISI 310 Stainless Steel Properties, Grade 310 SS Composition*. Accessed from: <https://www.theworldmaterial.com/aisi-310-stainless-steel/>. Accessed Date: 04.05.2021.
- Tijani, A. S., & Roslan, A. M. . (2014, July 2-4). *Simulation Analysis of Thermal Losses of Parabolic Trough Solar Collector in Malaysia Using Computational Fluid Dynamics*. [Conference presentation]. 2nd International Conference on System-Integrated Intelligence: Challenges for Product and Production Engineering, Bremen, Germany.
- Ullah, F., & Min, K. (2018, December 15-17). *Performance Evaluation of Dual-axis Tracking System of Parabolic Trough Solar Collector* [Conference presentation] The 5th Annual International Conference on Material Science and Environmental Engineering (MSEE2017), Xiamen, China.

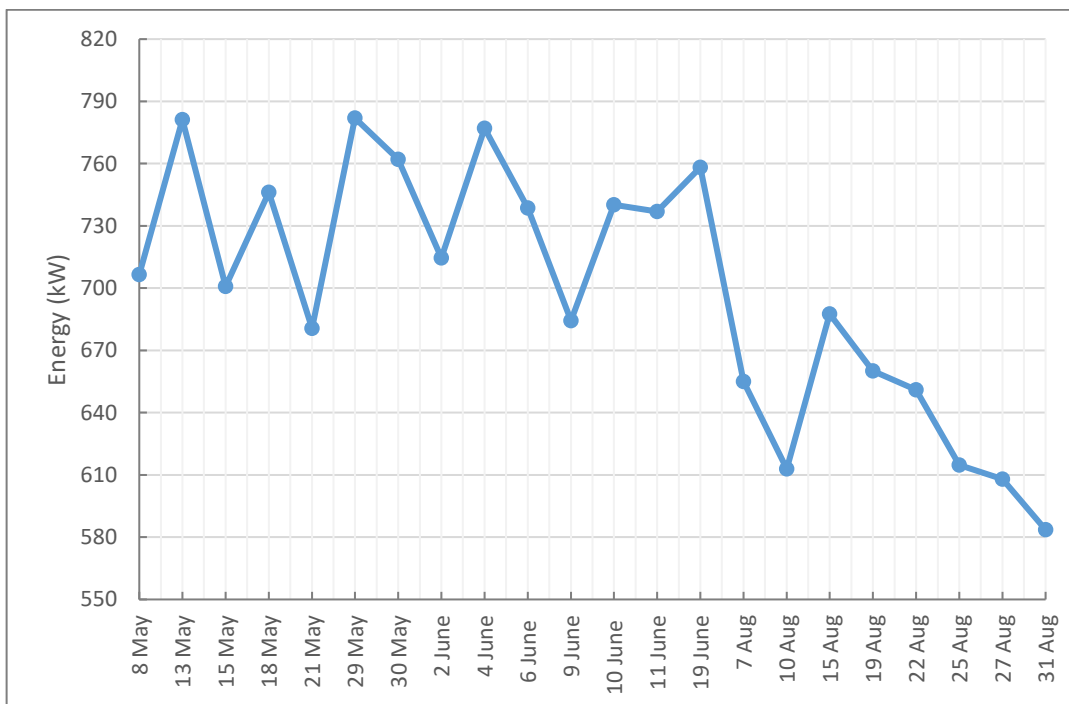
- Üçgöl, İ., Arslan, Ö., Elibüyük, U., & Emen, Y. (2019). *Parabolik Oluk Yoğunlaştırıcı Sistemlerin Isparta Organize Sanayi Bölgesinde Kullanımı*. Accessed from: <https://dergipark.org.tr/tr/download/article-file/900494> Accessed date: 16.10.2020
- Vijayan, G., & Rajasekaran, K. (2020). Performance evaluation of nanofluid on parabolic trough solar collector. *Journal of Thermal Science*, 24(2A), 853–864. <https://doi.org/10.2298/TSCII180509059G>
- Wang, J., Wang, J., Bi, X., & Wang, X. (2016). Performance Simulation Comparison for Parabolic Trough Solar Collectors in China. *Internal Journal of Photoenergy*, 2016(18), 1–16. <https://doi.org/10.1155/2016/9260943>
- Wikipedia. (2006). *Altimeter*. Accessed from: <https://tr.wikipedia.org/wiki/Altimetre> Accessed date: 28.04.2020.
- Woldemicheal, D. E., Cheng, H. K., Woldeyohannes, A. D., & Ing, L. C. (2012). Design Support System for Parabolic Trough Solar Collector. *Journal of Applied Sciences*, 12(23), 2474–2478. <https://doi.org/10.3923/jas.2012.2474.2478>
- Yahi, F., Belhamel, M., Berdja, M., Ouali, A., Tetbirt, Mokrane, M., & Djebiret, M. A. (2020, October 9-11). *Modelling and Exergetic Analysis of a Parabolic Trough Solar Collector* [Conference presentation]. 2019 International Conference on Environment, Resources and Energy Engineering, Bangkok, Thailand.
- Yassen, T. (2012). Experimental and Theoretical Study of a Parabolic Trough Solar Collector. *Anbar Journal for Engineering Sciences (AJES)*, 5(1), 109–125.
- Yeni Kıroba. (2018, February 25). ADÜ’den Dünyaya örnek dev proje.
- Yiğit, A., & Atmaca, İ. (2018). *Güneş enerjisi mühendislik uygulamaları*. Bursa: Dora Basım-Yayın Dağıtım.

APPENDICES

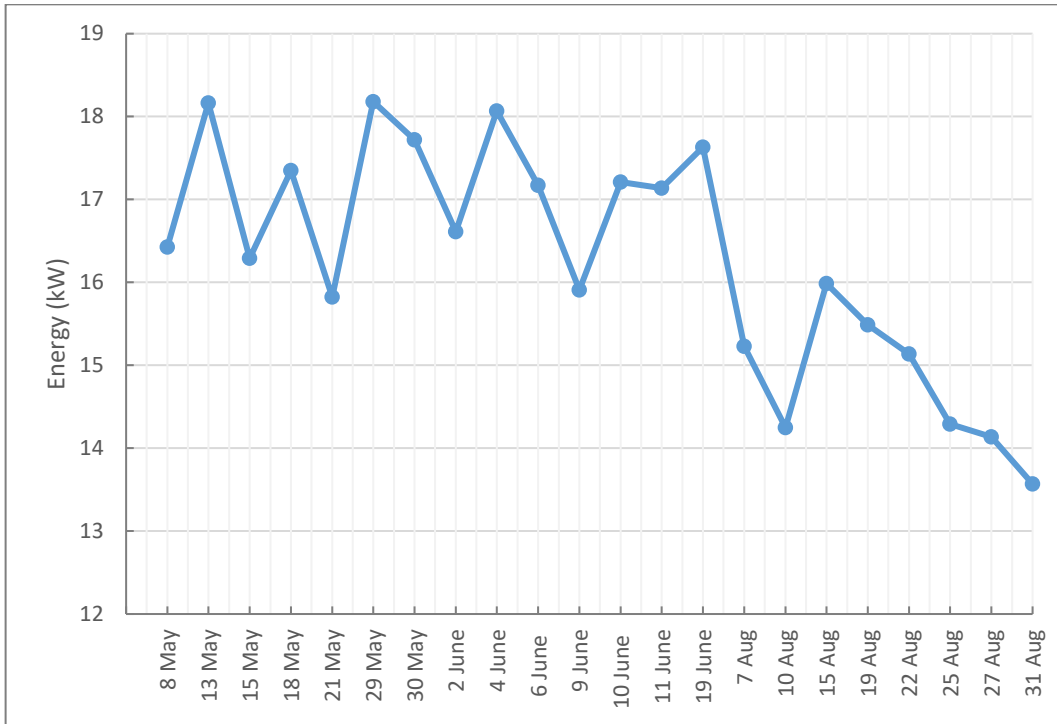
APPENDIX-I



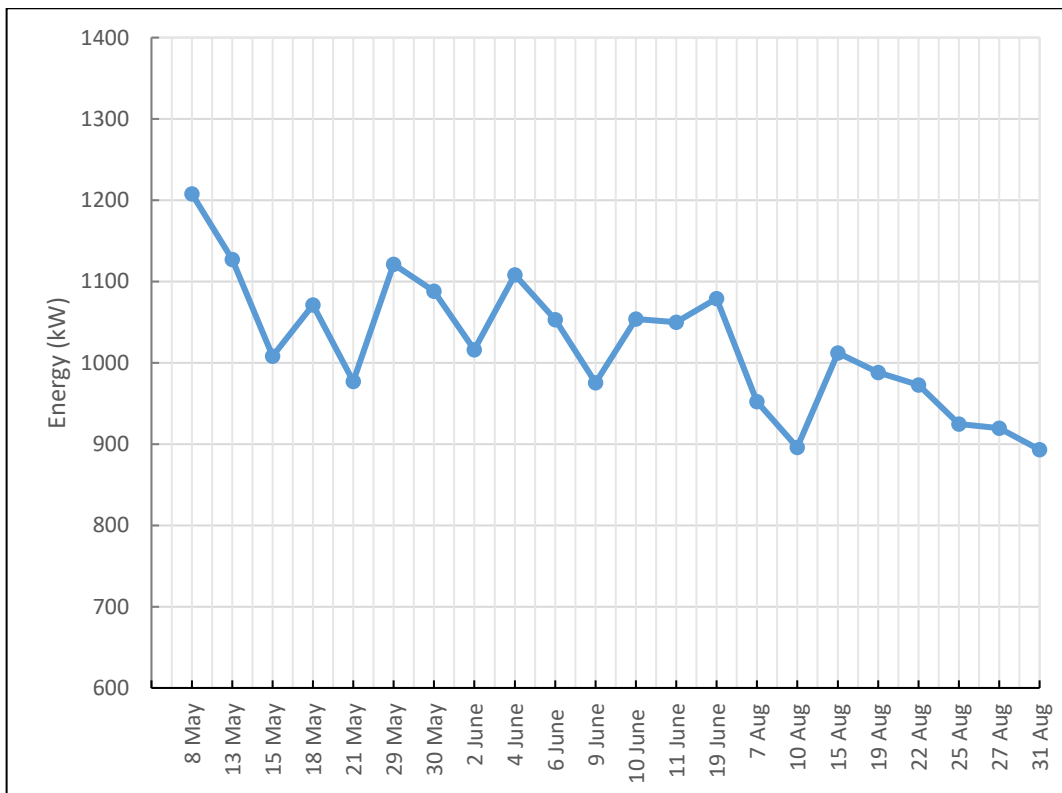
Variation of average DNI with respect to date



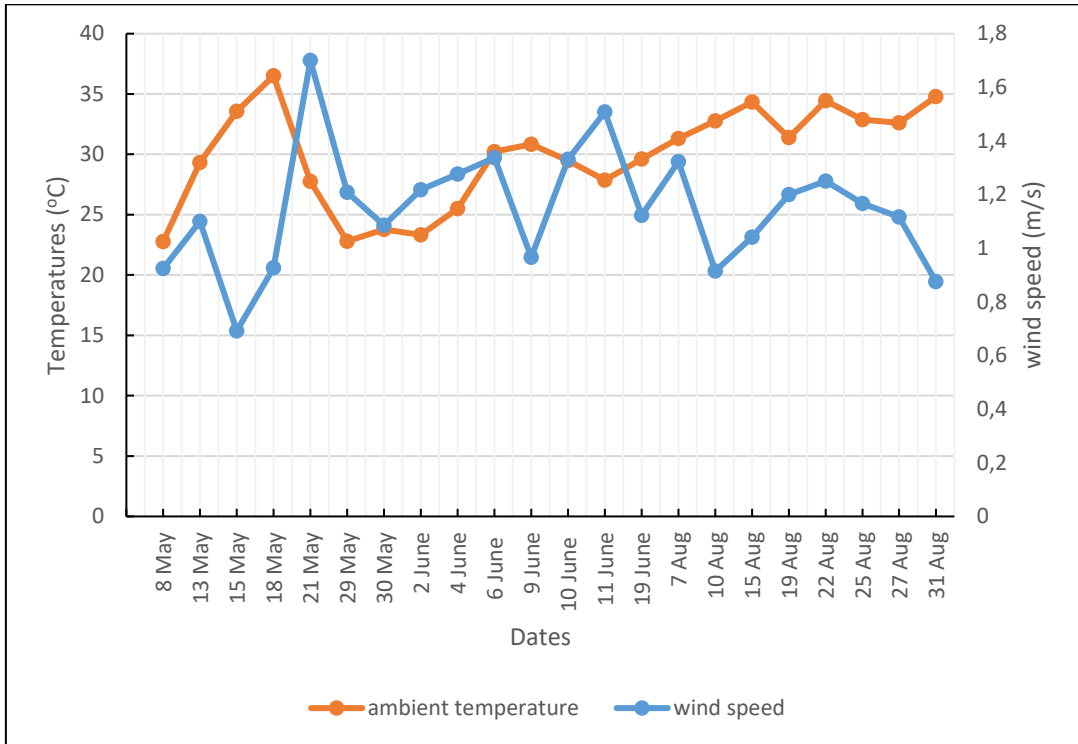
Variation of average energy concentrated on absorber tube



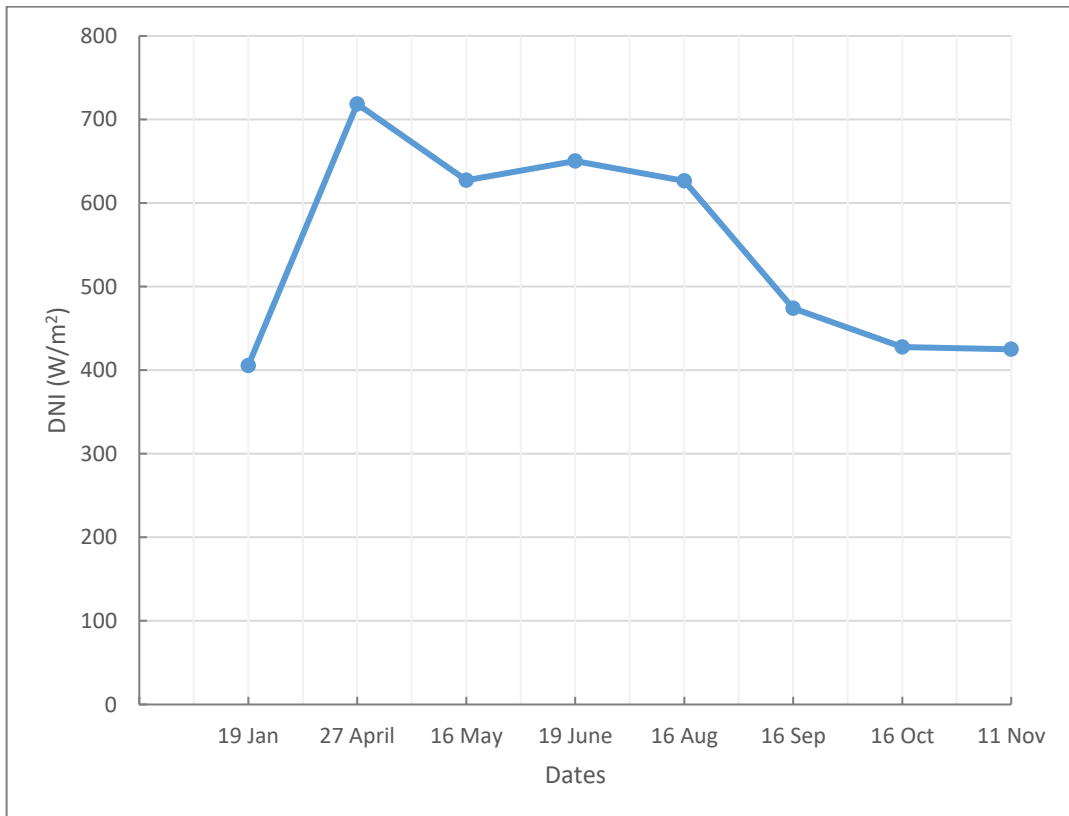
Variation of average energy concentrated on glass envelope



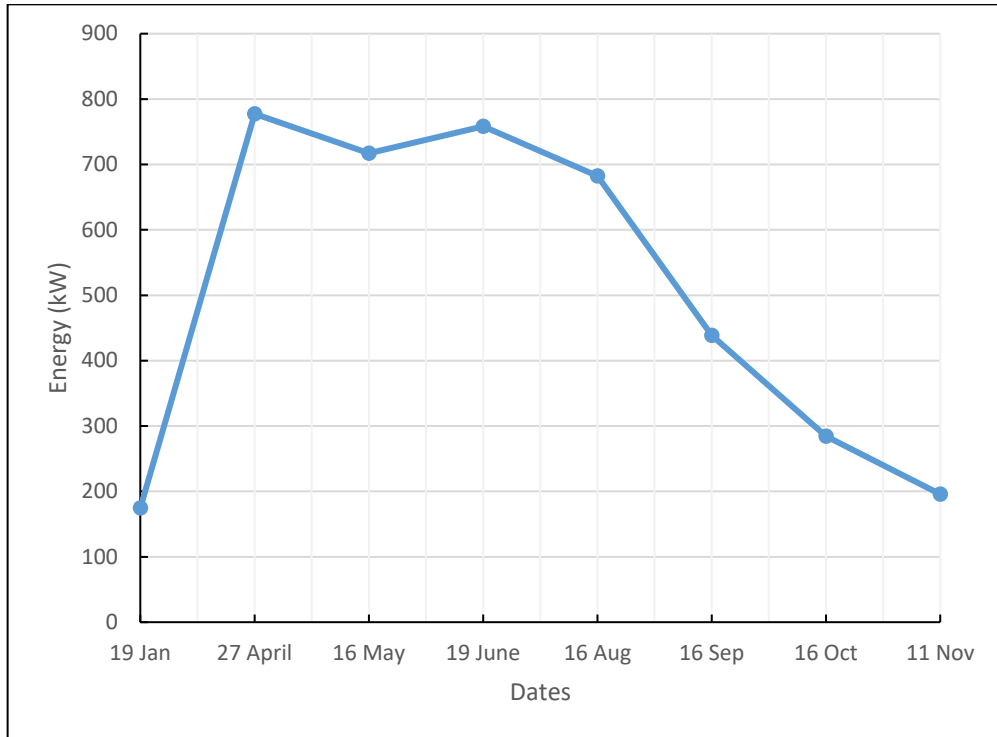
Variation of average solar energy input to the field



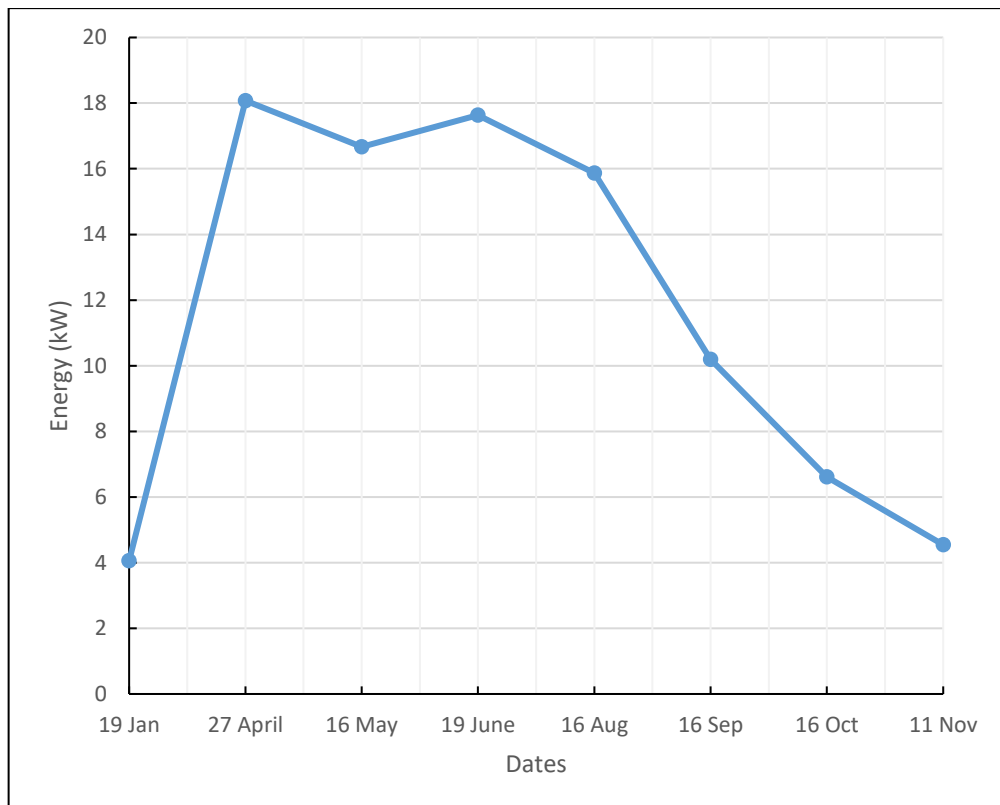
Variation of average wind speed and ambient temperature



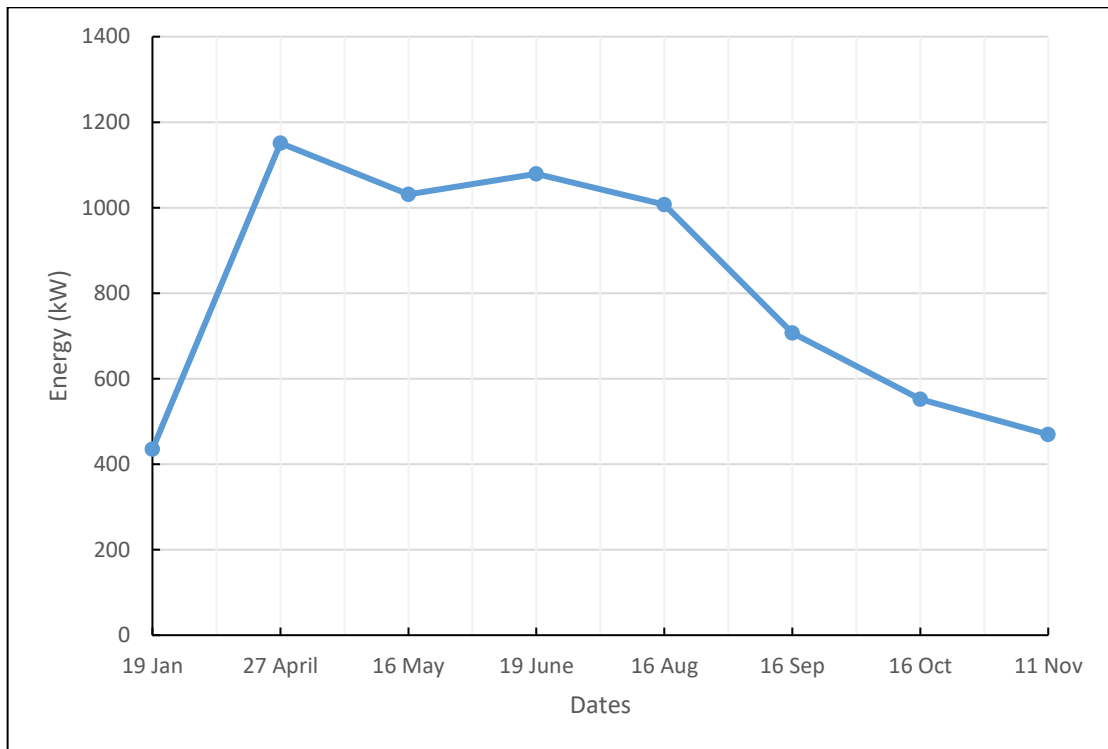
Variation of average annual DNI



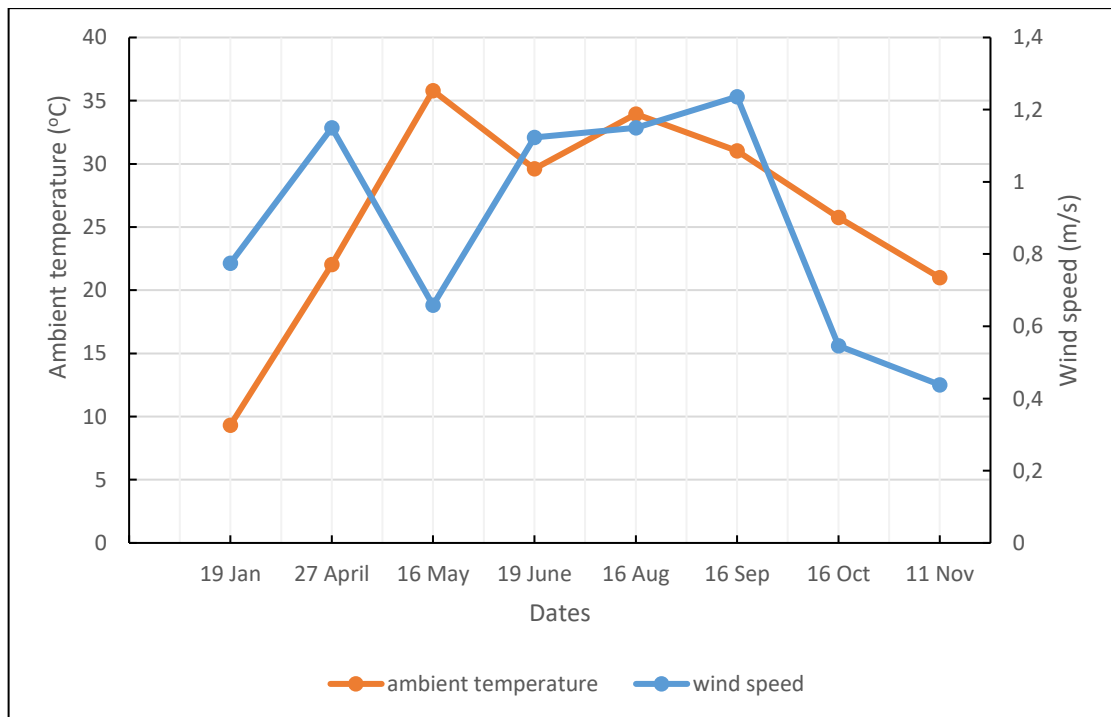
Variation of average annual concentrated energy on absorber tube



Variation of average annual concentrated energy on glass envelope



Variation of average annular solar energy input



Variation of average annual ambient temperature and wind speed

APPENDIX- II

"FUNCTION fq_12conv : Convective heat transfer rate from the HTF to the inside of the receiver tube"

FUNCTION fq_12conv (v_1; Tf_in;Tf_out; T_2)

\$COMMON v_1; D_2;Tf_in;Tf_out;T_2; L_absorber_loop

D_h=D_2 "[m]" "Hydraulic diameter of pipe for laminar and turbulent flow, equals inner diameter of absorber tube"

T_1ave= (Tf_in+Tf_out)/2 "[oC]"

"T_2 is inner surface temperature of absorber pipe" "[oC]"

"T_1ave is the mean(bulk) temperature of the HTF" "[oC]"

" Thermophysical properties of HTF "

MU_1 = INTERPOLATE('Therminol54';'MU';'T';T=T_1ave) "[kg/m-s]"

MU_2 = INTERPOLATE('Therminol54';'MU';'T';T=T_2) "[kg/m-s]"

Cp_1 = INTERPOLATE('Therminol54';'Cp';'T';T=T_1ave) "[J/kg-K]"

Cp_2 = INTERPOLATE('Therminol54';'Cp';'T';T=T_2) "[J/kg-K]"

k_1 = INTERPOLATE('Therminol54';'k';'T';T=T_1ave) "[W/m-K]"

k_2 = INTERPOLATE('Therminol54';'k';'T';T=T_2) "[W/m-K]"

RHO_1 = INTERPOLATE('Therminol54';'RHO';'T';T=T_1ave) "[kg/m^3]"

A_cs = PI*(D_2^2/4)

Re_D_2= (RHO_1 * D_h * (v_1/ A_cs)) / (MU_1) "Reynolds number apprasied at the mean (i.e bulk) temperature of the HTF, T_1ave "

Pr_2 = (Cp_2 * MU_2) / k_2 "Prandtl number apprasied at the absorber inner surface temperature, T_2"

Pr_1 = (Cp_1 * MU_1) / k_1 "Prandtl number apprasied at the mean (i.e bulk) temperature of the HTF, T_1ave"

"Determination of the HTF flow type in the absorber pipe and Nusselt number at D_2"

If (0,5<Pr_1) and (Pr_1<2000) Then

If (0,5<Pr_2) and (Pr_2<2000) Then

If (2300<Re_D_2) and (Re_D_2<5*10^6) Then " Turbulent/transitional flow Nusselt Number correlation developed by Gnielinski correlation)"

f_2 = (1,82 * LOG10(Re_D_2) - 1,64)^(-2) "friction factor for the inner surface of absorber pipe"

Nusselt_D2= (((f_2 / 8) * (Re_D_2 - 1000) * Pr_1) / (1 + 12,7 * (f_2 / 8)^(0,5) * (Pr_1^(0,6667) -1))) * (Pr_1 / Pr_2)^0,11"Nusselt number for turbulent pipe flow"

Else

Nusselt_D2 = 4,36 "uniform heat flux ""Nusselt number for laminar pipe flow"

EndIf

EndIf

EndIf

"Calculation of convection heat transfer and convection resistance between inner surface of absorber tube and HTF"

$h_{1} = \text{Nusselt_D2} * k_{1} / (D_{h})$ "[W/m²-K]" "convective heat transfer coefficient of HTF at T_{1ave}"

$fq_{12conv} = h_{1} * D_{2} * \text{PI} * (T_{2} - T_{1ave}) * L_{\text{absorber_loop}} * 5$ "[W]" "Useful heat gain for whole field"

END

"FUNCTION fq_23cond : Conduction heat transfer through receiver tube "

FUNCTION fq_23cond(T₂;T₃)

\$COMMON T₂;T₃;D₂;D₃; L_{absorber_loop}

"T₂ is inner surface temperature of absorber pipe" "[oC]"

"T₃ is outer surface temperature of absorber pipe" "[oC]"

$T_{23} = (T_{2} + T_{3}) / 2$ "average temperature of absorber pipe" "[oC]"

$k_{23} = (0,013 * T_{23}) + 15,2$ "[W/m-K]" "thermal conductivity of STAINLESS STEEL 304L absorber pipe material at T₂₃"

$fq_{23cond} = (2 * \text{PI} * k_{23} * (T_{3} - T_{2}) / \text{LN}(D_{3} / D_{2})) * L_{\text{absorber_loop}} * 5$ "[W]"

END

"FUNCTION fq_34conv : Convective heat transfer rate between the absorber outer surface and the inner surface of glass envelope"

FUNCTION fq_34conv(T₃; T₄)

\$COMMON T₀;D₃;D₄;g;T₃;T₄;L_{absorber_loop} ; P_{a1}

"T₃ is outer receiver temperature" "[oC]"

"T₄ is inner glass envelope temperature" "[oC]"

$T_{34} = (T_{3} + T_{4}) / 2$ "[oC]" "average temperature of annulus region"

$\text{MU}_{34} = \text{VISCOSITY}(\text{Air}; T = T_{34})$ "[kg/m-s]"

$\text{Cp}_{34} = \text{CP}(\text{Air}; T = T_{34})$ "[kJ/kg-K]"

$k_{34} = \text{CONDUCTIVITY}(\text{Air}; T = T_{34})$ "[W/m-K]" "thermal conductance of air apprasied at T₃₄"

$\text{Rho}_{34} = \text{DENSITY}(\text{Air}; T = T_{34} ; P = P_{a1})$ "[kg/m³]"

$\text{Alpha}_{34} = k_{34} / (\text{Cp}_{34} * \text{Rho}_{34} * 1000)$ "[m²/s]"

$\text{NU}_{34} = \text{MU}_{34} / \text{Rho}_{34}$ "[m²/s]"

$\text{Beta}_{34} = 1 / (T_{34} + T_{0})$ "[1/K]"

$\text{Pr}_{34} = \text{NU}_{34} / \text{Alpha}_{34}$

$\text{Ra}_{D3} = g * \text{Beta}_{34} * \text{ABS}(T_{3} - T_{4}) * (D_{3})^3 / (\text{Alpha}_{34} * \text{NU}_{34})$

$\text{Pr}_{\text{air}} = \text{NU}_{34} / \text{Alpha}_{34}$

$\text{Ra}_{\text{air}} = g * \text{Beta}_{34} * \text{ABS}(T_{3} - T_{4}) * ((D_{4} - D_{3}) / 2)^3 / (\text{Alpha}_{34} * \text{NU}_{34})$

$fq_{34conv} = (2,425 * k_{34} * (T_{3} - T_{4}) / (1 + (D_{3} / D_{4})^{(0,6)})^{(1,25)} * (\text{Pr}_{34} * \text{Ra}_{D3} / (0,861 + \text{Pr}_{34}))^{(0,25)}) * L_{\text{absorber_loop}} * 5$ "[W]" "convection heat transfer considering pressure in annulus case"

"FUNCTION fq_34rad : Radiation heat transfer rate between the absorber outer surface and glass envelope inner surface"

```

FUNCTION fq_34rad(T_3; T_4)
$COMMON D_3;D_4;EPSILON_4;sigma;T_0;T_3;T_4;L_absorber_loop
"T_3 is outer surface temperature of absorber" "[K]"
"T_4 is inner surface temperature of glass envelope" "[K]"
EPSILON_3= 0,000327*(T_3+273,15)-0,065971 "emittance of Luz cermet coating on absorber tube"
If (EPSILON_3<0,05) Then
EPSILON_3=0,05
EndIf
fq_34rad = (PI * D_3 * sigma * ((T_3 + T_0)^4 - (T_4 + T_0)^4) / (1 / EPSILON_3 + D_3 / D_4 * ( 1 /
EPSILON_4 - 1))) * L_absorber_loop * 5 "[W]"
h34_rad=(sigma*EPSILON_3*EPSILON_4*((T_3+T_0)^(2)+(T_4+T_0)^(2))*(T_3+T_0+T_4+T_0)/
(EPSILON_4+(EPSILON_3*((1-EPSILON_4)*(D_3/2))/(D_4/2))) "[W/m^2.K]" "Here units of T_3 and
T_4 are [K]"
END

"FUNCTION fq_45cond :Conduction heat transfer rate through the glass envelope"
FUNCTION fq_45cond(T_4;T_5)
$COMMON D_4;D_5;T_4;T_5;L_absorber_loop
"T_4 is inner surface temperature of glass envelope" "(K)"
"T_5 is outer surface temperature of glass envelope" "(K)"
k_45=1,04 "[W/m-K]" "thermal conductivity value of pyrex glass"
fq_45cond=(2*PI*k_45*(T_4-T_5)/(LN(D_5/D_4)))*L_absorber_loop*5 "[W]"
END

"FUNCTION fq_56conv: Convection heat transfer from glass envelope outer surface to ambient"
FUNCTION fq_56conv (T_5;T_amb)
$COMMON D_5;v_6;T_5;T_amb;L_absorber_loop ;P_6
" Thermophysical Properties for air "
MU_5 = VISCOSITY(Air;T=T_5) "[kg/m-s]"
MU_6 = VISCOSITY(Air;T=T_amb) "[kg/m-s]"
k_5 = CONDUCTIVITY(Air;T=T_5) "[W/m-K]"
k_6 = CONDUCTIVITY(Air;T=T_amb) "[W/m-K]"
Cp_5 = SPECHEAT(Air;T=T_5) "[kJ/kg-K]"
Cp_6 = SPECHEAT(Air;T=T_amb) "[kJ/kg-K]"
Rho_5 = DENSITY(Air;T=T_5; P=P_6) "[kg/m^3]"
Rho_6 = DENSITY(Air;T=T_amb; P=P_6) "[kg/m^3]"
Alpha_5 = k_5 / (Cp_5 * Rho_5) "[m^2/s]"
Alpha_6= k_6 / (Cp_6 * Rho_6) "[m^2/s]"
NU_5 = MU_5 / Rho_5 "[m^2/s]"
NU_6 = MU_6 / Rho_6 "[m^2/s]"
Pr_5 = NU_5 / Alpha_5

```

```

Pr_6 = NU_6 / Alpha_6
Re_D5 = v_6 * D_5 * Rho_6 / MU_6
"Zhukauskas's correlation for forced convection over a long horizontal cylinder"
If (Pr_6 <= 10) Then
n = 0,37
Else
n = 0,36
EndIf
If (Re_D5 < 40) Then
C = 0,75
m = 0,4
Else
If (40 <= Re_D5) and (Re_D5 < 10^3) Then
C = 0,51
m = 0,5
Else
If (10^3 <= Re_D5) and (Re_D5 < 2*10^5) Then
C = 0,26
m = 0,6
Else
If (2*10^5 <= Re_D5) and (Re_D5 < 10^6) Then
C = 0,076
m = 0,7
EndIf
EndIf
EndIf
EndIf
Nusselt_D5 = C * (Re_D5^m) * (Pr_6^n) * (Pr_6/Pr_5)^0,25
h_out= (k_6*Nusselt_D5) / D_5 "[W/m^2*K]" "convection heat transfer coefficient between glass
envelope outer surface and ambient"
fq_56conv = (h_out * PI * D_5 * (T_5 - T_amb))*L_absorber_loop*5 "[W]" "convection heat transfer
between glass envelope outer surface and ambient"
"FUNCTION fq_57rad : Radiation heat transfer rate between the glazing outer surface and the sky"
FUNCTION fq_57rad(T_5;T_amb)
$COMMON D_5;EPSILON_5;T_5;T_amb;L_absorber_loop;sigma
"T_5 = outer surface temperature of glass envelope" "[K]"
"T_7 = effective sky temperature" "[K]"
T_0= 273,15 "Convert temperature from degree celcius to kelvin"
T_7=T_amb-8

```

```

fq_57rad = EPSILON_5 * PI * D_5 * sigma * ((T_5 + T_0)^4 - (T_7 + T_0)^4)*L_absorber_loop*5 "[W]"
h_rad1=EPSILON_5*sigma*(T_5+T_0+T_7+T_0)*((T_5+T_0)^2+(T_7+T_0)^2) "[W/m^2*K]"radiative
resistance between glass envelope outer surface and the sky" "T_5 represnts glass envelope outer
surface temperature in celcius, T_7 represents effective sky temperature in celcius"
"FUNCTION fq_cond_bracket: Heat loss estimate through HCE support bracket"
FUNCTION fq_cond_bracket (T_3;T_amb;v_6)
$COMMON T_3;T_amb;v_6;L_absorber_loop ; P_6
"T_3 is absorber pipe outer surface temperature" "[oC]"
"T_amb (T_6) is atmosphere (ambient) temperature" "[oC]"
D_brac = 0,05 "[m]" "bracket diameter"
A_cs_brac = 0,21*0,85 "[m^2]" " minimum bracket cross-sectional area for conduction heat transfer"
P_brac = 0,21 "[m]" "effective bracket perimeter for convection heat transfer" "C shaped profile"
T_base = T_3 - 10 "[oC]" "effective bracket base temperature"
T_brac = (T_base + T_amb) / 3 "[oC]" " estimate average bracket temperature"
T_brac6 = (T_brac + T_amb) / 2 "[oC]" "estimate film temperature for support bracket"
"Thermophysical Properties for air"
MU_brac = viscosity(Air; T=T_brac) "[N-s/m^2]"
MU_6 = viscosity(Air; T=T_amb) "[N-s/m^2]"
Rho_6 = Density(Air; T=T_amb; P=P_6) "[kg/m^3]"
Rho_brac = Density(Air; T=T_brac; P=P_6) "[kg/m^3]"
k_brac = INTERPOLATE ('AISI 310';'k';'T'; T=T_brac) "[W/m-K]"
k_6 = conductivity(Air; T=T_amb) "[W/m-K]"
k_brac6 = conductivity(Air; T=T_brac6) "[W/m-K]"
Cp_brac = CP(Air; T=T_brac) "[kJ/kg-K]"
Cp_6 = CP(Air; T=T_amb) "[kJ/kg-K]"
NU_6 = MU_6 / Rho_6 "[m^2/s]"
Alpha_brac = k_brac / (Cp_brac * Rho_brac*1000) "[m^2/s]"
Alpha_6 = k_6 / (Cp_6 * Rho_6 *1000) "[m^2/s]"
Re_Dbrac = v_6 * D_brac / NU_6
NU_brac = MU_brac / Rho_brac "[m^2/s]"
Pr_brac = NU_brac / Alpha_brac
Pr_6 = NU_6 / Alpha_6
" Coefficients for external forced convection Nusselt Number correlation (Zhukauskas's correlation) "
If (Pr_6 <= 10) Then
n = 0,37
Else
n = 0,36
EndIf
If (Re_Dbrac < 40) Then

```

```

C = 0,75
m = 0,4
Else
If (40 <= Re_Dbrac) and (Re_Dbrac < 10^3) Then
C = 0,51
m = 0,5
Else
If (10^3 <= Re_Dbrac) and (Re_Dbrac < 2*10^5) Then
C = 0,26
m = 0,6
Else
If (2*10^5 <= Re_Dbrac) and (Re_Dbrac < 10^6) Then
C = 0,076
m = 0,7
EndIf
EndIf
EndIf
EndIf
Nu#_bar = C * (Re_Dbrac)^m * (Pr_6)^n * (Pr_6 / Pr_brac)^(0,25)
h_brac6 = Nu#_bar * k_brac6 / D_brac "[W/m^2-K]"
fq_cond_bracket = (SQRT(h_brac6 * P_brac * k_brac * A_cs_brac) * (T_base - T_amb)) * 72*5 "[W]" "1
loop" "estimated conduction heat loss through HCE support brackets "
END
"FUNCTION f_ETA_OptEff_env: Optical Efficiencies based on HCE type"
FUNCTION f_ETA_OptEff_env(THETA)
$COMMON THETA
Rho_mir_clean=0,935 "cleanliness of mirror"
ETA_Geo= 0,98 "Geometry effect"
ETA_mir_dirt= 0,984 "dirt factor of mirror."
ETA_shadow=0,974 "shadowing factor of HCE (bellows,shielding,supports)"
ETA_HCE_dirt= 0,992 "dirt factor of HCE"
ETA_Track=0,994 "Tracking error"
ETA_Gen= 0,96 "general error"
Rho_m=0,95 "mirror reflectance value"
K_Incidence=COS(THETA) + 0,00084 * THETA - 0,00005369 * (THETA)^2 "incident angle modifier
(IAM)"
f_ETA_OptEff_env=ETA_Geo*ETA_Track*ETA_shadow*ETA_Gen*Rho_mir_clean*ETA_mir_dirt*ET
A_HCE_dirt*K_Incidence " effective optical efficiency at the glass envelope"
"FUNCTION fq_3SolAbs: Solar Irradiation Absorption in absorber pipe"

```

```

FUNCTION fq_3SolAbs(THETA;DNI)
$COMMON THETA; DNI;W_a;D_5;ETA_OptEff_env; L_mirror_loop
Rho_mir_clean=0,935 "cleanliness of mirror"
ETA_Geo= 0,98 "Geometry effect"
ETA_mir_dirt= 0,984 "dirt factor of mirror."
ETA_shadow=0,974 "shadowing factor of HCE (bellows,shielding,supports)"
ETA_HCE_dirt= 0,992 "dirt factor of HCE"
ETA_Track=0,994 "Tracking error"
ETA_Gen= 0,96 "general error"
Rho_m=0,95 "mirror reflectance value"
ALPHA_abs= 0,92 "absorptance of absorber pipe"
TAU_env= 0,935 "transmittance value of glass envelope (pyrex glass) "
K_Incidence=COS(THETA) + 0,00084 * THETA - 0,00005369 * (THETA)^2 "incident angle modifier
(IAM)"
f_ETA_OptEff_env=ETA_Geo*ETA_Track*ETA_shadow*ETA_Gen*Rho_mir_clean*ETA_mir_dirt*ET
A_HCE_dirt*K_Incidence
A_aperture=W_a*L_mirror_loop*5 "[m^2]"
OptEff_abs = ETA_OptEff_env* TAU_Env "effective optical efficiency at the absorber "
fq_3SolAbs = q_i*OptEff_abs*ALPHA_abs "solar irradiation absorption rate into the absorber pipe [W]"
END

"FUNCTION fq_5SolAbs : Solar Irradiation Absorption in glass envelope"
FUNCTION fq_5SolAbs(THETA;DNI)
$COMMON THETA;DNI;W_a;D_5;L_mirror_loop
Rho_mir_clean=0,935 "cleanliness of mirror"
ETA_Geo= 0,98 "Geometry effect"
ETA_mir_dirt= 0,984 "dirt factor of mirror."
ETA_shadow=0,974 "shadowing factor of HCE (bellows,shielding,supports)"
ETA_HCE_dirt= 0,992 "dirt factor of HCE"
ETA_Track=0,994 "Tracking error"
ETA_Gen= 0,96 "general error"
Rho_m=0,95 "mirror reflectance value"
ALPHA_env=0,02 "absorptance of glass envelope"
K_Incidence=COS(THETA) + 0,00084 * THETA - 0,00005369 * (THETA)^2 "incident angle modifier
(IAM)"
ETA_OptEff_env=ETA_Geo*ETA_Track*ETA_shadow*ETA_Gen*Rho_mir_clean*ETA_mir_dirt*ETA_
HCE_dirt*K_Incidence
A_aperture=W_a*L_mirror_loop*5 "[m^2]"
q_i= DNI*COS(THETA)*A_aperture "Incoming solar irradiance [W]"

```

```

fq_5SolAbs = q_i*ETA_OptEff_env*ALPHA_env "solar irradiation absorption rate into the glass
envelope [W]"
"FUNCTION fq_heat loss_pipes: Heat losses from other pipes in solar field"
FUNCTION fq_pipes_above(Tf_out;Tf_in;T_amb)
$COMMON Tf_out;Tf_in;T_amb;D_2;T_2;v_1;v_6
T_1ave=(Tf_in+Tf_out)/2 "[oC]" "Average temperature of Therminol 54"
D_h=D_2 "[m]" "Hydraulic diameter of pipe for laminar and turbulent flow, equals inner diameter of
absorber tube"
D_pipe_outer=0,2388 "[m]"
k_INS= INTERPOLATE('Isover Rockwool';'k_INS';'T';T=T_1ave)
k_AISI= INTERPOLATE('AISI_1040';'k_AISI';'T';T=T_1ave)
" Thermophysical properties of HTF "
MU_1 = INTERPOLATE('Therminol54';'MU';'T';T=T_1ave) "[kg/m-s]"
MU_2 = INTERPOLATE('Therminol54';'MU';'T';T=T_2) "[kg/m-s]"
Cp_1 = INTERPOLATE('Therminol54';'Cp';'T';T=T_1ave) "[J/kg-K]"
Cp_2 = INTERPOLATE('Therminol54';'Cp';'T';T=T_2) "[J/kg-K]"
k_1 = INTERPOLATE('Therminol54';'k';'T';T=T_1ave) "[W/m-K]"
k_2 = INTERPOLATE('Therminol54';'k';'T';T=T_2) "[W/m-K]"
RHO_1 = INTERPOLATE('Therminol54';'RHO';'T';T=T_1ave) "[kg/m^3]"
A_cs = (PI*D_2^2)/4
Re_D_2= (RHO_1 * D_h * v_1/A_cs) / (MU_1) "Reynolds number apprasied at the mean (i.e bulk)
temperature of the HTF, T_1ave "
Pr_2 = (Cp_2 * MU_2) / k_2 "Prandtl number apprasied at the absorber inner surface temperature,
T_2"
Pr_1 = (Cp_1 * MU_1) / k_1 "Prandtl number apprasied at the mean (i.e bulk) temperature of the HTF,
T_1ave"
"Determination of the HTF flow type in the absorber pipe and Nusselt number at D_2"
If (0,5<Pr_1) and (Pr_1<2000) Then
If (0,5<Pr_2) and (Pr_2<2000) Then
If (2300<Re_D_2) and (Re_D_2<5*10^6) Then " Turbulent/transitional flow Nusselt Number
correlation developed by Gnielinski correlation)"
f_2 = (1,82 * LOG10(Re_D_2) - 1,64)^(-2) "friction factor for the inner surface of absorber pipe"
Nusselt_D2= (((f_2 / 8) * (Re_D_2 - 1000) * Pr_1) / (1 + 12,7 * (f_2 / 8)^(0,5) * (Pr_1^(0,6667) - 1))) *
(Pr_1 / Pr_2)^0,11"Nusselt number for turbulent pipe flow"
Else
Nusselt_D2 = 4,36 "uniform heat flux ""Nusselt number for laminar pipe flow"
EndIf
EndIf
EndIf
EndIf

```



```

h_1 = Nusselt_D2 * k_1 / (D_2) "[W/m^2-K]" "convective heat transfer coefficient of HTF at T_1ave"
h_outer= 4*(D_pipe_outer^(-0,42))*(v_6^(0,5)) "[W/m2-K]"
r_1=1/(h_1*PI*0,07792*1) "[oC/W]"
r_2=LN(4,445/3,896)/(2*PI*k_AISI*1) "[oC/W]"
r_3=LN(11,94/4,445)/(2*PI*k_INS*1) "[oC/W]"
r_4=1/(h_outer*PI*D_pipe_outer*1) "[oC/W]"
fq_pipes_above= ((T_1ave-T_amb)/(r_1+r_2+r_3+r_4))* 183 "(14+19)" "[W]" "1 loop"

```

"FUNCTION fq_pipe_vertical : Heat losses from the vertical pipes in which cold and hot Theminol 54 passes in 1 loop "

```

FUNCTION fq_pipes_vertical(Tf_out;Tf_in;T_amb)
$COMMON Tf_out;Tf_in;T_amb;D_2;T_2;v_1;v_6
T_1ave=(Tf_in+Tf_out)/2 "[oC]" "Average temperature of Therminol 54"
D_h=D_2 "[m]" "Hydraulic diameter of pipe for laminar and turbulent flow, equals inner diameter of absorber tube"
D_pipe_outer=0,1274 "[m]"
" Thermophysical properties of HTF "
MU_1 = INTERPOLATE('Therminol54';'MU';'T';T=T_1ave) "[kg/m-s]"
MU_2 = INTERPOLATE('Therminol54';'MU';'T';T=T_2) "[kg/m-s]"
Cp_1 = INTERPOLATE('Therminol54';'Cp';'T';T=T_1ave) "[J/kg-K]"
Cp_2 = INTERPOLATE('Therminol54';'Cp';'T';T=T_2) "[J/kg-K]"
k_1 = INTERPOLATE('Therminol54';'k';'T';T=T_1ave) "[W/m-K]"
k_2 = INTERPOLATE('Therminol54';'k';'T';T=T_2) "[W/m-K]"
RHO_1 = INTERPOLATE('Therminol54';'RHO';'T';T=T_1ave) "[kg/m^3]"
A_cs = (PI*D_2^2)/4
Pr_2 = (Cp_2 * MU_2) / k_2 "Prandtl number appraised at the absorber inner surface temperature, T_2"
Pr_1 = (Cp_1 * MU_1) / k_1 "Prandtl number appraised at the mean (i.e bulk) temperature of the HTF, T_1ave"
f_2 = (1,82 * LOG10(Re_D_2) - 1,64)^(-2) "friction factor for the inner surface of absorber pipe"
Nusselt_D2= (((f_2 / 8) * (Re_D_2 - 1000) * Pr_1) / (1 + 12,7 * (f_2 / 8)^(0,5) * (Pr_1^(0,6667) - 1))) * (Pr_1 / Pr_2)^0,11"Nusselt number for turbulent pipe flow"
Else
Nusselt_D2 = 4,36 "uniform heat flux ""Nusselt number for laminar pipe flow"
EndIf
EndIf
EndIf
EndIf
h_1 = Nusselt_D2 * k_1 / (D_2) "[W/m^2-K]" "convective heat transfer coefficient of HTF at T_1ave"
h_outer= 4*(D_pipe_outer^(-0,42))*(v_6^(0,5)) "[W/m2-K]"

```

```

r_1=1/(h_1*PI*0,05248*1) "[oC/W]"
r_2=LN(30,15/26,24)/(2*PI*k_AISI*1) "[oC/W]"
r_3=LN(6,37/3,015)/(2*PI*k_INS*1) "[oC/W]"
r_4=1/(h_outer*PI*D_pipe_outer*1) "[oC/W]"
fq_pipes_vertical= ((T_1ave-T_amb)/(r_1+r_2+r_3+r_4))* 8 "1loop" "[W]"
"FUNCTION fq_pipe_first : Heat losses from the pipes in which cold and hot Theminol 54 passes in 1
loop "
FUNCTION fq_pipe_first(Tf_out;Tf_in;T_amb)
$COMMON Tf_out;Tf_in;T_amb;D_2;T_2;v_1;v_6
T_1ave= (Tf_in + Tf_out) /2 "[oC]" "Average temperature of Theminol 54"
D_h=D_2 "[m]" "Hydraulic diameter of pipe for laminar and turbulent flow, equals inner diameter of
absorber tube"
D_pipe_outer=0,2388 "[m]"
" Thermophysical properties of HTF "
MU_1 = INTERPOLATE('Theminol54';'MU';'T';T=T_1ave) "[kg/m-s]"
MU_2 = INTERPOLATE('Theminol54';'MU';'T';T=T_2) "[kg/m-s]"
Cp_1 = INTERPOLATE('Theminol54';'Cp';'T';T=T_1ave) "[J/kg-K]"
Cp_2 = INTERPOLATE('Theminol54';'Cp';'T';T=T_2) "[J/kg-K]"
k_1 = INTERPOLATE('Theminol54';'k';'T';T=T_1ave) "[W/m-K]"
k_2 = INTERPOLATE('Theminol54';'k';'T';T=T_2) "[W/m-K]"
RHO_1 = INTERPOLATE('Theminol54';'RHO';'T';T=T_1ave) "[kg/m^3]"
A_cs = (PI*D_2^2)/4
Re_D_2= (RHO_1 * D_h * v_1/A_cs) / (MU_1) "Reynolds number apprasied at the mean (i.e bulk)
temperature of the HTF, T_1ave "
Pr_2 = (Cp_2 * MU_2) / k_2 "Prandtl number apprasied at the absorber inner surface temperature,
T_2"
Pr_1 = (Cp_1 * MU_1) / k_1 "Prandtl number apprasied at the mean (i.e bulk) temperature of the HTF,
T_1ave"
"Determination of the HTF flow type in the absorber pipe and Nusselt number at D_2"
f_2 = (1,82 * LOG10(Re_D_2) - 1,64)^(-2) "friction factor for the inner surface of absorber pipe"
Nusselt_D2= (((f_2 / 8) * (Re_D_2 - 1000) * Pr_1) / (1 + 12,7 * (f_2 / 8)^(0,5) * (Pr_1^(0,6667) -1))) *
(Pr_1 / Pr_2)^0,11"Nusselt number for turbulent pipe flow"
Else
Nusselt_D2 = 4,36 "uniform heat flux ""Nusselt number for laminar pipe flow"
EndIf
EndIf
EndIf
EndIf
h_1 = Nusselt_D2 * k_1 / (D_2) "[W/m^2-K]" "convective heat transfer coefficient of HTF at T_1ave"
END

```

```

"FUNCTION fq_pipe_1,16 : Heat losses from the pipes in which cold and hot Therminol 54 passes in 1
loop "
FUNCTION fq_pipe_116(Tf_out;Tf_in;T_amb)
$COMMON Tf_out;Tf_in;T_amb;D_2;T_2;v_1;v_6
T_1ave=(Tf_in+Tf_out)/2 "[oC]" "Average temperature of Therminol 54"
D_h=D_2 "[m]" "Hydraulic diameter of pipe for laminar and turbulent flow, equals inner diameter of
absorber tube"
D_pipe_outer=0,1274 "[m]"
k_INS= INTERPOLATE('Isover Rockwool';'k_INS';'T';T=T_1ave)
" Thermophysical properties of HTF "
MU_1 = INTERPOLATE('Therminol54';'MU';'T';T=T_1ave) "[kg/m-s]"
MU_2 = INTERPOLATE('Therminol54';'MU';'T';T=T_2) "[kg/m-s]"
Cp_1 = INTERPOLATE('Therminol54';'Cp';'T';T=T_1ave) "[J/kg-K]"
Cp_2 = INTERPOLATE('Therminol54';'Cp';'T';T=T_2) "[J/kg-K]"
k_1 = INTERPOLATE('Therminol54';'k';'T';T=T_1ave) "[W/m-K]"
k_2 = INTERPOLATE('Therminol54';'k';'T';T=T_2) "[W/m-K]"
RHO_1 = INTERPOLATE('Therminol54';'RHO';'T';T=T_1ave) "[kg/m^3]"
A_cs = (PI*D_2^2)/4
Re_D_2= (RHO_1 * D_h * v_1/A_cs) / (MU_1) "Reynolds number apprasied at the mean (i.e bulk)
temperature of the HTF, T_1ave "
Pr_2 = (Cp_2 * MU_2) / k_2 "Prandtl number appraised at the absorber inner surface temperature,
T_2"
Pr_1 = (Cp_1 * MU_1) / k_1 "Prandtl number appraised at the mean (i.e bulk) temperature of the HTF,
T_1ave"
"Determination of the HTF flow type in the absorber pipe and Nusselt number at D_2"
f_2 = (1,82 * LOG10(Re_D_2) - 1,64)^(-2) "friction factor for the inner surface of absorber pipe"
Nusselt_D2= (((f_2 / 8) * (Re_D_2 - 1000) * Pr_1) / (1 + 12,7 * (f_2 / 8)^(0,5) * (Pr_1^(0,6667) - 1))) *
(Pr_1 / Pr_2)^0,11"Nusselt number for turbulent pipe flow"
Else
Nusselt_D2 = 4,36 "uniform heat flux ""Nusselt number for laminar pipe flow"
EndIf
EndIf
EndIf
h_1 = Nusselt_D2 * k_1 / (D_2) "[W/m^2-K]" "convective heat transfer coefficient of HTF at T_1ave"
h_outer= 4*(D_pipe_outer^(-0,42))*(v_6^(0,5)) "[W/m2-K]"
r_1=1/(h_1*PI*0,05248*1) "[oC/W]"
r_2=LN(30,15/26,24)/(2*PI*k_AISI*1) "[oC/W]"
r_3=LN(6,37/3,015)/(2*PI*k_INS*1) "[oC/W]"
r_4=1/(h_outer*PI*D_pipe_outer*1) "[oC/W]"

```

```

"FUNCTION fq_bare_pipes_elbow_ : Heat losses from the bare short elbow pipes in which cold and
hot Therminol 54 passes in 1 loop "
FUNCTION fq_bare_pipes_elbow(Tf_out;Tf_in;T_amb)
$COMMON Tf_out;Tf_in;T_amb;D_2;T_2;v_1;v_6;T_2;T_3
T_1ave=(Tf_in+Tf_out)/2 "[oC]" "Average temperature of Therminol 54"
D_h=D_2 "[m]" "Hydraulic diameter of pipe for laminar and turbulent flow, equals inner diameter of
absorber tube"
D_pipe_outer=0,0424 "[m]"
k_INS= INTERPOLATE('Isover Rockwool';'k_INS';'T';T=T_1ave)
T_23= (T_2+T_3)/2 "average temperature of absorber pipe" "[oC]"
k_23= (0,013*T_23)+15,2 "[W/mK]" "thermal conductivity of STAINLESS STEEL 304L absorber pipe
material apprasied at T_23"
" Thermophysical properties of HTF "
MU_1 = INTERPOLATE('Therminol54';'MU';'T';T=T_1ave) "[kg/m-s]"
MU_2 = INTERPOLATE('Therminol54';'MU';'T';T=T_2) "[kg/m-s]"
Cp_1 = INTERPOLATE('Therminol54';'Cp';'T';T=T_1ave) "[J/kg-K]"
Cp_2 = INTERPOLATE('Therminol54';'Cp';'T';T=T_2) "[J/kg-K]"
k_1 = INTERPOLATE('Therminol54';'k';'T';T=T_1ave) "[W/m-K]"
k_2 = INTERPOLATE('Therminol54';'k';'T';T=T_2) "[W/m-K]"
RHO_1 = INTERPOLATE('Therminol54';'RHO';'T';T=T_1ave) "[kg/m^3]"
A_cs = (PI*D_2^2)/4
Pr_2 = (Cp_2 * MU_2) / k_2 "Prandtl number apprasied at the absorber inner surface temperature,
T_2"
Pr_1 = (Cp_1 * MU_1) / k_1 "Prandtl number apprasied at the mean (i.e bulk) temperature of the HTF,
T_1ave"
"Determination of the HTF flow type in the absorber pipe and Nusselt number at D_2"
If (0,5<Pr_1) and (Pr_1<2000) Then
If (0,5<Pr_2) and (Pr_2<2000) Then
If (2300<Re_D_2) and (Re_D_2<5*10^6) Then " Turbulent/transitional flow Nusselt Number
correlation developed by Gnielinski correlation)"
f_2 = (1,82 * LOG10(Re_D_2) - 1,64)^(-2) "friction factor for the inner surface of absorber pipe"
Nusselt_D2= (((f_2 / 8) * (Re_D_2 - 1000) * Pr_1) / (1 + 12,7 * (f_2 / 8)^(0,5) * (Pr_1^(0,6667) -1))) *
(Pr_1 / Pr_2)^0,11"Nusselt number for turbulent pipe flow"
Else
Nusselt_D2 = 4,36 "uniform heat flux ""Nusselt number for laminar pipe flow"
EndIf
EndIf
EndIf
h_1 = Nusselt_D2 * k_1 / (D_2) "[W/m^2-K]" "convective heat transfer coefficient of HTF at T_1ave"

```

```

r_1=1/(h_1*PI*0,0384*1) "[oC/W]"
r_2=LN(42,4/38,4)/(2*PI*k_23*1) "[oC/W]"
fq_bare_pipes_elbow= ((T_1ave-T_amb)/(r_1+r_2+r_3)) * 0,25 * 8 "1 loop" "[W]"
END
"FUNCTION fq_flex_pipes : Heat losses from the flex S pipes in which cold and hot Therminol 54
passes in 1 loop "
FUNCTION fq_flex_pipes(Tf_out;Tf_in;T_amb)
$COMMON Tf_out;Tf_in;T_amb;D_2;T_2;v_1;v_6; T_2;T_3
T_1ave=(Tf_in+Tf_out)/2 "[oC]" "Average temperature of Therminol 54"
D_h=D_2 "[m]" "Hydraulic diameter of pipe for laminar and turbulent flow, equals inner diameter of
absorber tube"
D_pipe_outer= 0,0732 "[m]"
T_23= (T_2+T_3)/2 "average temperature of absorber pipe" "[oC]"
k_23= (0,013*T_23)+15,2 "[W/mK]" "thermal conductivity of STAINLESS STEEL 304L absorber pipe
material appraised at T_23"
" Thermophysical properties of HTF "
MU_1 = INTERPOLATE('Therminol54';'MU';'T';T=T_1ave) "[kg/m-s]"
MU_2 = INTERPOLATE('Therminol54';'MU';'T';T=T_2) "[kg/m-s]"
Cp_1 = INTERPOLATE('Therminol54';'Cp';'T';T=T_1ave) "[J/kg-K]"
Cp_2 = INTERPOLATE('Therminol54';'Cp';'T';T=T_2) "[J/kg-K]"
k_1 = INTERPOLATE('Therminol54';'k';'T';T=T_1ave) "[W/m-K]"
k_2 = INTERPOLATE('Therminol54';'k';'T';T=T_2) "[W/m-K]"
RHO_1 = INTERPOLATE('Therminol54';'RHO';'T';T=T_1ave) "[kg/m^3]"
A_cs = (PI*D_2^2)/4
Re_D_2= (RHO_1 * D_h * v_1/A_cs) / (MU_1) "Reynolds number appraised at the mean (i.e bulk)
temperature of the HTF, T_1ave "
Pr_2 = (Cp_2 * MU_2) / k_2 "Prandtl number appraised at the absorber inner surface temperature,
T_2"
Pr_1 = (Cp_1 * MU_1) / k_1 "Prandtl number appraised at the mean (i.e bulk) temperature of the HTF,
T_1ave"
"Determination of the HTF flow type in the absorber pipe and Nusselt number at D_2"
If (0,5<Pr_1) and (Pr_1<2000) Then
If (0,5<Pr_2) and (Pr_2<2000) Then
If (2300<Re_D_2) and (Re_D_2<5*10^6) Then " Turbulent/transitional flow Nusselt Number
correlation developed by Gnielinski correlation)"
f_2 = (1,82 * LOG10(Re_D_2) - 1,64)^(-2) "friction factor for the inner surface of absorber pipe"
Nusselt_D2= (((f_2 / 8) * (Re_D_2 - 1000) * Pr_1) / (1 + 12,7 * (f_2 / 8)^(0,5) * (Pr_1^(0,6667) - 1))) *
(Pr_1 / Pr_2)^0,11"Nusselt number for turbulent pipe flow"
Else

```

```

Nusselt_D2 = 4,36 "uniform heat flux ""Nusselt number for laminar pipe flow"
EndIf
EndIf
EndIf
h_1 = Nusselt_D2 * k_1 / (D_2) "[W/m^2-K]" "convective heat transfer coefficient of HTF at T_1ave"
h_outer= 4*(D_pipe_outer^(-0,42))*(v_6^(0,5)) "[W/m2-K]"
r_1=1/(h_1*PI*0,015*1) "[oC/W]"
r_4=1/(h_outer*PI*D_pipe_outer*1) "[oC/W]"
fq_flex_pipes = ((T_1ave-T_amb)/(r_1+r_2+r_3+r_4)) * 1,35 * 4 "1 loop" "[W]"
"FUNCTION fq_bare_longpipes_elbow_ : Heat losses from the bare long elbow pipes in which cold
and hot Theminol 54 passes in 1 loop "
FUNCTION fq_bare_longpipes_elbow(Tf_out;Tf_in;T_amb)
$COMMON Tf_out;Tf_in;T_amb;D_2;T_2;v_1;v_6;T_2;T_3
T_1ave=(Tf_in+Tf_out)/2 "[oC]" "Average temperature of Therminol 54"
D_h=D_2 "[m]" "Hydraulic diameter of pipe for laminar and turbulent flow, equals inner diameter of
absorber tube"
D_pipe_outer=0,0424 "[m]"
k_INS= INTERPOLATE('Isover Rockwool';'k_INS';T;T=T_1ave)
T_23= (T_2+T_3)/2 "average temperature of absorber pipe" "[oC]"
k_23= (0,013*T_23)+15,2 "[W/m-K]" "thermal conductivity of STAINLESS STEEL 304L absorber pipe
material appraised at T_23"
" Thermophysical properties of HTF "
MU_1 = INTERPOLATE('Therminol54';'MU';T;T=T_1ave) "[kg/m-s]"
MU_2 = INTERPOLATE('Therminol54';'MU';T;T=T_2) "[kg/m-s]"
Cp_1 = INTERPOLATE('Therminol54';'Cp';T;T=T_1ave) "[J/kg-K]"
Cp_2 = INTERPOLATE('Therminol54';'Cp';T;T=T_2) "[J/kg-K]"
k_1 = INTERPOLATE('Therminol54';'k';T;T=T_1ave) "[W/m-K]"
k_2 = INTERPOLATE('Therminol54';'k';T;T=T_2) "[W/m-K]"
Re_D_2= (RHO_1 * D_h * v_1/A_cs) / (MU_1) "Reynolds number apprasied at the mean (i.e bulk)
temperature of the HTF, T_1ave "
Pr_2 = (Cp_2 * MU_2) / k_2 "Prandtl number apprasied at the absorber inner surface temperature,
T_2"
Pr_1 = (Cp_1 * MU_1) / k_1 "Prandtl number apprasied at the mean (i.e bulk) temperature of the HTF,
T_1ave"
"Determination of the HTF flow type in the absorber pipe and Nusselt number at D_2"
If (0,5<Pr_1) and (Pr_1<2000) Then
If (0,5<Pr_2) and (Pr_2<2000) Then
If (2300<Re_D_2) and (Re_D_2<5*10^6) Then " Turbulent/transitional flow Nusselt Number
correlation developed by Gnielinski correlation)"

```

```

f_2 = (1,82 * LOG10(Re_D_2) - 1,64)^(-2) "friction factor for the inner surface of absorber pipe"
Nusselt_D2= (((f_2 / 8) * (Re_D_2 - 1000) * Pr_1) / (1 + 12,7 * (f_2 / 8)^(0,5) * (Pr_1^(0,6667) -1))) *
(Pr_1 / Pr_2)^0,11"Nusselt number for turbulent pipe flow"
Else
Nusselt_D2 = 4,36 "uniform heat flux ""Nusselt number for laminar pipe flow"
Endlf
Endlf
Endlf
h_1 = Nusselt_D2 * k_1 / (D_2) "[W/m^2-K]" "convective heat transfer coefficient of HTF at T_1ave"
"FUNCTION fq_cylinders : Heat losses from the short and long cylinders on the absorber tube in
which cold and hot Theminol 54 passes in 1 loop "
FUNCTION fq_cylinders(Tf_out;Tf_in;T_amb)
$COMMON Tf_out;Tf_in;T_amb;D_2;T_2;v_1;v_6;T_2;T_3
T_1ave=(Tf_in+Tf_out)/2 "[oC]" "Average temperature of Therminol 54"
D_h=D_2 "[m]" "Hydraulic diameter of pipe for laminar and turbulent flow, equals inner diameter of
absorber tube"
D_pipe_outer=0,2070 "[m]"
T_23= (T_2+T_3)/2 "average temperature of absorber pipe" "[oC]"
k_23= (0,013*T_23)+15,2 "[W/m-K]" "thermal conductivity of STAINLESS STEEL 304L absorber pipe
material appraised at T_23"
" Thermophysical properties of HTF "
MU_1 = INTERPOLATE('Therminol54';'MU';'T';T=T_1ave) "[kg/m-s]"
MU_2 = INTERPOLATE('Therminol54';'MU';'T';T=T_2) "[kg/m-s]"
Cp_1 = INTERPOLATE('Therminol54';'Cp';'T';T=T_1ave) "[J/kg-K]"
Cp_2 = INTERPOLATE('Therminol54';'Cp';'T';T=T_2) "[J/kg-K]"
k_1 = INTERPOLATE('Therminol54';'k';'T';T=T_1ave) "[W/m-K]"
k_2 = INTERPOLATE('Therminol54';'k';'T';T=T_2) "[W/m-K]"
RHO_1 = INTERPOLATE('Therminol54';'RHO';'T';T=T_1ave) "[kg/m^3]"
Pr_2 = (Cp_2 * MU_2) / k_2 "Prandtl number appraised at the absorber inner surface temperature,
T_2"
Pr_1 = (Cp_1 * MU_1) / k_1 "Prandtl number appraised at the mean (i.e bulk) temperature of the HTF,
T_1ave"
"Determination of the HTF flow type in the absorber pipe and Nusselt number at D_2"
If (0,5<Pr_1) and (Pr_1<2000) Then
If (0,5<Pr) and (Pr<2000) Then
If (2300<Re_D_2) and (Re_D_2<5*10^6) Then " Turbulent/transitional flow Nusselt Number
correlation developed by Gnielinski correlation)"
f_2 = (1,82 * LOG10(Re_D_2) - 1,64)^(-2) "friction factor for the inner surface of absorber pipe"

```

```

Nusselt_D2= (((f_2 / 8) * (Re_D_2 - 1000) * Pr_1) / (1 + 12,7 * (f_2 / 8)^(0,5) * (Pr_1^(0,6667) - 1))) *
(Pr_1 / Pr_2)^0,11"Nusselt number for turbulent pipe flow"
Else
Nusselt_D2 = 4,36 "uniform heat flux ""Nusselt number for laminar pipe flow"
EndIf
EndIf
EndIf
h_1 = Nusselt_D2 * k_1 / (D_2) "[W/m^2-K]" "convective heat transfer coefficient of HTF at T_1ave"
"FUNCTION fq_isolated_elbow : Heat losses from the isolated elbow and flex S pipe in which cold and
hot Theminol 54 passes in 1 loop "
FUNCTION fq_isolated_elbow(Tf_out;Tf_in;T_amb)
$COMMON Tf_out;Tf_in;T_amb;D_2;T_2;v_1;v_6;T_2;T_3
T_1ave=(Tf_in+Tf_out)/2 "[oC]" "Average temperature of Therminol 54"
T_23= (T_2+T_3)/2 "average temperature of absorber pipe" "[oC]"
k_23= (0,013*T_23)+15,2 "[W/m-K]" "thermal conductivity of STAINLESS STEEL 304L absorber pipe
material appraised at T_23"
" Thermophysical properties of HTF "
MU_1 = INTERPOLATE('Therminol54';'MU';'T';T=T_1ave) "[kg/m-s]"
MU_2 = INTERPOLATE('Therminol54';'MU';'T';T=T_2) "[kg/m-s]"
Cp_1 = INTERPOLATE('Therminol54';'Cp';'T';T=T_1ave) "[J/kg-K]"
Cp_2 = INTERPOLATE('Therminol54';'Cp';'T';T=T_2) "[J/kg-K]"
k_1 = INTERPOLATE('Therminol54';'k';'T';T=T_1ave) "[W/m-K]"
k_2 = INTERPOLATE('Therminol54';'k';'T';T=T_2) "[W/m-K]"
RHO_1 = INTERPOLATE('Therminol54';'RHO';'T';T=T_1ave) "[kg/m^3]"
A_cs = (PI*D_2^2)/4
Pr_2 = (Cp_2 * MU_2) / k_2 "Prandtl number appraised at the absorber inner surface temperature,
T_2"
Pr_1 = (Cp_1 * MU_1) / k_1 "Prandtl number appraised at the mean (i.e bulk) temperature of the HTF,
T_1ave"
"Determination of the HTF flow type in the absorber pipe and Nusselt number at D_2"
If (0,5<Pr_1) and (Pr_1<2000) Then
If (0,5<Pr_2) and (Pr_2<2000) Then
If (2300<Re_D_2) and (Re_D_2<5*10^6) Then " Turbulent/transitional flow Nusselt Number
correlation developed by Gnielinski correlation)"
f_2 = (1,82 * LOG10(Re_D_2) - 1,64)^(-2) "friction factor for the inner surface of absorber pipe"
Nusselt_D2= (((f_2 / 8) * (Re_D_2 - 1000) * Pr_1) / (1 + 12,7 * (f_2 / 8)^(0,5) * (Pr_1^(0,6667) - 1))) *
(Pr_1 / Pr_2)^0,11"Nusselt number for turbulent pipe flow"
Else
Nusselt_D2 = 4,36 "uniform heat flux ""Nusselt number for laminar pipe flow"

```



```

Endlf
Endlf
Endlf
h_1 = Nusselt_D2 * k_1 / (D_2) "[W/m^2-K]" "convective heat transfer coefficient of HTF at T_1ave"
h_outer= 4*(D_pipe_outer^(-0,42))*(v_6^(0,5)) "[W/m2-K]"
r_1=1/(h_1*PI*0,015*1) "[oC/W]"
r_4=1/(h_outer*PI*D_pipe_outer*1) "[oC/W]"
"FUNCTION fq_T_pipe : Heat losses from the T pipe located between two parabolic trough on 1 row in
which cold and hot Theminol 54 passes in 1 loop "
FUNCTION fq_T_pipe(Tf_out;Tf_in;T_amb)
$COMMON Tf_out;Tf_in;T_amb;D_2;T_2;v_1;v_6
T_1ave=(Tf_in+Tf_out)/2 "[oC]" "Average temperature of Theminol 54"
D_h=D_2 "[m]" "Hydraulic diameter of pipe for laminar and turbulent flow, equals inner diameter of
absorber tube"
D_pipe_outer=0,1274 "[m]"
k_AISI= INTERPOLATE('AISI_1040';'k_AISI';'T';T=T_1ave)
" Thermophysical properties of HTF "
MU_1 = INTERPOLATE('Theminol54';'MU';'T';T=T_1ave) "[kg/m-s]"
MU_2 = INTERPOLATE('Theminol54';'MU';'T';T=T_2) "[kg/m-s]"
Cp_1 = INTERPOLATE('Theminol54';'Cp';'T';T=T_1ave) "[J/kg-K]"
Cp_2 = INTERPOLATE('Theminol54';'Cp';'T';T=T_2) "[J/kg-K]"
k_1 = INTERPOLATE('Theminol54';'k';'T';T=T_1ave) "[W/m-K]"
k_2 = INTERPOLATE('Theminol54';'k';'T';T=T_2) "[W/m-K]"
RHO_1 = INTERPOLATE('Theminol54';'RHO';'T';T=T_1ave) "[kg/m^3]"
A_cs = (PI*D_2^2)/4
Pr_2 = (Cp_2 * MU_2) / k_2 "Prandtl number appraised at the absorber inner surface temperature,
T_2"
Pr_1 = (Cp_1 * MU_1) / k_1 "Prandtl number appraised at the mean (i.e bulk) temperature of the HTF,
T_1ave"
"Determination of the HTF flow type in the absorber pipe and Nusselt number at D_2"
If (0,5<Pr_1) and (Pr_1<2000) Then
If (0,5<Pr_2) and (Pr_2<2000) Then
If (2300<Re_D_2) and (Re_D_2<5*10^6) Then " Turbulent/transitional flow Nusselt Number
correlation developed by Gnielinski correlation)"
f_2 = (1,82 * LOG10(Re_D_2) - 1,64)^(-2) "friction factor for the inner surface of absorber pipe"
Nusselt_D2= (((f_2 / 8) * (Re_D_2 - 1000) * Pr_1) / (1 + 12,7 * (f_2 / 8)^(0,5) * (Pr_1^(0,6667) - 1))) *
(Pr_1 / Pr_2)^0,11"Nusselt number for turbulent pipe flow"
Else
Nusselt_D2 = 4,36 "uniform heat flux ""Nusselt number for laminar pipe flow"

```

```

EndIf
EndIf
EndIf
h_1 = Nusselt_D2 * k_1 / (D_2) "[W/m^2-K]" "convective heat transfer coefficient of HTF at T_1ave"
h_outer= 4*(D_pipe_outer^(-0,42))*(v_6^(0,5)) "[W/m2-K]"
r_1=1/(h_1*PI*0,05248*1) "[oC/W]"
r_2=LN(30,15/26,24)/(2*PI*k_AISI*1) "[oC/W]"
r_4=1/(h_outer*PI*D_pipe_outer*1) "[oC/W]"
"FUNCTION fq_U_pipe : Heat losses from the U pipe located between two parallel rows in which cold
and hot Theminol 54 passes in 1 loop "
FUNCTION fq_U_pipe(Tf_out;Tf_in;T_amb)
$COMMON Tf_out;Tf_in;T_amb;D_2;T_2;v_1;v_6
T_1ave=(Tf_in+Tf_out)/2 "[oC]" "Average temperature of Therminol 54"
D_h=D_2 "[m]" "Hydraulic diameter of pipe for laminar and turbulent flow, equals inner diameter of
absorber tube"
D_pipe_outer=0,1274 "[m]"
k_INS= INTERPOLATE('Isover Rockwool';'k_INS';'T';T=T_1ave)
k_AISI= INTERPOLATE('AISI_1040';'k_AISI';'T';T=T_1ave)
" Thermophysical properties of HTF "
MU_1 = INTERPOLATE('Therminol54';'MU';'T';T=T_1ave) "[kg/m-s]"
MU_2 = INTERPOLATE('Therminol54';'MU';'T';T=T_2) "[kg/m-s]"
Cp_1 = INTERPOLATE('Therminol54';'Cp';'T';T=T_1ave) "[J/kg-K]"
Cp_2 = INTERPOLATE('Therminol54';'Cp';'T';T=T_2) "[J/kg-K]"
k_1 = INTERPOLATE('Therminol54';'k';'T';T=T_1ave) "[W/m-K]"
k_2 = INTERPOLATE('Therminol54';'k';'T';T=T_2) "[W/m-K]"
RHO_1 = INTERPOLATE('Therminol54';'RHO';'T';T=T_1ave) "[kg/m^3]"
A_cs = (PI*D_2^2)/4

Pr_2 = (Cp_2 * MU_2) / k_2 "Prandtl number appraised at the absorber inner surface temperature,
T_2"
Pr_1 = (Cp_1 * MU_1) / k_1 "Prandtl number appraised at the mean (i.e bulk) temperature of the HTF,
T_1ave"
"Determination of the HTF flow type in the absorber pipe and Nusselt number at D_2"
If (0,5<Pr_1) and (Pr_1<2000) Then
If (0,5<Pr_2) and (Pr_2<2000) Then
If (2300<Re_D_2) and (Re_D_2<5*10^6) Then " Turbulent/transitional flow Nusselt Number
correlation developed by Gnielinski correlation"
f_2 = (1,82 * LOG10(Re_D_2) - 1,64)^(2) "friction factor for the inner surface of absorber pipe"

```

```

Nusselt_D2= (((f_2 / 8) * (Re_D_2 - 1000) * Pr_1) / (1 + 12,7 * (f_2 / 8)^(0,5) * (Pr_1^(0,6667) - 1))) *
(Pr_1 / Pr_2)^0,11"Nusselt number for turbulent pipe flow"
Else
Nusselt_D2 = 4,36 "uniform heat flux ""Nusselt number for laminar pipe flow"
EndIf
EndIf
EndIf
h_1 = Nusselt_D2 * k_1 / (D_2) "[W/m^2-K]" "convective heat transfer coefficient of HTF at T_1ave"
h_outer= 4*(D_pipe_outer^(-0,42))*(v_6^(0,5)) "[W/m2-K]"
END
"FUNCTION fq_annular_bracket : Heat losses from the annular bracket in which glass tube passes
through and connecting to support bracket "
FUNCTION fq_annular_bracket(Tf_out;Tf_in;T_amb)
$COMMON T_3;v_6;T_5;T_amb;P_6;D_5
T_1ave = (Tf_in+Tf_out) / 2
" Thermophysical Properties for air "
MU_5 = VISCOSITY(Air;T=T_5) "[kg/m-s]"
MU_6 = VISCOSITY(Air;T=T_amb) "[kg/m-s]"
k_5 = CONDUCTIVITY(Air;T=T_5) "[W/m-K]"
k_6 = CONDUCTIVITY(Air;T=T_amb) "[W/m-K]"
Cp_5 = SPECHEAT(Air;T=T_5) "[kJ/kg-K]"
Cp_6 = SPECHEAT(Air;T=T_amb) "[kJ/kg-K]"
Rho_5 = DENSITY(Air;T=T_5; P=P_6) "[kg/m^3]"
Rho_6 = DENSITY(Air;T=T_amb; P=P_6) "[kg/m^3]"
Alpha_5 = k_5 / (Cp_5 * Rho_5 *1000) "[m^2/s]"
Alpha_6= k_6 / (Cp_6 * Rho_6*1000 ) "[m^2/s]"
NU_5 = MU_5 / Rho_5 "[m^2/s]"
NU_6 = MU_6 / Rho_6 "[m^2/s]"
Pr_5 = NU_5 / Alpha_5
Pr_6 = NU_6 / Alpha_6
Re_D5 = v_6 * D_5 * Rho_6 / MU_6
"Zhukauskas's correlation for forced convection over a long horizontal cylinder"
If (Pr_6 <= 10) Then
n = 0,37
Else
n = 0,36
EndIf
If (Re_D5 < 40) Then
C = 0,75

```

```

m = 0,4
Else
If (10^3 <= Re_D5) and (Re_D5 < 2*10^5) Then
C = 0,26
m = 0,6
Else
If (2*10^5 <= Re_D5) and (Re_D5 < 10^6) Then
C = 0,076
m = 0,7
EndIf
EndIf
Nusselt_D5 = C * (Re_D5^m) * (Pr_6^n) * (Pr_6/Pr_5)^0,25
h_out = (k_6*Nusselt_D5) / D_5 "[W/m^2*K]" "convection heat transfer coefficient between glass
envelope outer surface and ambient"
k = INTERPOLATE('AISI 310';'k';'T';T=T_1ave)
"FUNCTION fq_solar_field: Total solar radiation coming to ADU Solar Field"
FUNCTION fq_solar_field (DNI;W_a;L_mirror_loop)
$COMMON W_a; L_mirror_loop; DNI;THETA
A_aperture=W_a*L "[m^2]" "Total aperture area of whole field "
fq_solar_field= DNI*COS(THETA)*A_aperture "[W]" "True energy input of parabolic trough for whole
field"
D_2=0,038 "[m]" "inner diameter of absorber tube"
D_3= 0,043 "[m]" "outer diameter of absorber pipe"
D_4= 0,064 "[m]" "inner diameter of glass envelope"
D_5=0,070 "[m]" "outer diameter of glass envelope"
L_absorber_loop = 140,64 "[m]" "total length of absorber tube through 1 loop"
L_mirror_loop = 142,08 "[m]" "total length of mirror through 1 loop "
EPSILON_4=0,86 "[Emissivity value of glass envelope inner surface, (Pyrex glass)]"
EPSILON_5= 0,86 "[Emissivity value of glass envelope outer surface, (Pyrex glass)]"
sigma= 5,67*10^(-8) "[W/m^2.K^4]" "Stefan-Boltzmann constant"
T_0=273,15 "convert temperature from oC to K"
W_a=2,38 "[m]" "aperture width of parabolic mirror"
g= 9,81 "[m/s^2]" "gravitational constant"
"Variable parameters"
DNI = Lookup('10 AUGUST 2020';TableRun#;1) "[W/m^2]" "Direct Normal Irradiation"
Tf_in = Lookup('10 AUGUST 2020';TableRun#;2) "[W/m^2]" "[oC]" "inlet temperature of Therminol
54"
v_1 = Lookup('10 AUGUST 2020';TableRun#;5)"[m^3/s]" "HTF velocity"

```

T_amb = LookUp('10 AUGUST 2020';TableRun#;7) "[W/m^2]" "[oC]" "inlet temperature of Therminol 54"

"CALLING ALL FUNCTIONS"

q_12conv = fq_12conv(v_1;Tf_in;Tf_out;T_2)

q_23cond = fq_23cond(T_2;T_3)

q_34rad = fq_34rad(T_3;T_4)

q_34conv = fq_34conv(T_3;T_4)

q_45cond = fq_45cond(T_4;T_5)

q_56conv = fq_56conv(T_5;T_amb)

q_57rad = fq_57rad(T_5;T_amb)

q_3SolAbs = fq_3SolAbs(THETA;DNI)

q_5SolAbs = fq_5SolAbs (THETA;DNI)

q_cond_bracket= fq_cond_bracket(T_3;T_amb;v_6)

ETA_OptEff_env= f_ETA_OptEff_env(THETA)

q_pipes_above=fq_pipes_above(Tf_out;Tf_in;T_amb)

q_pipe_first=fq_pipe_first(Tf_out;Tf_in;T_amb)

q_pipe_116= fq_pipe_116(Tf_out;Tf_in;T_amb)

q_pipes_vertical = fq_pipes_vertical(Tf_out;Tf_in;T_amb)

q_bare_pipes_elbow = fq_bare_pipes_elbow(Tf_out;Tf_in;T_amb)

q_flex_pipes = fq_flex_pipes(Tf_out;Tf_in;T_amb)

q_bare_longpipes_elbow = fq_bare_longpipes_elbow(Tf_out;Tf_in;T_amb)

q_cylinders = fq_cylinders(Tf_out;Tf_in;T_amb)

q_isolated_elbow = fq_isolated_elbow(Tf_out;Tf_in;T_amb)

q_T_pipe= fq_T_pipe(Tf_out;Tf_in;T_amb)

q_U_pipe = fq_U_pipe(Tf_out;Tf_in;T_amb)

q_annular_bracket = fq_annular_bracket(Tf_out;Tf_in;T_amb)

ETA_Col = fETA_Col(q_12conv)

q_solar_field = fq_solar_field (DNI;W_a;L_mirror_loop)

q_12conv = q_23cond

q_3SolAbs = q_34conv + q_34rad + q_23cond + q_cond_bracket

q_34conv + q_34rad = q_45cond

q_45cond + q_5SolAbs = q_57rad + q_56conv

q_heat_loss = q_56conv + q_57rad + q_cond_bracket + (q_pipe_first+q_pipe_116 + q_pipes_vertical + q_bare_pipes_elbow + q_flex_pipes + q_bare_longpipes_elbow + q_cylinders + q_isolated_elbow + q_T_pipe + q_U_pipe + q_annular_bracket)*5 + q_pipes_above

APPENDIX – III

Liquid Properties of Therminol 54 HTF by Temperatures (SI units) (Eastman, (n.d))

T (°C)	ρ (kg/m³)	Cp (J/kg.K)	k (W/m.K)	μ (kg/m.s)
-28	904	1730	0,134	1,82
-20	899	1760	0,133	0,756
-10	892	1800	0,132	0,309
0	885	1830	0,131	0,143
10	878	1870	0,13	0,0738
20	872	1910	0,128	0,0416
30	865	1940	0,127	0,0252
40	858	1980	0,126	0,0163
50	852	2010	0,125	0,0111
60	845	2050	0,124	0,00793
70	838	2080	0,123	0,00589
80	831	2120	0,121	0,00452
90	825	2160	0,12	0,00356
100	818	2190	0,119	0,00288
110	811	2230	0,118	0,00238
120	804	2260	0,117	0,002
130	797	2300	0,116	0,00171
140	790	2330	0,114	0,00148
150	784	2370	0,113	0,00129
160	777	2400	0,112	0,00114
170	770	2440	0,111	0,00102
180	763	2470	0,11	0,00091
190	755	2510	0,109	0,00083
200	748	2540	0,107	0,00075
210	741	2580	0,106	0,00068
220	734	2610	0,105	0,00063
230	726	2650	0,104	0,00057
240	719	2680	0,103	0,00053
250	711	2720	0,102	0,00049
260	704	2750	0,1	0,00045
270	696	2790	0,099	0,00042
280	688	2830	0,098	0,00039
290	680	2860	0,097	0,00036
300	672	2900	0,096	0,00033
310	663	2930	0,095	0,00031

APPENDIX - IV

Properties of Air at 1 Atm Pressure (Çengel and Ghajar, 2014)

T (°C)	ρ (kg/m ³)	C _p (kJ/kg.K)	μ (kg/m.s)	k (W/m.K)
5	1,269	1,006	0,00001754	0,02401
10	1,246	1,006	0,00001778	0,02439
15	1,225	1,007	0,00001802	0,02476
20	1,204	1,007	0,00001825	0,02514
25	1,184	1,007	0,00001849	0,02551
30	1,164	1,007	0,00001872	0,02588
35	1,145	1,007	0,00001895	0,02625
40	1,127	1,007	0,00001918	0,02662
45	1,109	1,007	0,00001941	0,02699
50	1,092	1,007	0,00001963	0,02735
60	1,059	1,007	0,00002008	0,02808
70	1,028	1,007	0,00002052	0,02881
80	0,9994	1,008	0,00002096	0,02953
90	0,9718	1,008	0,00002139	0,03024
100	0,9458	1,009	0,00002181	0,03095
120	0,8977	1,011	0,00002264	0,03235
140	0,8542	1,013	0,00002345	0,03374
160	0,8148	1,016	0,00002420	0,03511
180	0,7788	1,019	0,00002504	0,03646
200	0,7459	1,023	0,00002577	0,03779
250	0,6746	1,033	0,00002760	0,04104
300	0,6158	1,044	0,00002934	0,04418

APPENDIX -V

Thermal conductivities of AISI 1040 Carbon Steel (MatWeb, (n.d))

T (°C)	k (W/m.K)
0	51,9
100	50,7
200	48,1
300	45,7
400	41,7
500	38,2
600	33,9

Thermal conductivities of AISI 310 Stainless Steel (Engineering Toolbox, 2019)

T (°C)	k (W/m.K)
-25	11,7
0	12,1
25	12,7
50	13,2
100	14,1
150	15
200	15,8
250	16,6
300	17,3
350	18

Thermal Conductivities of Isover Stonewool (Isover Saint Gobain, 2017)

T (°C)	k (W/m.K)
10	0,040
40	0,043
50	0,044
100	0,055
150	0,068
200	0,087
250	0,110
300	0,136

APPENDIX – VI

Measured data utilizing for analysis

8 MAY 2020

HOURS	DNI (W/m ²)	Tf_in (°C)	Tf_out (°C)	Theta (degree)	Flow Rate (m ³ /h)	Wind Speed (m/s)	Ambient Temp. (°C)
08:00	319,15	115,91	131,11	3,61	26,16	0,8	20,6
09:00	526,25	132,76	163,52	10,63	26,61	1,3	21,3
10:00	750,8	138,86	171,82	16,13	26,85	1,2	22,9
11:00	893,78	140,45	173,47	19,66	27,02	0,6	23,1
12:00	989,09	143,25	177,5	20,88	27,13	0,9	24,2
13:00	1008,63	147,4	183,72	19,66	27,19	0,9	24,5
14:00	984,41	151,13	189,09	16,13	27,15	0,8	24,9
15:00	909,40	149,72	183,48	10,63	27,13	0,6	25,5
16:00	189,85	104,31	113,41	3,61	26,65	0,9	23,6
17:00	540,64	139,47	169,08	4,50	26,65	1	21,6
18:00	366,03	121,1	141,97	13,32	26,51	1,3	21
19:00	106,25	108,4	121,89	22,48	26,50	0,8	20,2

13 MAY 2020

HOURS	DNI (W/m ²)	Tf_in (°C)	Tf_out (°C)	Theta (degree)	Flow Rate (m ³ /h)	Wind Speed (m/s)	Ambient Temp. (°C)
08:00	355,09	126,9	155,22	2,48	26,44	1	27,4
09:00	573,06	137,52	169,93	9,44	26,75	0,4	30,7
10:00	754,71	141,24	174,57	14,87	26,98	0,6	32
11:00	901,25	143,25	176,95	18,35	27,12	1,1	33,1
12:00	989,48	146,49	181,1	19,55	27,28	1,3	33
13:00	1022,69	148,75	185,49	18,35	27,3	1,4	33
14:00	1000,42	147,71	188,42	14,87	29,1	1,4	32,4
15:00	907,45	142,83	181,04	9,44	28,89	1,2	31
16:00	757,84	140,26	177,37	2,48	28,73	1,6	27,9
17:00	566,03	133,73	166,39	5,57	25,58	1,5	25,5
18:00	344,93	120,85	145,76	14,35	28,38	1	23,8
19:00	78,13	98,57	111,88	23,5	28,21	0,7	21,9

15 MAY 2020

HOURS	DNI (W/m ²)	Tf_in (°C)	Tf_out (°C)	Theta (degree)	Flow Rate (m ³ /h)	Wind Speed (m/s)	Ambient Temp. (°C)
07:00	110,94	42,60	42,36	5,97	26,60	1,4	26,9
08:00	295,32	94,73	100,96	2,06	27,80	1,3	29,9
09:00	498,45	95,22	110,35	8,99	28,03	1	32,1
10:00	676,19	102,30	120,55	14,4	28,26	0,6	34,4
11:00	822,68	107,36	127,99	17,86	28,48	0,5	36,8
12:00	898,07	111,88	133,92	19,06	28,66	0,5	38
13:00	934,79	116,34	140,14	17,86	28,74	0,7	38,7
14:00	901,98	119,82	144,90	14,4	28,68	0,6	38,6
15:00	815,65	121,40	146,49	8,99	28,56	0,7	36,8
16:00	661,74	116,70	138,07	2,06	28,43	0,7	33,2
17:00	478,92	107,36	123,36	5,97	28,23	0,2	29,6
18:00	274,23	92,96	101,2	14,74	28,1	0,1	28

18 MAY 2020

HOURS	DNI (W/m ²)	Tf_in (°C)	Tf_out (°C)	Theta (degree)	Flow Rate (m ³ /h)	Wind Speed (m/s)	Ambient Temp. (°C)
08:00	287,12	64,39	64,27	1,47	27,47	1,4	32,8
09:00	506,66	105,78	115,6	8,37	28,13	1,3	35,2
10:00	674,24	101,08	116,52	13,74	28,29	1,1	37,4
11:00	828,15	106,08	123,84	17,17	28,5	0,6	39,9
12:00	880,5	107,24	124,64	18,36	28,66	0,6	40,3
13:00	894,17	110,54	129,22	17,17	28,69	0,9	41,3
14:00	905,11	117,25	139,04	13,74	28,69	1,2	39,4
15:00	711,35	116,58	137,27	8,37	28,54	0,8	38,1
16:00	689,08	115,97	135,81	1,47	28,44	0,7	34,9
17:00	498,06	108,1	122,93	6,53	28,28	0,9	32,3
18:00	289,85	94,67	103,15	15,28	28,12	0,7	29,9

21 MAY 2020

HOURS	DNI (W/m ²)	Tf_in (°C)	Tf_out (°C)	Theta (degree)	Flow Rate (m ³ /h)	Wind Speed (m/s)	Ambient Temp. (°C)
07:00	134,77	45,9	45,72	7,05	26,61	0,6	28,8
08:00	175,01	49,13	48,46	0,93	26,84	0,8	29,8
09:00	277,74	90,03	92,1	7,79	27,96	1,1	30,4
10:00	707,83	109,32	131,84	13,12	28,37	2	30,3
11:00	838,31	126,77	148,26	16,54	28,67	2,1	32,1
12:00	925,03	116,76	142,46	17,71	28,76	2	31,1
13:00	965,65	120,06	147,65	16,54	28,81	2,5	29,9
14:00	964,48	128,73	160,65	13,12	28,80	2,2	29,2
15:00	888,09	132,94	167,12	7,79	28,74	2,2	28,1
16:00	747,68	132,08	164,98	0,93	28,59	2,3	24,6
17:00	574,24	127,93	157,17	7,05	28,46	1,6	23,1
18:00	359,78	117,44	140,2	15,77	28,32	1,5	22
19:00	159,77	102,24	116,15	24,89	28,2	1,2	21,5

29 MAY 2020

HOURS	DNI (W/m ²)	Tf_in (°C)	Tf_out (°C)	Theta (degree)	Flow Rate (m ³ /h)	Wind Speed (m/s)	Ambient Temp. (°C)
09:00	564,86	28,99	27,95	6,47	24,22	1	22,8
10:00	772,29	130,25	159	11,74	26,51	1,2	23,7
11:00	934,40	135,93	168,71	15,1	26,88	1,2	24
12:00	1023,47	139,71	172,55	16,25	27,07	1,2	26,3
13:00	1181,29	129,03	156,13	15,1	27,12	1,5	25,5
14:00	623,46	104,62	116,64	11,74	26,84	1,7	24,1
15:00	375,4	132,02	156,93	6,47	27,17	1,6	24,5
16:00	815,26	121,34	145,39	0,30	26,55	1,4	22
17:00	619,94	132,94	161,63	8,22	26,83	1,2	20,3
18:00	392,59	128,79	154,24	16,9	26,85	0,8	19,1
19:00	178,91	111,45	127,63	26	26,68	0,5	18,6

30 MAY 2020

HOURS	DNI (W/m ²)	Tf_in (°C)	Tf_out (°C)	Theta (degree)	Flow Rate (m ³ /h)	Wind Speed (m/s)	Ambient Temp. (°C)
07:00	164,46	64,64	66,1	8,34	25,57	1,3	21,6
08:00	364,85	123,66	149,78	0,43	26,43	0,9	23,1
09:00	578,53	131,47	160,77	6,33	26,70	0,6	24,4
10:00	766,04	135,01	166,14	11,59	26,86	0,8	24,9
11:00	914,87	138,74	171,33	14,94	27,04	0,9	26,5
12:00	997,69	141,67	175,3	16,1	27,19	1	26,9
13:00	1035,58	146,92	183,05	14,94	27,24	1,3	26,2
14:00	1018,39	151,13	188,79	11,59	27,23	1,6	26,1
15:00	1027,77	113,59	132,94	6,33	26,51	1,6	24,9
16:00	933,23	81,61	84,11	0,43	26,33	1,4	23,2
17:00	189,85	113,10	127,75	8,34	26,62	1,2	21,5
18:00	385,17	112,37	129,15	17,01	26,42	0,7	20,3
19:00	182,04	110,78	126,69	26,11	26,47	0,8	19,4

2 JUNE

HOURS	DNI (W/m ²)	Tf_in (°C)	Tf_out (°C)	Theta (degree)	Flow Rate (m ³ /h)	Wind Speed (m/s)	Ambient Temp. (°C)
09:00	565,64	116,7	137,03	5,95	26,21	0,7	22,6
10:00	759,01	122,38	143,68	11,19	26,51	0,7	24,7
11:00	336,73	111,15	126,16	14,53	26,69	1,4	25,4
12:00	398,06	110,66	111,09	15,68	26,54	1,6	26,1
13:00	264,46	117,01	135,56	14,53	26,74	1,7	26,1
14:00	1245,74	89,24	88,02	11,19	26,35	1,6	26,1
15:00	961,36	118,84	143,07	5,95	26,42	1,7	24,6
16:00	939,09	118,41	128,97	0,79	26,40	1,5	21,9
17:00	657,05	116,40	139,1	8,68	26,45	0,9	20,8
18:00	426,97	103,7	118,29	17,34	26,33	0,7	19,3
19:00	185,55	110,11	113,59	26,43	26,38	0,9	19

4 JUNE 2020

HOURS	DNI (W/m ²)	Tf_in (°C)	Tf_out (°C)	Theta (degree)	Flow Rate (m ³ /h)	Wind Speed (m/s)	Ambient Temp. (°C)
07:00	160,55	63,48	63,42	8,88	25,49	1,6	22,9
08:00	369,93	127,81	149,3	1,00	26,34	1,3	24,7
09:00	581,66	125,43	151,9	5,73	26,67	0,7	25,2
10:00	769,16	120,24	151,8	10,95	26,65	0,9	27,1
11:00	916,82	126,29	154	14,28	26,74	1,1	28,7
12:00	999,25	129,95	158,7	15,43	26,84	1,3	29,1
13:00	1033,63	132,27	161,93	14,28	26,88	1,7	28,6
14:00	1000,42	132,94	162,18	10,95	26,81	1,8	27,7
15:00	913,31	134,1	163,58	5,73	26,74	1,8	26,5
16:00	784,40	135,01	164,68	1	26,72	1,6	24,7
17:00	595,33	129,15	155,16	8,88	26,6	1,1	23,2
18:00	391,03	113,35	131,47	17,53	26,41	0,8	21,8
19:00	188,29	103,58	116,64	26,62	26,33	0,9	21,3

6 JUNE 2020

HOURS	DNI (W/m ²)	Tf_in (°C)	Tf_out (°C)	Theta (degree)	Flow Rate (m ³ /h)	Wind Speed (m/s)	Ambient Temp. (°C)
07:00	124,61	40,53	39,67	9,06	25,27	1,8	25,2
08:00	312,12	68,48	66,9	1,20	25,79	1,6	28,9
09:00	566,42	98,15	105,53	5,53	26,23	1,3	32
10:00	651,19	103,46	118,05	10,74	26,33	1,4	32,7
11:00	906,28	99,73	115,24	14,06	26,33	1	33,4
12:00	936,75	111,09	129,03	15,2	26,54	1,3	34,2
13:00	1064,10	100,89	115,3	14,06	26,49	1,8	33,4
14:00	997,69	119,45	141,42	10,74	26,57	2	32,8
15:00	911,36	126,9	152,1	5,53	26,63	2	31,6
16:00	673,07	103,27	116,89	1,20	26,36	1,3	30
17:00	585,96	116,46	136,11	9,06	26,39	0,9	28,1
18:00	374,23	107,24	122,62	17,7	26,31	0,4	25,6
19:00	163,68	91,25	99,12	26,78	26,17	0,6	24,9

9 JUNE 2020

HOURS	DNI (W/m ²)	Tf_in (°C)	Tf_out (°C)	Theta (degree)	Flow Rate (m ³ /h)	Wind Speed (m/s)	Ambient Temp. (°C)
09:00	529,7	110,54	111,45	5,27	26,09	1	32
10:00	709,40	102,60	120,67	10,47	26,32	0,9	32,6
11:00	850,81	107,30	126,53	13,78	26,46	0,4	33,1
12:00	948,08	112,92	133,24	14,92	26,6	0,6	35
13:00	433,22	88,93	97,9	13,78	26,5	1,1	34,1
14:30	791,04	60,12	60,91	10,47	25,82	1,7	33
15:00	937,17	107,55	126,35	5,27	26,33	1,8	32
16:00	779,71	121,04	144,17	1,44	26,64	1,4	30,5
17:00	547,67	112,67	130,25	9,28	26,55	1,4	29,1
18:00	349,62	104,13	116,95	17,92	26,45	0,9	27,6
19:00	167,58	88,75	95,28	26,99	26,28	0,3	25,7
20:00	27,74	65,86	64,52	36,17	25,88	0,1	25,2

11 JUNE 2020

HOURS	DNI (W/m ²)	Tf_in (°C)	Tf_out (°C)	Theta (degree)	Flow Rate (m ³ /h)	Wind Speed (m/s)	Ambient Temp. (°C)
07:00	161,72	69,15	69,34	9,41	25,59	1	26,5
08:00	362,12	116,82	137,64	1,57	26,33	1,1	28,6
09:00	568,77	121,95	145,27	5,13	26,53	1,3	29,8
10:00	751,59	119,82	145,15	10,32	26,57	1,4	30,9
11:00	899,64	123,36	148,26	13,63	26,70	1,6	31,3
12:00	989,87	125,61	151,68	14,76	26,80	1,8	32,1
13:00	1008,23	124,21	146,67	13,63	26,82	2,5	29,6
14:00	991,05	133,3	161,87	10,32	26,84	2,5	28,5
15:00	938,31	137,58	167,3	5,13	26,82	1,8	27,9
16:00	422,67	113,47	127,02	1,57	26,71	1,7	26
17:00	613,69	120,3	139,59	9,41	26,43	1,4	24,8
18:00	391,03	119,33	136,36	18,04	26,48	1	23,5
19:00	138,29	96,32	104,07	27,11	26,32	0,5	22,7

10 JUNE 2020

HOURS	DNI (W/m ²)	Tf_in (°C)	Tf_out (°C)	Theta (degree)	Flow Rate (m ³ /h)	Wind Speed (m/s)	Ambient Temp. (°C)
07:00	118,36	39,25	38,33	9,35	25,30	0,9	27,7
08:00	334,78	106,51	119,21	1,50	26,13	1	28,8
09:00	546,89	112,49	132,94	5,20	26,43	1	31,3
10:00	731,66	116,15	138,31	10,39	26,56	1,3	32,3
11:00	874,25	120,37	142,46	13,7	26,70	1,4	33,2
12:00	949,64	124,39	146,55	14,84	26,81	1,6	33,9
13:00	1009,8	128,91	152,47	13,7	26,86	1,8	32,1
14:00	967,22	132,76	157,11	10,39	26,86	1,8	31,4
15:00	895,34	137,21	162,18	5,20	26,82	1,7	29,9
16:00	748,07	136,05	159,18	1,50	26,77	1,6	27,4
17:00	567,20	128,18	146,79	9,35	26,64	1,2	26,1
18:00	354,31	114,08	126,35	17,98	26,48	1,1	24,9
19:00	172,66	94,85	106,75	27,06	26,32	0,9	24,1

19 JUNE 2020

HOURS	DNI (W/m ²)	Tf_in (°C)	Tf_out (°C)	Theta (degree)	Flow Rate (m ³ /h)	Wind Speed (m/s)	Ambient Temp. (°C)
07:00	181,26	41,75	40,89	9,69	25,30	0,6	26,6
08:00	351,18	117,19	129,09	1,86	26,14	0,7	28,9
09:00	543,38	112,13	135,69	4,82	26,39	1	30,7
10:00	737,13	114,02	137,88	10	26,53	0,8	31,1
11:00	914,09	118,47	144,29	13,29	26,66	0,8	32,1
12:00	1100,82	111,15	132,94	14,42	26,63	1,7	33,4
13:00	307,82	89,85	99,31	13,29	26,46	1,6	33,2
14:00	1107,46	79,04	86,67	10	26,14	1,4	31,6
15:00	949,64	119,45	146,98	4,82	26,49	1,6	31,7
16:00	879,71	123,29	149,24	1,86	26,56	1	28,4
17:00	697,68	67,81	67,81	9,59	25,83	1,8	26,5
18:00	484,78	81,91	92,17	18,3	25,98	1,3	25,7
19:00	200,01	91,86	100,47	27,37	26,11	0,3	25

7 AUGUST 2020

HOURS	DNI (W/m ²)	Tf_in (°C)	Tf_out (°C)	Theta (degree)	Flow Rate (m ³ /h)	Wind Speed (m/s)	Ambient Temp. (°C)
07:00	71,49	31,62	32,04	3,93	24,59	0,6	30,4
08:00	262,51	73,37	77,76	4,21	25,77	0,7	32,1
09:00	464,08	89,72	98,57	11,27	26,08	1	34,3
10:00	654,32	95,77	106,02	16,8	26,22	1,4	35,3
11:00	787,91	98,64	109,35	20,36	26,32	1,6	35,5
12:00	900,42	101,63	112,98	21,59	26,40	1,7	34,7
13:00	940,26	105,35	117,37	20,36	26,44	1,8	34,1
14:00	938,31	111,03	125,86	16,8	26,44	2,1	33,4
15:00	864,87	116,58	131,41	11,27	26,45	1,8	30,5
16:00	719,55	116,76	131,11	4,21	26,41	1,5	29,2
17:00	541,81	116,76	130,44	3,93	26,39	1,6	27,4
18:00	325,40	109,93	120,24	12,77	26,33	0,8	25,8
19:00	138,68	96,38	102,66	21,93	26,22	0,6	24,2

10 AUGUST 2020

HOURS	DNI (W/m ²)	Tf_in (°C)	Tf_out (°C)	Theta (degree)	Flow Rate (m ³ /h)	Wind Speed (m/s)	Ambient Temp. (°C)
07:00	63,67	31,07	27,34	3,21	24,99	0,3	27,7
08:00	256,26	43,15	38,03	4,97	25,34	0,5	29,4
09:00	178,91	71,23	75,08	12,07	25,87	0,9	31,1
10:00	676,58	86,67	94,06	17,65	26,06	1,1	33,1
11:00	817,21	94,42	103,64	21,24	26,28	1,5	33,4
12:00	894,17	98,70	108,52	22,49	26,34	1,5	35,1
13:00	950,03	103,82	114,87	21,24	26,40	1,4	35,9
14:00	915,65	107,97	121,83	17,65	26,43	0,6	37
15:00	819,56	110,78	122,99	12,07	26,42	1,1	35,8
16:00	696,51	112,80	125	4,97	26,42	0,9	34,1
17:00	509,78	105,96	115,73	3,21	26,36	0,7	32,4
18:00	302,74	97,11	103,82	12,08	26,23	0,8	31,2
19:00	112,89	83,86	88,50	21,24	26,15	0,6	30

15 AUGUST 2020

HOURS	DNI (W/m²)	Tf_in (°C)	Tf_out (°C)	Theta (degree)	Flow Rate (m³/h)	Wind Speed (m/s)	Ambient Temp. (°C)
08:00	268,37	90,58	92,04	6,30	25,99	0,8	31,1
09:00	476,58	110,11	117,56	13,49	26,30	1,2	32,5
10:00	668,38	99,98	114,99	19,14	26,42	1,2	34,6
11:00	826,98	101,63	116,46	22,8	26,45	0,9	36,4
12:00	924,25	99,67	113,71	24,07	26,48	1,4	37,6
13:00	962,92	96,87	110,05	22,8	26,40	1,9	37,1
14:00	926,98	100,89	115,24	19,14	26,40	1,6	37,1
15:00	846,90	104,50	119,82	13,49	26,40	0,7	37,2
16:00	710,18	105,78	121,04	6,30	26,37	0,8	35,4
17:00	521,89	104,07	117,68	1,94	26,34	1	33,8
18:00	305,48	98,51	109,2	10,84	26,29	0,7	31,8
19:00	110,55	87,22	93,02	20,2	26,19	0,3	27,4

19 AUGUST 2020

HOURS	DNI (W/m²)	Tf_in (°C)	Tf_out (°C)	Theta (degree)	Flow Rate (m³/h)	Wind Speed (m/s)	Ambient Temp. (°C)
08:00	250,01	78,92	79,84	7,43	25,85	0,6	29,9
09:00	464,86	108,65	113,04	14,69	26,30	1	31,3
10:00	654,32	109,38	113,77	20,41	26,44	1,3	33,7
11:00	805,10	105,53	116,76	24,12	26,43	1,4	35,7
12:00	903,54	106,88	114,38	25,4	26,49	1,5	35
13:00	942,61	101,50	117,44	24,12	26,53	1,6	35,3
14:00	927,76	99,98	115,24	20,41	26,42	1,8	34,2
15:00	838,7	101,32	116,76	14,69	26,36	1,7	32,4
16:00	707,05	103,52	119,08	7,43	26,34	1,3	29,8
17:00	519,16	102,18	116,28	0,86	26,30	0,9	27,8
18:00	301,18	96,01	106,69	9,80	26,26	0,7	26,3
19:00	97,27	80,63	86,86	18,98	26,12	0,6	25,4

22 AUGUST 2020

HOURS	DNI (W/m ²)	Tf_in (°C)	Tf_out (°C)	Theta (degree)	Flow Rate (m ³ /h)	Wind Speed (m/s)	Ambient Temp. (°C)
08:00	255,09	91,56	102,6	8,32	27,77	2,2	31,5
09:00	475,01	114,81	121,46	15,62	28,14	1,9	33
10:00	668,77	105,84	125	21,39	28,23	2,2	34,5
11:00	817,99	102,11	118,96	25,14	28,32	1,8	35,1
12:00	918,39	103,09	123,3	26,45	28,41	1,4	36,8
13:00	950,81	106,57	125,31	25,14	28,46	0,9	37,5
14:00	923,86	111,51	132,51	21,39	28,45	0,7	37,8
15:00	831,28	115,97	138,55	15,62	28,37	0,7	35,7
16:00	674,63	117,19	139,71	8,32	28,34	0,5	34
17:00	477,36	114,38	134,40	0,02	28,26	0,3	33,2
18:00	267,20	106,45	121,46	8,98	28,18	1,3	32,8
19:00	82,42	87,65	93,26	18,17	27,99	1,1	31,3

25 AUGUST 2020

HOURS	DNI (W/m ²)	Tf_in (°C)	Tf_out (°C)	Theta (degree)	Flow Rate (m ³ /h)	Wind Speed (m/s)	Ambient Temp. (°C)
08:00	222,27	80,2	82,71	9,22	27,58	0,9	32
09:00	435,17	109,93	119,02	16,57	28,09	0,5	34,8
10:00	628,93	104,62	122,87	22,41	28,26	1,1	35,5
11:00	778,54	104,86	124,64	26,20	28,35	1,2	37,1
12:00	876,20	114,44	122,26	27,52	28,49	1,4	37,3
13:00	922,29	103,03	121,46	26,20	28,43	1,5	36,7
14:00	895,34	107,06	126,96	22,41	28,36	1,9	34,9
15:00	804,32	109,68	130,62	16,57	28,28	1,6	33
16:00	659	110,23	130,56	9,22	28,22	1,4	30,4
17:00	466,03	107,73	126,41	0,83	28,13	1,1	28,7
18:00	260,55	100,71	114,99	8,14	28,05	0,8	27,8
19:00	72,66	81,3	86	17,33	27,87	0,6	26,5

27 AUGUST 2020

HOURS	DNI (W/m²)	Tf_in (°C)	Tf_out (°C)	Theta (degree)	Flow Rate (m³/h)	Wind Speed (m/s)	Ambient Temp. (°C)
08:00	233,21	85,76	88,56	9,83	27,64	0,7	30,6
09:00	445,33	114,44	121,65	17,23	28,09	0,6	32,9
10:00	640,25	107,12	122,32	23,1	28,33	1	33,4
11:00	791,04	116,7	123,29	26,92	28,44	1,3	35,5
12:00	885,18	114,44	122,87	28,25	28,56	1,7	36,2
13:00	922,29	104,62	118,47	26,92	28,5	1,8	35,7
14:00	889,09	105,66	125,31	23,1	28,37	1,5	36,4
15:00	796,12	109,07	130,01	17,23	28,29	1,1	34,5
16:00	648,46	109,93	130,44	9,83	28,22	1,5	31,4
17:00	450,01	106,69	125,43	1,43	28,17	1,1	29,1
18:00	244,54	99,49	113,47	7,56	28,07	0,7	28,5
19:00	69,14	79,35	78,74	16,75	27,88	0,4	27,2

31 AUGUST 2020

HOURS	DNI (W/m²)	Tf_in (°C)	Tf_out (°C)	Theta (degree)	Flow Rate (m³/h)	Wind Speed (m/s)	Ambient Temp. (°C)
08:00	217,58	77,52	80,14	11,09	27,57	0,3	32
09:00	438,29	113,47	118,78	18,56	28,11	0,7	33,8
10:00	633,61	104,62	122,07	24,5	28,31	1	36,3
11:00	779,71	108,65	120,43	28,39	28,46	0,9	38,1
12:00	888,31	105,96	125,98	29,75	28,52	1,1	39,1
13:00	917,61	115,48	125	28,39	28,59	0,9	40,2
14:00	877,76	105,72	125,37	24,5	28,39	1,3	38,5
15:00	780,49	108,34	128,85	18,56	28,26	1	36,8
16:00	628,53	108,89	129,46	11,09	28,21	1	33,4
17:00	438,69	106,39	124,58	2,63	28,15	0,9	30,9
18:00	228,52	97,23	110,17	6,39	28,06	0,9	29,7
19:00	49,61	76,11	79,41	15,58	27,81	0,5	28,6

19 JANUARY 2020

HOURS	DNI (W/m ²)	Tf_in (°C)	Tf_out (°C)	Theta (degree)	Flow Rate (m ³ /h)	Wind Speed (m/s)	Ambient Temp. (°C)
10:00	260,55	75,38	76,54	50,77	27,69	1,3	10,7
11:00	418,76	94,73	101,02	56,31	28,27	0,9	11,6
12:00	542,99	96,44	107,06	58,39	28,56	1,2	11,9
13:00	584,39	98,33	110,60	56,31	28,30	1,1	11,7
14:00	524,63	110,35	128,3	50,77	28,33	1	9,8
15:00	469,62	117,19	139,16	43,11	28,35	0,6	7,2
16:00	319,15	119,82	142,58	34,36	28,40	0,1	6,4
17:00	125	94,97	103,64	25,2	28,23	0,001	5,3

27 APRIL 2020

HOURS	DNI (W/m ²)	Tf_in (°C)	Tf_out (°C)	Theta (degree)	Flow Rate (m ³ /h)	Wind Speed (m/s)	Ambient Temp. (°C)
10:00	720,73	55,24	54,87	19,3	25,47	0,8	23,9
11:00	898,86	125,8	158,39	22,96	26,72	1,1	25
12:00	995,73	144,29	186,41	24,23	27,15	1,1	25,8
13:00	1024,64	149,66	193,49	22,96	27,35	1,3	25,6
14:00	996,91	154,97	201,79	19,3	27,43	1,4	24,7
15:00	885,18	159,49	208,56	13,64	27,51	1,6	22,2
16:00	734,4	159,55	208,08	6,44	27,5	1,7	20,7
17:00	530,9	150,88	192,94	1,81	27,40	1,2	19,1
18:00	300,79	136,66	166,75	10,72	27,19	0,8	17,3
19:00	98,05	106,69	118,35	19,89	26,74	0,5	16

16 MAY 2020

HOURS	DNI (W/m ²)	Tf_in (°C)	Tf_out (°C)	Theta (degree)	Flow Rate (m ³ /h)	Wind Speed (m/s)	Ambient Temp. (°C)
07:00	121,1	40,59	39,37	6,16	26,80	1,5	29
08:00	299,23	77,27	85,33	1,86	27,69	1,3	32,2
09:00	507,44	94,73	111,03	8,78	28,04	1	34,9
10:00	690,26	100,41	120,79	14,17	28,30	0,7	36,4
11:00	834,79	107,55	128,54	17,63	28,52	0,5	38,5
12:00	923,47	112	134,89	18,82	28,68	0,3	39,9
13:00	936,36	116,46	141,18	17,63	28,78	0,5	41,5
14:00	915,65	121,95	148,63	14,17	28,74	0,6	40,4
15:00	833,62	125,74	151,07	8,78	28,62	0,9	39
16:00	680,88	121,34	145,45	1,86	28,51	0,3	35,9
17:00	488,3	113,53	131,9	6,16	28,34	0,2	32,7
18:00	295,71	101,14	112,86	14,92	28,2	0,1	29,2

19 JUNE 2020

HOURS	DNI (W/m ²)	Tf_in (°C)	Tf_out (°C)	Theta (degree)	Flow Rate (m ³ /h)	Wind Speed (m/s)	Ambient Temp. (°C)
07:00	181,26	41,75	40,89	9,69	25,30	0,6	26,6
08:00	351,18	117,19	129,09	1,86	26,14	0,7	28,9
09:00	543,38	112,13	135,69	4,82	26,39	1	30,7
10:00	737,13	114,02	137,88	10	26,53	0,8	31,1
11:00	914,09	118,47	144,29	13,29	26,66	0,8	32,1
12:00	1100,82	111,15	132,94	14,42	26,63	1,7	33,4
13:00	307,82	89,85	99,31	13,29	26,46	1,6	33,2
14:00	1107,46	79,04	86,67	10	26,14	1,4	31,6
15:00	949,64	119,45	146,98	4,82	26,49	1,6	31,7
16:00	879,71	123,29	149,24	1,86	26,56	1	28,4
17:00	697,68	67,81	67,81	9,59	25,83	1,8	26,5
18:00	484,78	81,91	92,17	18,3	25,98	1,3	25,7
19:00	200,01	91,86	100,47	27,37	26,11	0,3	25

16 AUGUST 2020

HOURS	DNI (W/m ²)	Tf_in (°C)	Tf_out (°C)	Theta (degree)	Flow Rate (m ³ /h)	Wind Speed (m/s)	Ambient Temp. (°C)
08:00	264,07	86,73	87,83	6,58	25,91	0,5	31
09:00	480,87	100,34	114,87	13,78	26,35	0,7	33,4
10:00	669,94	100,83	117,07	19,46	26,4	0,8	34,8
11:00	826,98	98,51	113,35	23,12	26,43	1,1	35,6
12:00	918,78	95,95	108,65	24,4	26,43	1,4	35,8
13:00	959,40	97,84	110,72	23,12	26,43	2	37,2
14:00	927,76	102,30	118,05	19,46	26,43	1,8	37,7
15:00	834,40	104,86	120,12	13,78	26,42	2	36,4
16:00	698,07	105,9	120,49	6,58	26,38	1,8	34,4
17:00	522,28	103,76	117,01	1,68	26,33	0,9	32,1
18:00	308,21	98,51	108,89	10,59	26,29	0,5	29,7
19:00	109,38	85,51	90,4	19,77	26,19	0,3	29

16 SEPTEMBER 2020

HOURS	DNI (W/m ²)	Tf_in (°C)	Tf_out (°C)	Theta (degree)	Flow Rate (m ³ /h)	Wind Speed (m/s)	Ambient Temp. (°C)
08:00	162,51	50,78	45,53	16,36	25,21	0,4	31,6
09:00	367,20	78,68	86,73	24,12	25,96	0,9	31,9
10:00	555,10	84,17	93,75	30,41	26,16	1	33
11:00	703,54	94,06	103,03	34,57	26,41	1,1	36
12:00	656,27	99,37	110,17	36,04	26,55	1,3	35,3
13:00	330,09	92,29	100,16	34,57	26,47	1,6	32,5
14:00	778,54	104,86	118,23	30,41	26,43	2,1	31,4
15:00	690,26	106,51	119,75	24,12	26,42	2,1	29,8
16:00	481,26	78,13	81	16,36	26,14	1,4	28
17:00	348,84	102,48	114,51	7,68	26,27	1,2	26,6
18:00	139,46	91,49	98,51	1,43	26,28	0,5	25,2

16 OCTOBER 2020

HOURS	DNI (W/m²)	Tf_in (°C)	Tf_out (°C)	Theta (degree)	Flow Rate (m³/h)	Wind Speed (m/s)	Ambient Temp. (°C)
08:00	110,94	26,49	25,70	26,03	23,75	1	22
09:00	312,90	73,92	82,64	34,33	25,88	1,5	24,8
10:00	505,87	81,61	90,27	41,3	26,23	1,5	26,2
11:00	655,49	83,68	93,02	46,09	26,38	0,5	28,7
12:00	608,22	82,71	91,37	47,82	26,43	0,5	29,4
13:00	737,13	94,06	108,22	46,09	26,42	0,001	31,2
14:00	684,79	105,23	124,03	41,3	26,44	0,5	28,4
15:00	430,09	88,93	98,88	34,33	26,29	0,001	25,8
16:00	413,68	108,34	127,93	26,03	26,41	0,5	23,7
17:00	206,26	101,87	116,46	17,04	26,42	0,001	22,3
18:00	38,28	73,12	76,66	7,85	26,07	0,001	20,8

11 NOVEMBER 2020

HOURS	DNI (W/m²)	Tf_in (°C)	Tf_out (°C)	Theta (degree)	Flow Rate (m³/h)	Wind Speed (m/s)	Ambient Temp. (°C)
10:00	361,73	36,99	35,28	48,69	25,31	1	22,8
11:00	498,84	52,25	49,81	54,04	25,44	1	23,5
12:00	581,27	67,08	64,21	56,02	25,96	1	24,2
13:00	607,44	94,49	98,7	54,04	26,32	0,5	24
14:00	525,41	117,25	121,22	48,69	26,57	0,001	22,1
15:00	451,97	111,58	131,72	41,18	26,49	0,001	18,9
16:00	284,38	113,1	130,86	32,53	26,64	0,001	17
17:00	89,85	89,42	99,12	23,4	26,37	0,001	15,5

REPUBLIC OF TURKEY
AYDIN ADNAN MENDERES UNIVERSITY
GRADUATE SCHOOL OF NATURAL AND APPLIED SCIENCES

SCIENTIFIC ETHICAL STATEMENT

I hereby declare that I composed all the information in my master's thesis entitled "PERFORMANCE ANALYSIS OF PARABOLIC TROUGH SOLAR COLLECTORS" within the framework of ethical behavior and academic rules, and that due references were provided and for all kinds of statements and information that do not belong to me in this study in accordance with the guide for writing the thesis. I declare that I accept all kinds of legal consequences when the opposite of what I have stated is revealed.

Mehmet Aktaş

26/07/2021